



Faculty of Science and Technology  
Department of Mathematics and Statistics

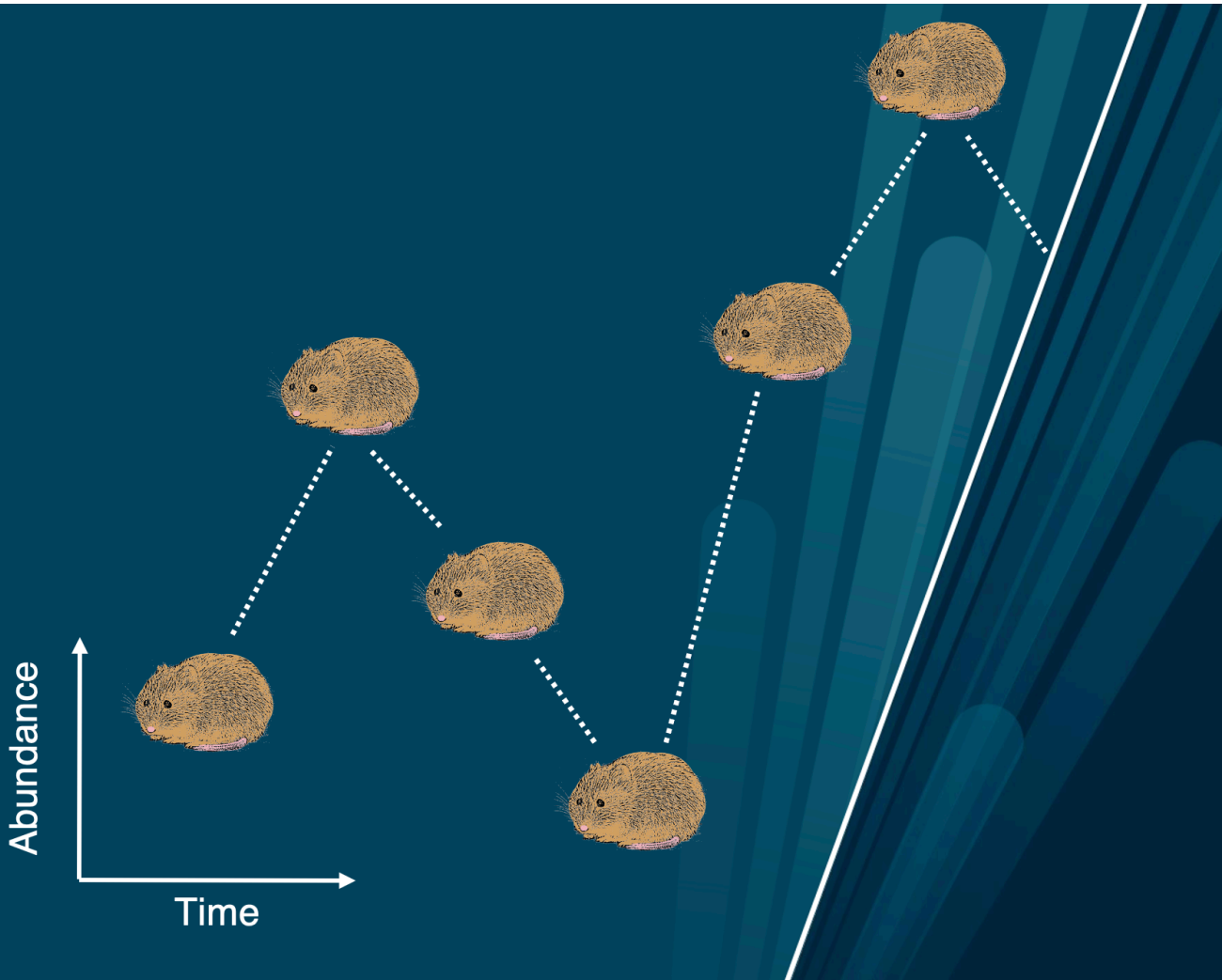
## Boreal rodents fluctuating in space and time

Tying the observation process to the modeling of seasonal population dynamics

—

**Pedro Guilherme Nicolau**

*A dissertation for the degree of Philosophiae Doctor – March 2022*





A dissertation for the degree of Philosophiae Doctor

# **Boreal rodents fluctuating in space and time**

Tying the observation process to the modelling  
of seasonal population dynamics

Pedro Guilherme Antunes Lopes da Silva Nicolau



Supervised by:

Sigrunn H. Sørbye  
Nigel G. Yoccoz

Faculty of Science and Technology  
Department of Mathematics and Statistics  
UiT- The Arctic University of Norway

Tromsø – March 2022





*“Mathematics without natural history is sterile,  
but natural history without mathematics is muddled”*

John Maynard Smith (1982)



## Abstract

Small rodents are some of the most important elements of boreal and arctic food webs in which they play essential functional roles. Their population dynamics are characterized by large amplitude multi-annual cycles regulated by direct and delayed density-dependence. These drastic variations in abundance have deep cascading effects into the whole ecosystem. Hence, the study boreal rodent population processes and drivers is important if seeking to understand and predict future states of northern ecosystems.

To monitor animal populations, it is important to obtain reliable estimates of population size, which involves accounting for errors in the observation process. For small rodents, a common way of doing so is through the capture-recapture methodology, which collects information on both the number of observed animals and on their detectability, allowing to infer the number of non-observed individuals. Time series of abundance corrected for the observation process can then be used to model population processes of interest. Capture-recapture, although being optimal, is resource-intensive and limited to favorable field conditions, restricting the spatial and temporal resolution of the abundance data. This can be particularly limiting when studying populations of multivoltine rodents, with fast-changing population dynamics subject to strong effects of seasonality. New methods based on camera traps allow to increase spatial and temporal resolution of rodent data (together with other species which are otherwise not monitored). However, as they cannot provide measures of detectability if the animals cannot be identified individually, they require species-specific calibration studies.

This thesis works on advancing the observation process of boreal rodents to study characteristic population processes: density-dependence and spatial synchrony. For this purpose, three specific research goals were defined. (1) Develop a statistical framework to account for different sources of sampling error (i.e., capture heterogeneity) when estimating direct and delayed density-dependence in rodent population processes. In addition,

---

assess estimation biases for different process parameters through a comprehensive simulation study. (2) Assess the adequacy of tunnel-based camera trap activity data as an index for abundance, calibrated against estimates obtained from capture-recapture in two different small rodent species, with differential space use and trappabilities. (3) Devise a protocol to estimate spatial synchrony in populations subject to geographical- and seasonal-specific density-dependence, allowing to separate those deterministic effects from the stochastic (i.e., weather) effects in driving the observed population synchrony.

## Acknowledgements

The onset of this journey started with both of my supervisors, which selected me to take part in the PhD program – Sigrunn Sørbye and Nigel Yoccoz. My background combined statistics and ecology, and my supervisors helped me make the most of both worlds. Sigrunn ensured I had as much supervision as I wished for, always keeping her door open to ensure I did not get stuck at any part of the process. She pushed me to be more precise, more rigorous and always did the most to ensure the quality of our research through frequent and timely feedback. Nigel sat across the campus, often being somewhere in the tundra or forest, and still never made me feel like he was actually far away. He strove to give me my own space and as much creative control as possible, within the scopes of the project, while making sure the rigor and assumptions held. Above all, he made me feel like I would be OK no matter what, and that is truly incalculable. I would also like to acknowledge Professor Rolf Ims, my unofficial supervisor, which collaborated with me in two of the projects and truly helped taking the research to the next level. Always kind, positive and forever passionate about his research.

To welcome me at the Mathematics and Statistics department, I could count on a number of people, which made my life better in several ways. First Helge, and then Tine Hågensen, both provided all the bureaucratic and personal support I needed. The Algebra group deserves a special mention. Cordian, for being such a friendly person with a great positive energy and providing many loud laughs, making it feel a bit closer to home. Hugues, for all kinds of help, from computer support to tax-related problems, to all sorts of life hacks. Sebastian, for many nice soul-sharing moments. And Robin, for the swimming company, puzzle pints, deep ear for all my rants and overall for being such a good cultured friend with great positive energy.

Although originally from the Algebra group, he has now left so I can technically make his own paragraph. In between his sarcastic humor, his olive yellow jacket, his French ‘accént’ and his ginger tea, Philippe became my friend. He was there for ALL my downs. Always making the perfect

---

joke at the most inappropriate time possible, sucking out the bad from any situation tarnishing my brain. We clashed, we laughed, we cried (not him, just me). He became not just a friend, but also a role model for his academic integrity and selflessness.

I would also like to mention all the group of PhD students (and associates) at IMS which seemed to follow not only an exponential growth in terms of size, but also in greatness. In particular, the PhD focus group, with Børge, Åse Mari, Andreu and Anna Karpova. Clara and Luc, for such fun times, the TTT's out in the sunny/windy/snowy cold, and the Céline Dion knowledge. And Kessy, Carla, Alessandro Schena, Örs, Alessandro Cotronei, Michele, Rakhi and Magda. Also, my former office mates, namely Eirik, which provided guidance and support throughout, and Dávid. Additionally, Øistein, for his help and for the template of his thesis.

A few selected people made sure I always had ears and shoulders available, while sharing incredible moments with. The Pattern Recognition duo: Eduard, my extravagant (in all the best ways) and incredibly caring friend; and Sophie, with her extensive linear Algebra knowledge and true free spirit. And the super-Helene and wonder-Verena duo, for the endless fun, aurora/whale watching, skiing trips, dinners, deep conversations and true friendship.

Many other people in Tromsø enriched my life in a number of ways, for longer or shorter periods. The volleyball group, with people rotating almost weekly and often being the highlight of the week, with a special mention to Artem, Johannes and Martine. The Tromsø birding community, including Björn, Mikołaj, Jan and Unni. The party group of Knut, Natalia, Antonio, Isabel, among others. Dan, a true Tromsø local and my gaming friend. All my different room mates including Lukas, Enrico, Aakash and Junia. My landladies, with a very kind mention to Hilde, for being such a brilliant host, with the deepest knowledge of the region, amazing dishes and most contagious laugh. My Norwegian teacher, Lene, which took my rather short journey in learning Norwegian farther than it would have otherwise gone.

A big part of my time was spent at the top of campus on the biology building. Despite me not being technically a member there, I was welcomed with open arms from the first day I stepped into the building. Truly every single person was kind to me and was curious about what I had to say. The

---

list of people that have made a positive contribution is long, but I will try to cover most of it here. Starting with the NorPop group, which I only really joined towards the end of my journey but made such a positive impact on both my research and life quality. Amazing discussions, fantastic baking skills, endless brainstorming. Eivind, Julia, Florent, Simon, Isabell, Stijn, Michele and Eva made going up the campus hill, and getting up earlier on Mondays, worth it. Two special members deserve to be highlighted. Julia, for her friendship, the incredibly wide knowledge, kind heart, altruism and, last but not least, her beautiful blueberry pie. And Eivind, for being the best co-author I could have hoped for, always teeming with ideas, with the right type of optimism, his readiness to help others, and his ability to disagree to keep me in check. Other people deserve to be mentioned. Laffen, for his friendship, kindness and incredible efficiency with bureaucracy. John-André for giving me the opportunity to go live the tundra and assist him, together with Matthias which gave me a glimpse of wild living in Norway. Finally, Chloé, which could be a little bit sprinkled through the different paragraphs, for always providing useful advice, knowledge and friendship throughout.

One of the great assets of taking a PhD is being able to attend conferences, present your work and meet fantastic people. Of the different conferences I attended, the International Statistical Ecology Conference deserves to be highlighted. Both Saint Andrews 2018 and Virtual Sydney 2020 were unique opportunities to truly become part of the ecological statistics community and become inspired to do more and better. Of the many incredible people I had the privilege to meet, a few deserve special mention. Sunny & the ‘Uropeans – Chris and Pablo –, made my experience in Kentucky truly memorable at such a tough time of my life. All the crew in Amarante, at the Sociedade Portuguesa de Estatística 2019 Conference, made it unforgettable, with the added pleasure of being able to present to an audience so dear to my heart.

Before I was able to step on that plane and go live above the Arctic circle, I could count on the help of many people which, in one way or another, contributed to make me the scientist and human I am today. Most importantly, I would like to acknowledge Ali and Tiago, my two MSc supervisors, without whom I would have surely not pursued a PhD. Their

---

knowledge, expertise, humanity and friendship were simply beyond, and set the standard for what I could hope to achieve and wish to become. An important mention goes to DEIO, the Statistics Department at the University of Lisbon. All the incredible professors took care of me and took me from the world of biology into the world of statistics. Professors Marília Antunes, Lisete Sousa, Salomé Cabral, Helena Mouriño were among the many sharing their knowledge and inspiring me to continue.

A number of true friends have remained so until this day and deserve a very special mention. Carolina, my madrinha, going through the same journey as me but across the Atlantic, always there when I need her, with her words, knowledge, lively discussions and inspiring me daily with her perseverance. All my Pica-Pau siblings, particularly Maria, Mateus e Gonçalo; for showing me they will always have my back no matter what, when or how distant in space we may be. Rita, for being the strongest person I know and never failing to make sure I am doing OK, no matter what is going on with her life. Costa, for being my metaphysical brother. My university friends, Filipa, Manel, Marcos and Madalena, with whom I have grown so much. All my birding friends, especially Pedro Ramalho, not only a true friend but also a role model. Stephen, the kindest soul, bawdy-humor-partner and adventure buddy. Flávio, Samuel, Frederico, Luís, Matthias and the rest of the Portuguese birding community, making me feel like the only thing I have missed out while being away were 'just' lifers. And the AVESDOMUNDOPT crew: Gonçalo, João, Paulo and José, which have been unmatched partners in this project for the last 2 years of my PhD.

After almost 4 pages, in which I surely forgot people to thank, comes the part where I could spend at the very least 4 pages more. My family. Mom Luísa and Dad Jorge, my heroes, which taught me to think and to question, taught me humanity and taught me joy. My sister Joana, for showing me how to stay true to myself and being the other side to my soul. Sofia, the purest being to ever wander the Earth. My grandma São, for teaching me infinite love and strength. My late grandparents which I lost during this journey: Avô António, Avô Nicolau and Avó Maria, which I will forever bring inside me at all times. And my new family. Zaula and Roberto, for accepting me as their own son and showing me unconditional kindness through their souls. Finally, Jennifer, my team mate, who believes



---

in me even when I cannot, knows all the corners of my brain and teaches me bravery every single day.

Four years have passed by in the blink of an eye. Somehow, cold, arctic winds and overcast have become the norm, replacing my familiar warm, Atlantic breeze and sunny clear skies. What now feels normal was not for a long time, and it took a lot of people to get me to where I am. To all of you a sincere thank you.



## List of publications

### Paper I

Nicolau, P. G.; Sørbye, S. H.; Yoccoz, N. G. (2020). **Incorporating capture heterogeneity in the estimation of autoregressive coefficients of animal population dynamics using capture-recapture data**, *Ecol. Evol.*, 10 (23), 12710–12726. doi: 10.1111/jav.02646.

### Paper II

\*Kleiven, E. F.; \*Nicolau, P. G.; Sørbye, S. H.; Aars, J.; Yoccoz, N. G.; Ims, R. A., **Using camera traps to study population dynamics of small rodents**. \*These authors contributed equally to this work. Manuscript.

### Paper III

Nicolau, P. G.; S. H. Sørbye; Ims, R. A.; Yoccoz, N. G., **Seasonality, density dependence and spatial population synchrony**. Pre-print at arXiv.org. doi: 10.48550/arXiv.2203.16118.

### Other publications

Sørbye, S. H.; Nicolau, P. G.; Rue, H. (2021). **Finite-sample properties of estimators for first and second order autoregressive processes**, *Stat. Inference Stoch. Process.* doi: 10.1007/s11203-021-09262-4.

Nicolau, P. G.; Burgess, M. D.; Marques, T. A.; Baillie, S. R.; Moran, N. J.; Leech, D. I.; Johnston, A. (2021). **Latitudinal variation in arrival and breeding phenology of the pied flycatcher *Ficedula hypoleuca* using large-scale citizen science data**, *J. Avian Biol.*, 52 (2). doi: 10.1111/jav.02646.

# Contents

Abstract	i
Acknowledgments	iii
List of publications	ix
Other publications	ix
Chapter 1. Introduction	1
1.1. State of the Arctic	1
1.2. The COAT Project	1
1.2.1. Ecological role of small rodents	3
1.3. Aims of the Thesis	4
1.4. Outline	5
Chapter 2. Monitoring Methods for Small Rodents	7
2.1. Capture-recapture	7
2.1.1. Closed populations	8
2.1.2. Discrete-time capture-recapture models	8
2.2. Camera traps	12
2.2.1. Tunnel-based camera traps	13
Chapter 3. Population Dynamics of Boreal Rodents	15
3.1. Population processes	15
3.1.1. Density-dependence	16
3.1.2. Seasonality	18
3.2. Spatial population synchrony	19
3.2.1. Extending the Moran Effect	19
3.2.2. Measuring spatial synchrony	20
3.2.3. Investigating the causes of synchrony	21
3.2.4. Climate change and population synchrony	22

---

Chapter 4. Summary of Papers	23
Paper 1 – Accounting for capture heterogeneity in the estimation of density-dependence	23
Paper 2 – Tunnel-based camera traps as an alternative to capture-recapture in estimating vole abundance	28
Paper 3 – Seasonality and Population Synchrony	33
Chapter 5. Discussion	37
Chapter 6. Future Outlook	41
Closing Note	43
Bibliography	45
Paper I	59
Paper II	93
Paper III	137



## CHAPTER 1

# Introduction

### 1.1 State of the Arctic

The Arctic is changing. This statement hardly surprises anyone, as we are constantly reminded of it through the media, documentaries and political figures. Climate change has brought the entire world under severe stress, but no other region has been subjected to more challenges (Corell, 2006). The Arctic region, composed of tundra and transitional boreal forest habitat (Sirois, 1992), has picked the interest of scientists for centuries. It is an environment of extremes, in terms of its climate, its range of habitats, as well as the life cycles which both fauna and flora have had to develop in order to thrive. The Arctic has always impressed due to its resilience, with its tight communities evolving together to withstand the environmental variability and unpredictability over eons (Bliss, 1991). But, more than any other, Arctic ecosystems are most vulnerable to disturbance. Adding to the already extensive direct anthropogenic disturbances, climate change has brought new tests which might simply prove too difficult for Arctic communities to overcome (Malhi et al., 2020). The amplified temperature rise is having numerous repercussions such as thawing permafrost, changes in snow conditions, reduced sea ice extent, intensification of the hydrological cycles, northwards migration of the tree line, mismatches in phenology and other worrying large-scale ecosystem impacts (Serreze and Barry, 2011; Box et al., 2019). To understand what might be done to mitigate this problem, we must first comprehend the current state to potentially predict what lies ahead.

### 1.2 The COAT Project

To help solve the Arctic state conundrum, the Climate ecological Observatory for the Arctic Tundra (COAT) was established in Norway. COAT is

a long-term, ecosystem-based research scheme which intends to clarify the current state of the arctic ecosystems, specifically the arctic tundra, as well as predict future effects of climate change (Ims et al., 2013b). COAT intends to provide a framework which goes all the way from ecological theory, passing through data collection, statistical analysis, outputting the research content to both the general public, as well as managers and decision-makers (e.g., Henden et al., 2020). This methodological framework is further linked to the COAT Tools project, funded by UiT, which specifically focuses on developing methods for efficient analysis of the ecological data collected within COAT.

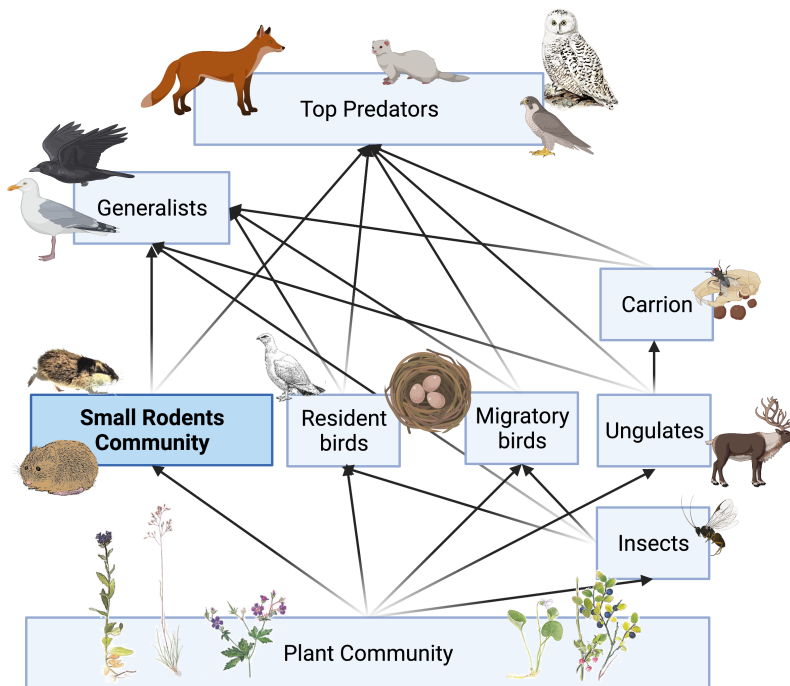


FIGURE 1.1. Illustrative example of simplified food web of Arctic tundra ecosystems, based on Ims et al. (2013b) and Mossberg et al. (2012). Created with BioRender.com



COAT is built on a food-web approach, monitoring the different components of the ecosystem chain from the bottom up (see Fig. 1.1 for a simplified version of the tundra food web). This approach is strongly founded on ecological theory, linking the different chains of the ecosystem to the climate and focusing on deriving prediction models. There are seven different modules contained within COAT, based on the food web: tundra-forest ecotone, tall shrub, small rodent, ungulate, ptarmigan, goose and arctic fox. This thesis will focus specifically on the small rodents module.

### 1.2.1 Ecological role of small rodents

Small rodents are one of the most abundant groups of mammals on the planet, which play particularly relevant functions in northern ecosystems (Ims and Fuglei, 2005). In addition to being linked to most elements of the food web, their ecological role is amplified due to their deeply marked population cycles. These abundance fluctuations are characterized by very high abundance peaks followed by large crashes, which have important and cascading effects into the ecosystem. Due to their high abundances, small rodents consume a larger amount of plant material than all the remaining herbivores in the tundra, with a key effect for the vegetation communities (Batzli et al., 1980). This impact on the vegetation directly affects nutrient turnover and species composition (Dahlgren et al., 2009). In addition, small rodents constitute prey for both specialist (e.g. owls and mustelids) and generalist predators (e.g. red fox), and so their fluctuations in abundance have a direct effect on their predators. Moreover, in peak years, the abundance of small rodents allows for other species, such as ground-nesting birds, to suffer from less predation by generalist predators, resulting in higher reproductive success (Ims et al., 2013a). In contrast, low rodent abundance years are associated with high predation for other species. In fact, it has been postulated that small rodent cycles may have played a role in shaping migration strategies of tundra-nesting birds (Gilg and Yoccoz, 2010). These aspects make rodent populations very good system predictors, as predicting change in rodent populations can shed a light on the degree of global change of the complete ecosystem (Ims et al., 2013a).

The rodent communities of northern Norway are dominated, in most

years, by gray-sided voles *Myodes rufocanus*. This corresponds to the microtine species with the largest amount of available data. This species has a boreal and low-Arctic distribution, ranging from Fennoscandia, through Siberia, all the way to Northeast Asia. They occupy a variety of habitats, in particular birch forests and dwarf-birch tundra (Kaneko et al., 1998; Ims et al., 2013b). In the winter, they highly favor the presence of bilberry to feed on (Dahlgren et al., 2007). Gray-sided voles are a short-lived multivoltine species, meaning they mature and reproduce fast, with 2-4 litters per season, being able to reproduce in the season in which they are born (Kaneko et al., 1998). The reproduction of this species happens essentially during the snow-free months, being typically between May and October in northern Norway. The breeding is influenced by population density, cycle phase, food conditions, as well as social hierarchy, in which age and size play a relevant role (Nakata, 1984). Another key component of arctic rodent communities is the Norwegian lemming *Lemmus lemmus*. This species has a more alpine distribution, whereas the gray-side vole dominates the northern sub-arctic/artic ecotone (Henttonen et al., 1992) which this thesis focuses on. In addition, due to its unpredictability and difficulty in trapping, the lemming is not here addressed.

### 1.3 Aims of the Thesis

This project is a part of COAT Tools, at the heart of statistical ecology. The general focus is improving statistical methods to better monitor and comprehend the population ecology of small rodent communities, linked to the tundra. It is important to note that most data which will be used in this thesis is not from actual tundra habitat, but rather collected in the sub-arctic boreal forest and tundra-forest transition area of northern Norway. This habitat, which corresponds to the largest vegetation transition on the planet, has a close relationship to the tundra and has been moving northwards with recent climatic warming (Hofgaard et al., 2012). In addition, the vole species, dynamics and monitoring methods are virtually identical to those of the actual tundra, but with the added benefit of the data being more practical to collect.

The specific aims of this thesis are described below.

- (1) Evaluate the importance of explicitly incorporating capture heterogeneity when estimating density-dependence parameters, which regulate the population processes of small rodents. In addition, evaluate biases in parameter estimation, as well as the conditions affecting it.
- (2) Develop a framework where both observed and unobserved heterogeneity from the capture process may be efficiently included in the estimation of abundance.
- (3) Establish a bridge between current gold standard monitoring methods and new data collection techniques. In particular, compare abundance metrics from the newly developed tunnel-based camera traps to those obtained from resource-intensive capture-recapture.
- (4) Devise a protocol to study spatial population synchrony in animal populations subjected to strong seasonal effects. This includes estimating the scale and strength of synchrony, partialing out the effects of the density-dependence structure and investigating possible meteorological drivers.

### 1.4 Outline

The research developed in this project is presented in this document which constitutes my thesis. This thesis is article-based, which means that it seeks to provide the relevant theory, summary of research and an overarching discussion of the research detailed in the manuscripts. The manuscripts, which have been either published or submitted to peer-reviewed field-relevant journals, and are appended at the end of this document. The chapters composing this thesis follow the structure outlined below.

The statistical and ecological theory which serves as the basis to understand the research is introduced in the chapters 2–3. Chapter 2 summarizes the two main field methodologies used to collect small rodent population data. The first methodology is capture-recapture, a well-known technique which provides information regarding the observation process error. The second is the recently developed tunnel-based camera trap method, tailored for the monitoring of small mammals using natural corridors. Both methods are introduced with respective features and challenges. Chapter 3 describes

the general topic of population dynamics of boreal rodents, focusing on two key aspects: density-dependent processes (with a focus on the importance of seasonality) and population synchrony. Chapter 4 summarizes and discusses the scientific research presented in the three individual manuscripts, complemented by three figures/schemes serving as graphical abstracts. Chapter 5 discusses and integrates the research outputs, contextualizing them into a bigger picture and the COAT project. Finally, chapter 6 provides a future outlook in the field, highlighting emerging lines of research and containing some final considerations, followed by the Bibliography and the appended papers.

## CHAPTER 2

# Monitoring Methods for Small Rodents

To monitor population dynamics of animals, it is important to obtain accurate estimates of abundance, which involves both collecting information on the number of animals (state of the populations), as well as information of the detectability of the animals (observation process). Due to being so elusive, monitoring small rodents typically requires actual trapping, either in the form of snap-trapping or capture-recapture. Snap-trapping results in the killing of animals for the single purpose of monitoring, which is highly unethical. Moreover, it does not provide much information on the observation process, i.e., regarding which animals are more likely to be captured (Kleiven et al., 2018). Therefore, traditional capture-recapture (often referred to as capture-mark-recapture; CMR) has become the most popular method to estimate the abundance of small mammals, considered to be the gold standard (Seber, 1986; Jareño et al., 2014). Nonetheless, a recent effort has been put into improving and optimizing other methods, such as camera traps. These allow for automated data collection in continuous time and already see widespread use in many groups of animals (Trolliet et al., 2014).

### 2.1 Capture-recapture

The traditional capture-recapture (CR) method for small rodents consists of setting up baited traps (with or without pre-baiting in preceding days), and re-checking the traps the following day(s) for any trapped animals. Trapped animals are then marked and released into the general population, which is subsequently re-sampled for as many days as the trapping experiment takes. The proportion of recaptured animals can then be used to estimate the population size (abundance). The longer the duration of the trapping experiment, the more precise the abundance estimation. More complex

methods, such as spatially explicit capture-recapture, allow further estimation of densities by making use of the animal locations in specialized grids (Efford, 2004; Romairone et al., 2018). Nevertheless, capture-recapture methods do not come without limitations, which include the unwanted animal mortality in the traps (Stephens and Anderson, 2014), trap saturation (Krebs et al., 2011), as well as providing low temporal resolution of the abundance estimates.

### 2.1.1 Closed populations

An important assumption when estimating population size and capture probabilities, is whether we are dealing with closed or open populations. In theory, most natural populations are open, subject to mortality/natality and dispersal/immigration. In practice, however, if we define short temporal intervals in a population, we may consider those effects to be negligible and we may assume closed populations. This assumption offers a number of practical advantages, such as being simpler, easier to implement, and requiring less resource-intensive data to estimate population parameters (Young and Young, 1998; Chao, 2001). Due to the relatively short life cycles of small rodents and the difficulties of long-term monitoring, monitoring methods are often short in time (2–3 trapping days for the data used in this thesis). This makes the populations fairly constant at the time of sampling, with (assumed) negligible losses in terms of survival and dispersal, as well as no additions in terms of births and immigration. With these aspects in mind, the closed population assumption becomes reasonable.

### 2.1.2 Discrete-time capture-recapture models

To monitor populations, we typically resort to a measure of the population state, abundance, which we want to estimate. Given a population of  $N$  independent individuals, indexed by  $i = 1, \dots, N$ , we perform a capture-recapture experiment with  $\tau$  sampling events. We can define the presence and absence of each individual with  $\{0, 1\}$ , and the capture histories can be expressed in a matrix with dimension  $N \times \tau$ , where each row corresponds to the capture history of a single individual. The number of rows with only zeros corresponds to the number of individuals which are never captured. A simplistic model may assume that all animals have equal probability of

being trapped, which remains constant over the  $\tau$  sampling events. However, dependence among samples may arise from two main sources: local dependence within each animal, i.e, a previous capture event may impact the probability of a following capture event, provoking trap-happy and trap-shy effects; and heterogeneous capture probabilities between different animals (Chao, 2001). This dependency among samples leads to significant bias of estimators assuming independence, such as the well-known and intuitive Lincoln-Peterson (LP) estimator (see Fig. 2.1). In this case, if the recapture rate increases after the first marking session, the LP-estimator will underestimate the number of animals present, and vice-versa.

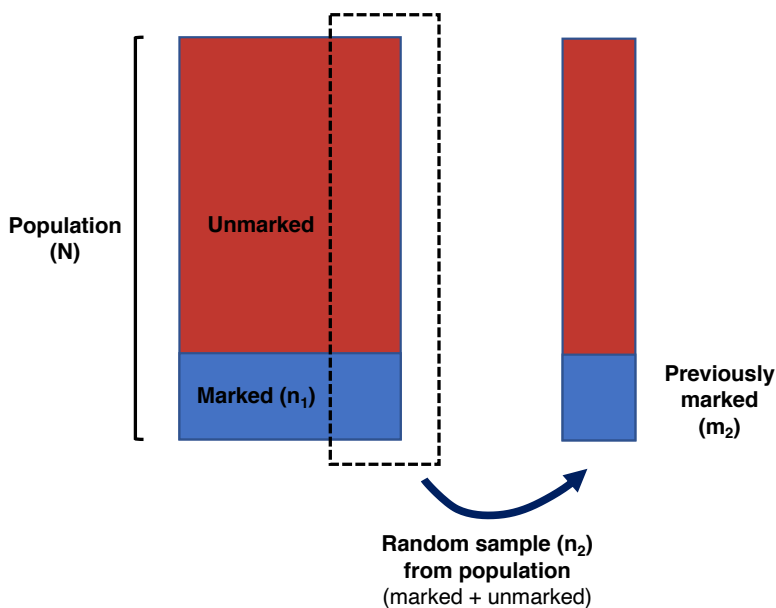


FIGURE 2.1. Logic behind the Lincoln-Peterson estimator. We mark a part of the initial population, which becomes composed by marked and unmarked individuals. The proportion of marked individuals is here  $n_1/N$ . By random sampling from that population, we estimate the total number of individuals using the proportion of marked ones in the new sample ( $m_2/n_2$ ). The Lincoln-Peterson estimator is then defined by  $\hat{N}_P = n_1 n_2 / m_2$ . Inspired by Powell and Gale (2015).

A variety of models have been proposed to overcome sample-dependency, with the famous model framework proposed by Otis et al. (1978) having taken central stage in literature (Huggins and Hwang, 2011; King and McCrea, 2019). Otis et al. (1978) addressed three main sources of variation in the capture probabilities:

- (1) temporal heterogeneity, in which probabilities can change with time, as a consequence of natural changes between different trapping events, such as weather or disturbance (Model  $M_t$ );
- (2) behavioral heterogeneity, in which the previous trapping of an individual can alter its future behavior, and therefore change its capture probability (Model  $M_b$ );
- (3) individual heterogeneity, in which different individuals have different probabilities of being captured, possibly affected by other variables (Model  $M_h$ ).

These three main factors constitute the basic foundation of variation in capturability, and each can be combined with each other to obtain the models denoted by  $M_{tb}$ ,  $M_{th}$ ,  $M_{bh}$  and  $M_{tbh}$ . The model which assumes constant probabilities is referred to as  $M_0$ . Many different models and frameworks have been developed over the years to model capture heterogeneity, and there is extensive literature on how to handle it. For a comprehensive review of multistate, random-effect and finite-mixture capture-recapture models, see Gimenez et al. (2017). Huggins and Hwang (2011) provided a review on the conditional likelihood framework to model capture heterogeneity in closed populations, which this thesis makes use of, particularizing on the cases where heterogeneity can be modeled from covariates.

The general conditional likelihood problem can be summarized as follows. Assume a closed population with  $N$  individuals, for which a capture-recapture experiment is conducted over  $\tau$  capture sessions. Let  $\mathbf{y}'_i = (y_{i1}, \dots, y_{i\tau})$  denote the capture history for each individual  $i = 1, \dots, n$ . Here,  $y_{ij} \sim \text{Bernoulli}(p_{ij})$ , for individual  $i$  and capture session  $j = 1, \dots, \tau$ , where 1 denotes a capture and 0 denotes an absence. This implies that  $2^\tau - 1$  possible capture histories can be observed for the captured individuals. All the  $i = n + 1, \dots, N$  individuals with capture history  $\mathbf{y}_0 = (0, \dots, 0)$  are never observed. If we assume independence between individuals, the complete



likelihood is

$$\begin{aligned}
 L(N, \{p_{ij}\} | \{y_{ij}\}) &= \prod_{i=1}^N \prod_{j=1}^{\tau} p_{ij}^{y_{ij}} (1 - p_{ij})^{1-y_{ij}} \\
 &= \left\{ \prod_{i=1}^n \prod_{j=1}^{\tau} p_{ij}^{y_{ij}} (1 - p_{ij})^{1-y_{ij}} \right\} \left\{ \prod_{i=n+1}^N \prod_{j=1}^{\tau} (1 - p_{ij}) \right\}
 \end{aligned}
 \tag{2.1}$$

The computation of this likelihood is analytically intractable as it depends on the unknown population size  $N$  (Huggins and Hwang, 2011; Yee et al., 2015). A conditional likelihood can however be obtained and maximized, based on the individuals captured at least once. It is then possible to estimate the set of capture probabilities  $\{p_{ij}\}$  by making some assumptions regarding the observation process. As an example, I will particularize on the case of a capture history over  $\tau = 2$  capture days, for the case where the capture process can be described using model  $M_{th}$ . This implies that each individual is assumed to have an independent probability of being captured on day 1 ( $p_1$ ) and day 2 ( $p_2$ ), according to Table 1.

TABLE 1. Capture history probabilities according to temporal heterogeneity model  $M_{th}$ .

Capture History	Day 1	Day 2	Probability
"11"	$p_1$	$p_2$	$p_{11} = p_1 p_2$
"01"	$1 - p_1$	$p_2$	$p_{01} = (1 - p_1) p_2$
"10"	$p_1$	$1 - p_2$	$p_{10} = p_1 (1 - p_2)$
"00"	$1 - p_1$	$1 - p_2$	$p_{00} = (1 - p_1)(1 - p_2)$

Assuming independence, the probability of obtaining a given capture history for an individual will correspond to the product of the capture probabilities on each day, described by the sets of probabilities  $\{p_{11}, p_{01}, p_{10}, p_{00}\}$ . The vector for the observable capture histories will then have a multinomial distribution with three categories. The success probabilities for these categories are defined by

$$p_{11}^* = \frac{p_{11}}{1 - p_{00}}, \quad p_{01}^* = \frac{p_{01}}{1 - p_{00}}, \quad p_{10}^* = \frac{p_{10}}{1 - p_{00}},$$

ensuring that the probabilities sum to 1. These probabilities can then be estimated for each individual by fitting a multinomial regression model to the observed capture history data, in which the predictor is a function of individual covariates (observed heterogeneity) and/or random effects (unobserved heterogeneity). Under  $M_{th}$ , this gives the equations

$$\frac{\frac{p_1 p_2}{1 - p_{00}}}{p_1(1 - p_2)} = \frac{\widehat{p_{11}^*}}{\widehat{p_{10}^*}} \Leftrightarrow p_2 = \frac{\widehat{p_{11}^*}}{\widehat{p_{10}^*} + \widehat{p_{11}^*}} \quad (2.2)$$

$$\frac{\frac{p_1 p_2}{1 - p_{00}}}{(1 - p_1)p_2} = \frac{\widehat{p_{11}^*}}{\widehat{p_{01}^*}} \Leftrightarrow p_1 = \frac{\widehat{p_{11}^*}}{\widehat{p_{01}^*} + \widehat{p_{11}^*}} \quad (2.3)$$

This gives estimates for the individual capture probabilities on day 1 ( $\widehat{p_{i,1}}$ ) and day 2 ( $\widehat{p_{i,2}}$ ), for all individuals  $i = 1, \dots, n$ . We can then use these probabilities to obtain  $\hat{N}$ , using an empirical estimator such as the Horvitz-Thompson estimator (Horvitz and Thompson, 1952)

$$\hat{N} = \sum_{i=1}^n (1 - \widehat{p_{i,0}})^{-1}, \quad (2.4)$$

where  $\widehat{p_{i,0}} = (1 - \widehat{p_{i,1}})(1 - \widehat{p_{i,2}})$ , corresponding to the estimated probability that individual  $i$  is captured at least once.

## 2.2 Camera traps

In recent times, camera traps have become increasingly predominant as ecological monitoring tools. They are particularly appealing to ecologists as they provide mostly non-invasive and cost-efficient monitoring. In comparison, the capture-recapture methods require a lot of manual and specialized labor, more resources (including time), and are notoriously more invasive (Wearn and Glover-Kapfer, 2019). The use of camera traps to monitor rodents has so far been limited, with much of the camera traps methodologies being dedicated to larger mammals, such as large carnivores (Burton et al., 2015). Nonetheless, camera traps have a large potential for small rodents

monitoring (Rendall et al., 2014; Palencia et al., 2021), and their use has been increasing (Soininen et al., 2015; Villette et al., 2015; Littlewood et al., 2021; Mölle et al., 2021). Still, given that no direct detectability measure has been developed for camera trap methods where there are no distinguishable individual markings (like most small mammals), they require further studies to assess their reliability (Gilbert et al., 2021). Nonetheless, for many species, camera traps are outright the best methods because they are actually capable of detecting them and otherwise they would simply not be sampled (Boonstra and Krebs, 1978; Jensen et al., 1993), such as lemmings or small mustelids like stoats (Möller et al., 2021). Furthermore, camera traps provide much better temporal resolution, allowing to sample year-round even in harsh weather and field conditions which prevent the use of other standard methods, unlocking a new world of data for several species. An increase in the spatial resolution is also a further possibility, as it is easier to cover larger spatial extents with camera traps (Soininen et al., 2015).

### 2.2.1 Tunnel-based camera traps

In the specific case of boreal rodents, one of the largest barriers has always been the presence of snow for most of the year. Camera traps circumvent this by automated collection in remote locations. Soininen et al. (2015) developed a tunnel-based camera trap methodology to monitor small rodents. These consist of metal devices simulating natural cavities, placed in natural corridors that small mammals use. A camera with an infra-red sensor is then placed at the top of the tunnel (Fig. 2.2), which is triggered by the passage of animals with 1 minute spaced intervals. This methodology and others alike allow for the monitoring of the presence of several species, particularly useful to monitor subnivean communities. However, unlike other camera trap methods developed for large mammals, it does not allow for the estimation of animal density using area and animal movement information (Rowcliffe et al., 2008; Nakashima et al., 2017).

Annotation of the photos can then be performed manually by specialized ecologists, or by recently developed pattern recognition algorithms, although their performance is dependent on the existence of well annotated data sets (Tabak et al., 2019). One handicap from using this methodology is the

fact that they require expertise in the placement of the cameras, as well as being of restricted use in areas subject to flooding and other environmental factors. Spatial replication may help circumvent this by helping to cover a large area and therefore being less subject to the biases caused by the animals' space use, including local changes in space use through time.

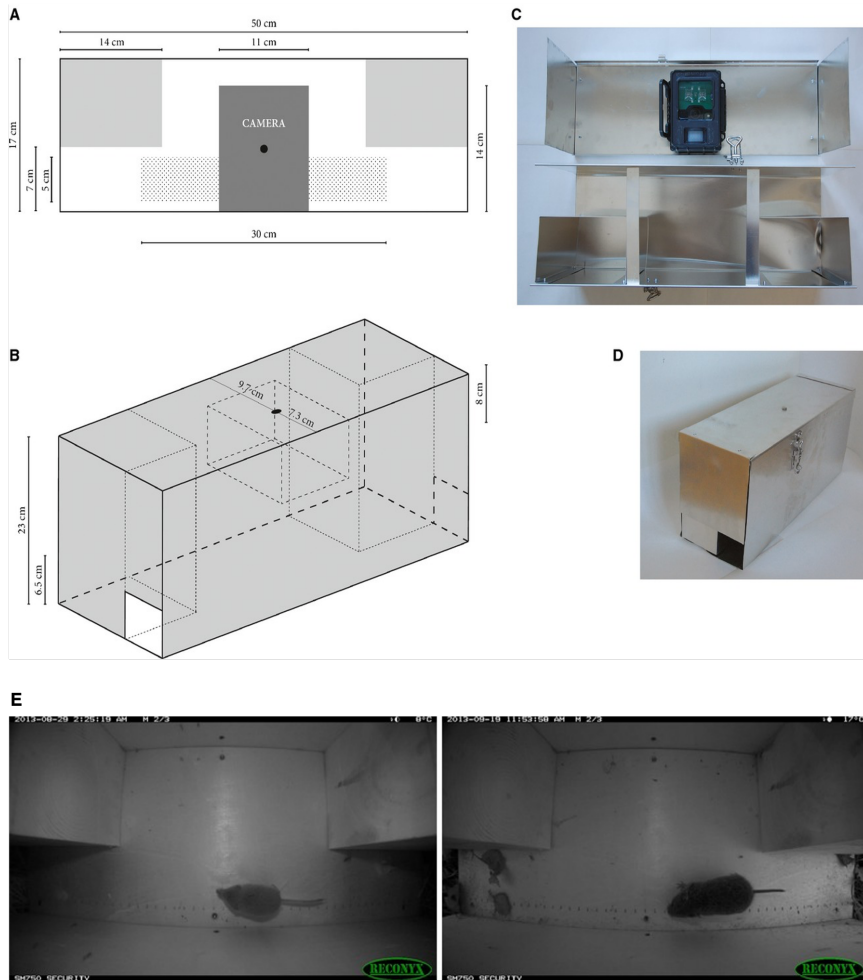


FIGURE 2.2. Example of tunnel-based camera traps for small mammals. Panels A–B display dimensions, C–D show internal and external appearance, and E shows two images of small mammals photographed while crossing the tunnel. Composite of Figs. 1–2 in Soininen et al. (2015). Used in agreement with publisher (John Wiley and Sons).

## CHAPTER 3

# Population Dynamics of Boreal Rodents

Many rodent species display marked fluctuations in their abundances, including both seasonal fluctuations and multi-annual fluctuations. These cycles have raised the interest of scientists for almost one hundred years (starting with Elton, 1924), and both the existence of such cycles, as well as their causes, have been amply studied and discussed (Stenseth, 1999; Krebs, 2013). The role of small rodents in boreal environments is thus tightly linked to these population cycles, which act as spatio-temporal pacemakers for ecosystem processes (Korpela et al., 2013). Understanding the drivers of these population processes therefore holds generalized importance, beyond the local scale of these ecosystems.

### 3.1 Population processes

The population processes of small rodents have two main components, a multi-annual and a multi-seasonal. The seasonal component is widespread across many rodent populations and species but, in Fennoscandia, latitude plays a major role. Multi-annual fluctuations arise generally only above 60°N (Hansson and Henttonen, 1988; Hanski et al., 1991). These cycles are propelled by the interaction between density-dependence, as well as the stochasticity and seasonality of the environment (Stenseth, 1999). They are remarkable due to their regularity, i.e., their relatively fixed period, and their variation in amplitude – with densities increasing up to 2-3 magnitude orders from the low phase to the peak (Andreassen et al., 2021) – with deep cascading effects into the ecosystem. These cycles have an intrinsic effect into the small rodent ecology, with prominent changes in body mass, social behavior, age distributions, sexual maturation, survival and growth rates (Oli, 2019).

### 3.1.1 Density-dependence

The concept of density-dependence in ecology refers to the regulation of population growth by the number of individuals in a population (Hixon and Johnson, 2006). In general, at lower densities, most individuals are likely to be able to meet their resource needs. However, at very high densities, there is an increase in competition, predation, food depletion and disease spread, leading to the decrease of population growth rates. Density-dependence is thus tightly linked to the carrying capacity of the environment (often known as  $K$ , signaling the population size at which the multiplicative growth rate reaches 1). Essentially, it corresponds to a mechanism which may allow for populations to maintain long-term stable cycles, depending on the strength and delays of the density-dependence.

The most common way of estimating density-dependence in ecological studies has been through the use of autoregressive models (Slade, 1977; Lande et al., 2002; Thorson et al., 2015). An autoregressive model is denoted as  $\text{AR}(p)$ , where  $p$  indicates the order of the model and is defined by

$$X_t = c + \sum_{i=1}^p \phi_i X_{t-i} + \epsilon_t \quad , \quad t = 1, \dots, T. \quad (3.1)$$

The variable  $X_t$  corresponds to abundance at time  $t$  modeled in the log scale,  $\phi_1, \dots, \phi_p$  are the autoregressive coefficients,  $c$  is a constant, and  $\epsilon_t$  represents white noise. It is important to note that linear autoregressive models evidently correspond to an approximation of reality, and come with the important assumption of linearity. Still, linear models are easily interpretable, which is a great advantage in comparison with non-linear models when it comes to studying the properties of the cycles, as well as its causes.

In ecology, the standard  $\text{AR}(1)$  and  $\text{AR}(2)$  models are generally the most popular when it comes to estimating density-dependence. The  $\text{AR}(1)$  model, often known as the Gompertz model, has had widespread use to estimate density-dependence, fitting well within state-space model frameworks (Dennis et al., 2006; Lebreton and Gimenez, 2012; Thorson et al., 2015). However,  $\text{AR}(1)$  models only relate to direct density-dependence, where the population state at time  $t$  given the population state at time  $t-1$  is assumed conditionally independent of previous states. While this model

has a number of advantages, it typically refers to irregular fluctuations, regulated by density-independent factors (Stenseth et al., 2003), and is thus not always adequate. If large amplitude fluctuating cycles are of concern, then delayed regulation is generally present and the order of the autoregressive process should be increased, having  $p \geq 2$  (Korpela et al., 2014). Certain rodent species, such as the gray-sided vole, have empirically been shown to display population cycles well approximated by a linear AR(2) process for the log-abundance  $X_t$  (Bjørnstad et al., 1995):

$$X_t = c + \phi_1 X_{t-1} + \phi_2 X_{t-2} + \epsilon_t. \quad (3.2)$$

This is a special case of 3.2, where  $\phi_1$  can be interpreted as the annual direct density-dependence (often measured in the fall),  $\phi_2$  as the annual delayed density dependence, and  $\epsilon_t$  is related to environmental stochasticity (see Fig. 3.1 for the parameter space where the model is stationary).

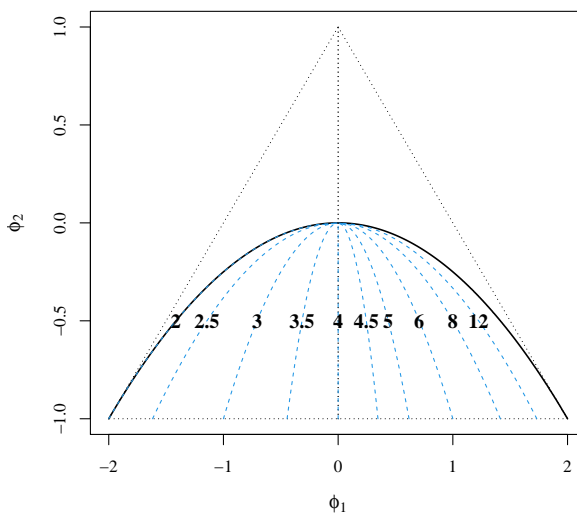


FIGURE 3.1. Parameter space of the AR(2) coefficients for stationary processes, contained inside the dotted triangle.  $\phi_1$  and  $\phi_2$  correspond to the direct and delayed density-dependence, respectively. Pairs of the parameters being below the bold semi-circle correspond to cyclic dynamics (pseudo-periodic behavior) with the period given by the number in the middle of the blue dashed lines. The pseudo-periodic area is given by  $\phi_1^2 + (1 - \phi_2)^2 + 4\phi_2^2 < 0$ .

The AR(2) model can be further interpreted as a trophic interaction model, where the direct density-dependence will correspond to the effect of the vole abundance in the previous season, and the delayed density-dependence corresponds to a predator/food source, regulated by the number of voles two seasons before (Agrell et al., 1995; Stenseth, 1999). In the particular case of rodent cycles, Stenseth et al. (1998) empirically investigated the presence of non-linearity by resorting to threshold autoregressive models (TAR), allowing for phase-dependency in the cycles, i.e., for the density-dependence coefficients to vary with density. Their empirical study revealed a degree of non-linearity on the direct density-dependence coefficient, which appeared to be affected by the phase of the growth cycle. However, the delayed density-dependence, responsible for regulating the periodicity, was revealed to be approximately linear. This reinforces the notion that linear AR(2) models may be used to analyze population regulation processes of microtines.

### 3.1.2 Seasonality

Northern ecosystems are subject to strong seasonal effects which have a deep impact on the population dynamics of all present species. Essentially, the two main seasons constitute two distinct life cycle events, subject to different effects on population growth, alternating between two modes. Winter is linked to survival, with mostly only negative population growth due to the practically negligible reproduction. Summer is linked to reproduction, where the population growth will be a product of the reproduction rates and the survival of the young, adding to survival of the overwintered (Stenseth et al., 1998). For voles, it has been suggested that the multi-annual periodicity may be in fact associated to the duration of the winter season (Hansson and Henttonen, 1985; Stenseth et al., 2002), which can help produce long term cycles and stability (but see Rodríguez-Pastor et al., 2018; Cornulier et al., 2013 for additional contributing factors). However, even though seasonality plays a major role in small rodent cycles, it has historically been insufficiently addressed, a consequence of the limitations of field data collection, particularly in the harsh winters (Stenseth, 1999). For that reason, seasonal models treating the different seasons separately are important to fully understand the sources of density-dependence (Stenseth et al., 2003;



Fauteux et al., 2021). Hansen et al. (1999) proposed modeling the population cycles using bivariate linear autoregressive models, treating spring and fall log-abundances independently:

$$X_t = \beta_1 Y_{t-1} + \beta_2 X_{t-1} + \beta_3 Y_{t-2} + \beta_4 X_{t-2} + \epsilon_t \quad (3.3)$$

$$Y_t = \eta_1 X_t + \eta_2 Y_{t-1} + \eta_3 X_{t-1} + \eta_4 Y_{t-2} + \omega_t. \quad (3.4)$$

The parameters  $\boldsymbol{\beta} = (\beta_1, \dots, \beta_4)$  and  $\boldsymbol{\eta} = (\eta_1, \dots, \eta_4)$  correspond to the seasonal autoregressive coefficients associated with predicting either spring log-abundance  $X_t$ , or fall log-abundance  $Y_t$ , respectively. The series  $\epsilon_t$  and  $\omega_t$  are white noise terms. This model can easily be written in terms of predicting seasonal growth rates, using response variables  $X_t - Y_{t-1}$  for winter growth rates in (3.3), and  $Y_t - X_t$  for summer growth rates in (3.4).

### 3.2 Spatial population synchrony

Population synchrony is defined as the simultaneous changes in the fluctuations of different populations across space (Liebhold et al., 2004; Hansen et al., 2020). Synchrony typically refers to abundance, but several other population features, such as reproduction/mortality, mean size or age distribution, can be spatially correlated. It is a phenomenon widely present in many animal and plant populations, with greatly varying patterns (Koenig, 1999), and it can even occur between different species. Studying synchrony reveals different important aspects of populations, including regulating factors and population/community structure. Three key processes are typically associated with the presence of spatial synchrony. First, dispersal, acting by coupling locally regulated populations (Ripa, 2000). Second, community processes and trophic interactions, which may include (nomadic) predators (Ims and Andreassen, 2000), competition (Ulrich et al., 2019), or parasites (Vogwill et al., 2009). And finally, density-independent environmental (abiotic) factors, such as the climate (Bjørnstad et al., 1999a; Allstadt et al., 2015).

#### 3.2.1 Extending the Moran Effect

The environmental stochasticity effect has taken center stage when it comes to studying synchrony, starting back in 1953. The landmark study by Pat Moran (Moran, 1953) presented a model linking local weather conditions

and the cycles of two separate populations, in what is now amply referred to as the "Moran effect" (Hansen et al., 2020). Moran (1953) ascertained that the dynamics of different populations having the same intrinsic density dependence structure and subject to the same effects of the environment, should showcase the same synchrony in their populations as they do in their environment. This means that the cause of synchrony can be completely independent from the mechanisms regulating the population cycles. As an example, if the cycles of two populations  $X_t^{(1)}$  and  $X_t^{(2)}$  are given by identical coefficients  $\phi_1$  and  $\phi_2$  in 3.2, then

$$\text{Cor}(X_t^{(1)}, X_t^{(2)}) = \text{Cor}(\epsilon_t^{(1)}, \epsilon_t^{(2)}). \quad (3.5)$$

This theorem follows strict assumptions, including log-linear density dependence, identical population processes between populations, and no dispersal/migration. However, the strict assumptions of the Moran theorem are rarely fulfilled in nature. This has led to some necessary extensions to account for exceptions, such as non-linear density regulation (Engen and Sæther, 2005; Royama, 2005) and spatially heterogeneous dynamics (Hugueny, 2006). Hence, the term 'generalized Moran effect' has been coined to denote the general synchronizing effect of correlated environments on population cycles (Hansen et al., 2020).

### 3.2.2 Measuring spatial synchrony

The occurrence of spatial synchrony is often noticeable simply by visually inspecting population time series, which was the initial method to assess synchrony before formal statistical analyses were developed (Liebhold et al., 2004). To quantitatively assess spatial synchrony, a measure of association between different time series observed at different spatial locations must be employed. A common choice is to use Pearson's correlation coefficient to measure the linear association between two series, which is easily interpretable. Assessing spatial synchrony by correlations carries two relevant problems, including long-term trends and temporal autocorrelation. Long-term trends may cause the patterns of synchrony to be obfuscated in short-term analysis. This may be solved using a de-trending technique, such as using the growth rates of the series (Buonaccorsi et al., 2001). The presence of temporal autocorrelation violates the assumption of independence among

samples when conducting inference on correlations. A solution for this is fitting an adequate model, in particular an autoregressive model (also called "pre-whitening") (Liebhold et al., 2004), especially relevant when working with density-dependent population processes. We can then use the correlations between the model residuals from the different spatial locations as our measure for population synchrony. To further study spatial synchrony at a broad spatial scale, i.e. to assess the scale, shape or geography of synchrony, we can model synchrony as a function of distance. A number of different methods have been employed for this purpose, in particular variations of the Mantel correlogram (e.g., Bjørnstad et al., 1999a; Bjørnstad et al., 1999b; Gouhier and Guichard, 2014; Gouveia et al., 2015; Turkia et al., 2020).

### 3.2.3 Investigating the causes of synchrony

While measuring synchrony holds intrinsic value in defining population units (i.e. meta-populations), one of the main research interest in studying synchrony comes from understanding its causes. A particular problem in this case corresponds to the inability of fully separating the different variables contributing to it, and no single factor is generally responsible for driving population synchrony (Liebhold et al., 2004; Vogwill et al., 2009). Dispersal has been postulated as one of the key factors driving large scale synchrony, even when acting at a local scale, and has been thoroughly investigated using different autoregressive/nonlinear models (Abbott, 2011). However, the role of intra-specific dispersal in synchronizing populations has been deemed limited, as it may not hold the stabilizing power to maintain large scale synchrony (Briggs and Hoopes, 2004; Wall et al., 2013; Zhang et al., 2015). As a consequence of the limitations of dispersal for large-scale synchrony, attention has been drawn to a number of external drivers, both biotic and abiotic, as a mean to synchronize populations. To investigate the effect of the environment on synchronizing populations, population synchrony can be often modeled as a function of the spatial correlations in other variables, such as the weather (e.g Post and Forchhammer, 2004) or predator breeding performance (e.g Fay et al., 2020).

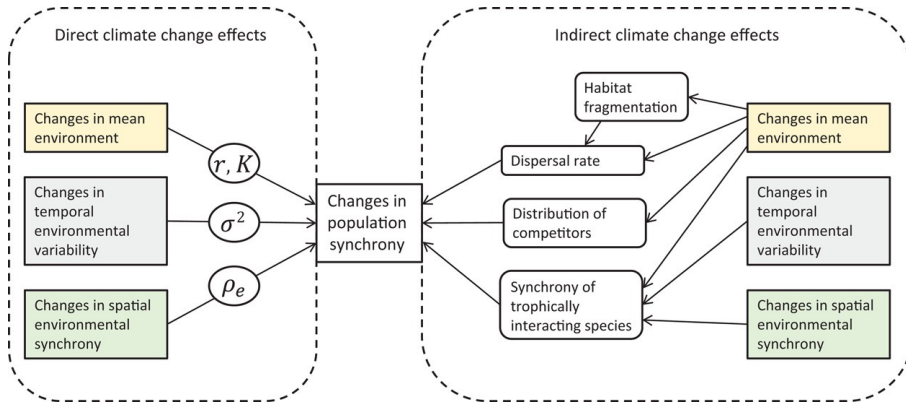


FIGURE 3.2. Effects of climate change on population synchrony. The parameters inside the circles are:  $r$ , growth rate;  $K$ , carrying capacity of the environment;  $\sigma^2$ , the environmental variance; and  $\rho_e$ , the correlation in the environment. Figure withdrawn from Hansen et al. (2020), used here under the Creative Commons CC BY license.

### 3.2.4 Climate change and population synchrony

Recent research has put emphasis on the implications of climate change on synchrony and the subsequent impact on the sustainability of populations (Sheppard et al., 2015; Koenig and Liebhold, 2016; Hansen et al., 2020). Fig. 3.2 describes the complex web of interactions between climate change and the consequences for population synchrony. In sum, climate change will lead to new normal states in the environment, with direct consequences to the growth rates and carrying capacity. Furthermore, changes in the environmental variability through time, as well changes in the spatial environmental synchrony, will likely alter population cycles. Indirectly, climate change may act as an enabler of habitat fragmentation, thus affecting dispersal rates, as well as changing competitor/predator distributions. Spatial population synchrony can greatly influence both the rate of extinction of certain species (Heino et al., 1997), as well as shape community dynamics (Haynes et al., 2009). Thus, studying the interplay between climate change and synchrony, particularly in Arctic ecosystems, may help reveal the challenges many populations are predicted to face, with direct implications for conservation and management.

## CHAPTER 4

### Summary of Papers

#### **Paper 1 – Accounting for capture heterogeneity in the estimation of density-dependence**

The importance of addressing the sampling uncertainty when estimating animal abundance has been a hot topic in research for several decades. In particular, the discussion around capture heterogeneity has remained lively up to this day, with numerous new extensions and approaches still being investigated (Gimenez et al., 2017; Herliansyah et al., 2022). Uncertainty in animal abundance estimates is a problem when seeking to estimate population parameters, such as density-dependence parameters (Yoccoz and Ims, 2004; Lebreton and Gimenez, 2012). However, it has been common practice to resort to simplistic models to describe the observation process – in fact disregarding capture heterogeneity. This has been done assuming either a homogeneous Poisson process (e.g. Stenseth et al., 2003), negative Binomial (e.g., Santin-Janin et al., 2014) or Log-normal distribution (e.g. Santin-Janin et al., 2014; Ono et al., 2019) for the observation model.

This first study had the following specific goals:

- (1) Develop a framework to analyze capture-recapture data for closed populations, combining both observed (via covariates) and unobserved heterogeneity (random effects) to estimate capture probabilities and abundance.
- (2) Assess the importance of accounting for capture heterogeneity when estimating population process parameters, specifically when estimating the density-dependence structure described by AR(2) models. Simultaneously, understand how the intrinsic AR(2) parameters may affect the estimation process.
- (3) Understand the effects of assuming a simple Poisson process when estimating the density-dependence, compared to either using an

explicit capture-recapture model or ignoring the observation error.

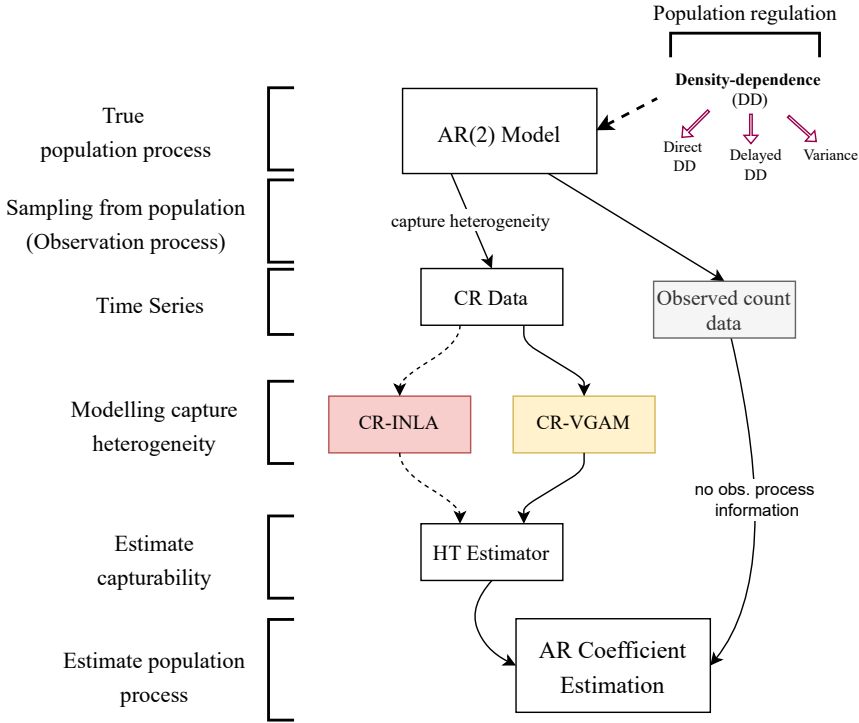


FIGURE 4.1. Schematic figure of the methodological setting for the simulation study of paper 1. The underlying process of this population is regulated by both direct and delayed density-dependence, according to an AR(2) process. Here, the goal is to estimate the true parameters of this population process to further understand the regulating mechanisms driving the population cycles. When sampling from this population, there is sampling error deriving from capture heterogeneity. This can be addressed using one of three different methods, with two methods incorporating capture-recapture information (CR-INLA and CR-VGAM), and one which disregards it (Observed counts). From the time series adjusted for detectability, is then possible to model the true population process and estimate the AR(2) parameters. Figure created with `draw.io`.

---

For these purposes, we implemented a simulation study based on real capture-recapture data of gray-sided voles in Northeast Norway. First, we generated a time series of length 20 simulating the true vole population process (in the log scale), regulated by both direct and delayed density-dependence. This process followed an AR(2) model, with varying coefficients  $\{\phi_1, \phi_2\}$ , and for different process variances  $\{\epsilon\}$  (equation 3.2). Second, we simulated the capture process with observed heterogeneity (model  $M_{th}$ ) in two days, where the capture probabilities depended on the effect of a single covariate. This allowed to obtain a given number of captured individuals at each trapping session, with associated capture histories. Finally, we estimated the AR(2) coefficients using three different approaches, as shown in Fig. 4.1:

- (1) The first method (CR-INLA) used the methodology of Integrated Nested Laplace Approximation (INLA) (Rue et al., 2017) to estimate the capture probabilities using the conditional likelihood approach (see section 2.1). INLA allows for the natural integration of both covariates and random effects in a computationally efficient Bayesian framework. Then, we used the Horvitz-Thompson (HT) estimator to estimate the log-abundance at each time point. Finally, we fitted AR(2) models to estimate the AR(2) coefficients using the log-abundance time series, now corrected for the observation process.
- (2) The second method (CR-VGAM) used the R-package VGAM (Yee et al., 2015) to estimate the capture probabilities. This method also uses the conditional likelihood approach but in a vectorial generalized additive model framework. This method does not allow for the modeling of random effects, but nonetheless provided a basis of comparison with the first method. After estimating the capture probabilities, we once again used the HT estimator to obtain the log-abundances, and then estimated back the AR(2) parameters.
- (3) For our final method, we simply used the simulated log-counts for each time point, ignoring the observation process, and directly estimated the AR(2) coefficients from the log-count time series.

Furthermore, we tested the assumption of a homogeneous observation model,

and repeated the process described above but modeling the log-abundances obtained through methods 1–3 as a Poisson process instead, before estimating the AR(2) coefficients.

From this simulation study, it was possible to better understand the role capture heterogeneity plays when seeking to estimate density-dependence. Overall, the approaches which modeled the observation process outperformed the method which disregarded it, as one would expect (Lebreton and Gimenez, 2012). However, the effects differed according to the AR(2) parameters themselves and the process variance. Overall, the estimation of the  $\{\phi_1, \phi_2\}$  coefficients was biased towards zero. This is a well-known phenomenon of estimating AR coefficients when using short time series, and can be corrected (Sørbye et al., 2021). In practice, this phenomenon translated into an underestimation of the strength of direct  $\phi_1$  and delayed  $\phi_2$  density-dependence, and an overestimation of the process variance of the AR(2) model.

The most relevant factor affecting parameter estimation appeared to be the process variance ( $\epsilon_t$ ). For lower values (below 0.16), there was a larger separation between methods, and it appeared more important to model capture heterogeneity. For high values of process variance, however, the differences in performance were only marginal. This suggests that in systems where the variations in amplitude are very pronounced, as is the case of vole cycles, the sampling error does not obfuscate the population patterns as much as in cases with low process variance. This could be explained by the fact that when the population process variance is high, the observation variance becomes only a minor component of the total variance, which happens in the context of the gray-sided vole. Other animal populations, particularly larger mammals, often show much smaller fluctuations in abundance. In addition, other systems have much larger observation errors (much lower detectability compared to these voles), which should be accounted for whenever possible.

When assuming a Poisson process, the estimation was generally worse (again, better seen for the low process variance simulations), with an overall larger bias. This occurred even when comparing simply the raw counts with those modeled directly as a Poisson process. There was also an associated larger uncertainty in the coefficient estimates, even if the coverage in



---

parameters was generally very high. This highlights a potential problem of assuming a homogeneous observation process which does not reflect capture heterogeneity, when this is present.

**Paper 2 – Tunnel-based camera traps as an alternative to capture-recapture in estimating vole abundance**

To monitor animal populations and be able to study their population dynamics, it is important to have sound estimates of abundance. In the previous paper, we focused on using capture-recapture data to estimate population parameters of interest. However, capture-recapture has several limitations, in particular due to being resource-intensive, requiring a lot of effort to deploy live traps and baiting on successive days. This limits the possibility of covering large areas, providing reduced spatial resolution, which can constrain the scope of the monitoring. For these reasons, automated camera-traps have become popular alternatives to standard capture-recapture to study a host of animal groups, particularly large mammals, and those which can be individually identified with distinctive features (Gilbert et al., 2021). However, for small animals that are often very difficult to detect, camera-traps have a very large potential which is only now starting to be realized. Camera traps provide a measure of activity, and it is not always clear whether the resulting activity indices are a good reflection of the population state (Jennelle et al., 2002). As such, calibration studies are required to ensure whether indices derived from camera traps can be considered sound indices for abundance.

For this paper, we used two case studies in boreal/sub-arctic biomes to assess the suitability of camera-trap indices to monitor populations of two small rodent species, the gray-sided vole and tundra vole (*Microtus oeconomus*). To perform this study, reliable abundance data and camera trap data collected at the same locations were required. The field methodology for our study consisted of placing a single tunnel-based camera trap (CT) in a grid of capture-recapture (CR) traps, at different spatial locations. The CR-based (log) abundances were corrected for the observation process using the CR-INLA method of paper 1, modeling capture history probabilities as a function of individual covariates *weight* and *sex*, and spatial random effects. For the CT-indices, we used the mean (log) number of photos of the given species, taken over different time windows of varying lengths, either encompassing or preceding the live trapping experiment period. Prior to performing calibration, we first assessed the linearity in the relationships

---

between the CT-indices and the CR-estimates (in the log-scale) using non-parametric smoothing models. Generally, the relationships proved to be approximately linear, and considering that linear models are easily interpretable and applicable, particularly in a calibration context, we decided to use them. The calibration analysis consisted of two main steps. First, the CT-indices of different time windows (exposure variables) were modeled as a function of the log CR-abundances (ground-truthing variable), resulting in a calibration line. The goodness-of-fit was assessed through the coefficient of determination ( $R^2$ ). The time window which maximized the  $R^2$  was considered optimal. Second, we performed inverse prediction optimal CT-index where we could assess the predictive capacities of the model (through k-fold cross validation) and obtain prediction intervals with correctly estimated uncertainty.

Our two case studies provided different results. The gray-sided vole calibration study contained 120 calibration points collected at 15 different spatial locations (scattered across 170 km in a straight line). The optimal calibration regression was achieved using the interval of 5 days (encompassing the live trap experiment days) and revealed an  $R^2 = 0.57$ . Moreover, the model was able to correctly predict the correct abundance phase (either low, intermediate or high) two thirds of the time. This can be taken as a successful calibration for different reasons. First, the  $R^2$  is roughly in line with those from other studies with similar species (Villette et al., 2015; Parsons et al., 2021). Moreover, our methodology differed from those studies, which used cameras pointing at single CMR-traps (checked every day), and performed a direct calibration between the animals photographed and captured. In contrast, our tunnel-based camera traps were not pointing directly any of the multiple CMR-traps, making it a more challenging task. In addition, there is bound to exist some confounding with the animals which get physically trapped and are not able to cross the camera traps and be recorded. Finally, we purposely excluded a spatial term from the regression models so that the calibration regressions could be generalizable to any new location. This means that we disregard the local variations of the different stations, as well as the different placements of the camera traps. These factors suggest that indeed the activity measures obtained from the cameras are able to provide a reliable image of the population state of gray-sided

voles.

The tundra vole study highlighted some of the challenges one might face with these studies. It consisted of 60 calibration points collected at 4 different spatial locations, located within  $1\text{km}^2$ . In this case, however, the calibration regressions were much worse, achieving an optimal  $R^2 = 0.21$  which corresponded to the day preceding the beginning of the live trapping. This poor calibration further resulted in a poor predictive performance, with higher bias compared to the gray-sided vole case, and only successfully predicting the abundance phase one third of the times. Different factors may help explain these results. On one hand, tundra voles are typically harder to catch and already required pre-baiting for the live traps, which may have an effect in the spatial distribution of the species. Moreover, this species has a much more heterogeneous use of space, with rapid home range shifts (Tast, 1966). This was evidenced by the lower and scattered correlations in the number of photos taken by the cameras in adjacent days when comparing with the gray-sided vole, in which the number of photos remained highly correlated for a long period. For the tundra vole, we additionally detected an effect of the animal entrapment on the calibration, as the days preceding the experiment exhibited higher goodness-of-fit than the experiment days, unlike what had occurred with the gray-sided vole. Due to these complications and given the close proximity of the trapping stations, we further performed a calibration analysis but taking the mean of all stations, effectively treating them as replicates of the same spatial location. With this setup, the  $R^2$  with the optimized temporal window rose to 0.81. This rise is likely linked to the smoothing out of the differences in space use of the different animals, highlighting the necessity of using actual camera trap replicates, in specific for unpredictable species such as the tundra vole.

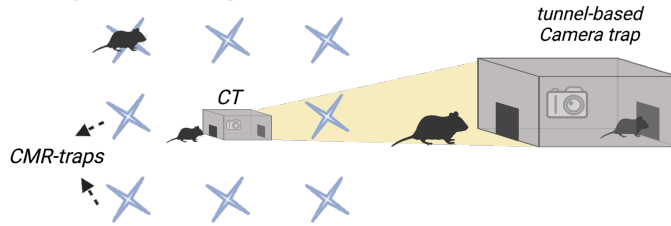
It is relevant to add that  $R^2$  is an imperfect measure, in particular because the ground-truthing abundance estimates are prone to error themselves, and do not correspond to the absolute true abundances – simply the closest to them we can get. Even in perfect scenarios, the  $R^2$  is not expected to be 1 when error is present in both variables. It has thus been recommended that such calibration studies are only conducted in good conditions, namely high capture probabilities (such as the case of the voles) and low sampling error (Gopalaswamy et al., 2015). Additionally, it is important

---

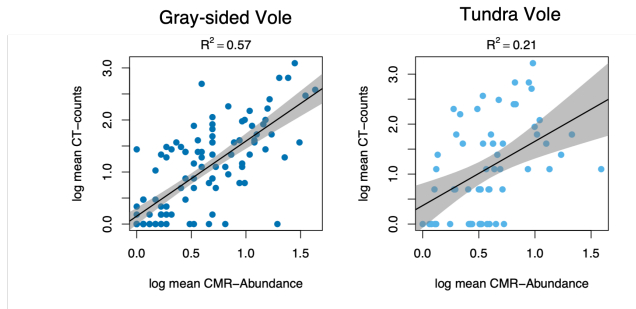
to take into account the observation process, which we did in this study by modeling the capture probabilities as a function of capture heterogeneity (Knape and de Valpine, 2011).

Overall, this study highlights the potential of tunnel-based camera traps as a monitoring method for small mammals. In addition to being able to reflect local vole abundances, camera traps have the added benefit of drastically increasing spatial (being relatively easy to spread out in space) and temporal resolution (collecting data continuously throughout the year). Furthermore, our cameras collected a lot more information on other species, such as shrews, lemmings and small mustelids, which are usually not adequately sampled (Möller et al., 2021). Still, performing calibration studies (when possible) remains important, as different species may use the space differently (Kolowski et al., 2021).

### 1. Live experiment setup



### 2. Calibration regression



### 3. Inverse Prediction

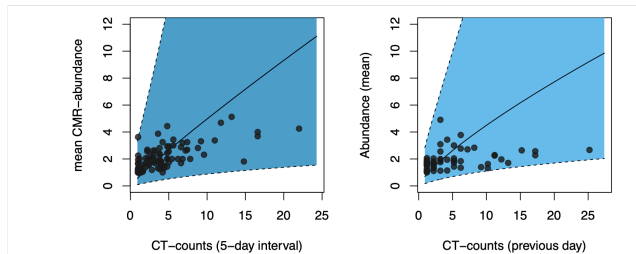


FIGURE 4.2. Schematic figure of the methodological setting of paper 2. A field study was developed to collect both capture-mark-recapture data and a single tunnel-based camera trap data of small rodents (panel 1; created with BioRender.com). This study was conducted for two species. Calibration was then performed using the number of photos obtained from the camera traps as the CT-index, calibrated as a function of abundance estimates from CMR (panel 2). Finally, we can use the CT-index to predict abundance (panel 3).

---

### Paper 3 – Seasonality and Population Synchrony

Spatial synchrony has been a widely studied phenomenon across different taxa and ecosystems, in a hope to achieve a better understanding of mechanisms driving ecological dynamics. The effect of the climate on population synchrony was formalized and popularized by Moran (1953), applied to populations of Canadian lynx, in a region with striking differences between winter and summer. Even though Moran himself recognized the importance of these seasonal differences, he was not able to account for seasonal density-dependence given the lynx time series were annual only. The so-called “Moran effect” has been subject to many extensions ever since, hoping to account for a number of exceptions not included in the original theorem specification, such as dispersal (Ripa, 2000), non-linear (Engen and Sæther, 2005) or spatially heterogeneous density-dependence (Hugueny, 2006). Nevertheless, the effect of seasonal-specific density-dependence has not been addressed in synchrony studies, even if seasonality has a well-known profound effect on many different systems (White and Hastings, 2020; Fauteux et al., 2021), on top of being greatly influenced by climate change (Xu et al., 2013).

For this study, we devised an analytical protocol to account for the contributions of season-specific density-dependence to the total observed spatial population synchrony, before estimating the effects of weather on driving the synchrony. We based and applied this framework to a population of gray-sided voles from Northeast Norway, known for its seasonal density-dependence and marked spatial synchrony (Hansen et al., 1999). This protocol and case study application are illustrated in Fig. 4.3, showing the main steps required to partial out different density-dependence contributions from the observed synchrony, and investigating ecologically relevant effects. The figure steps are structured as follows:

- (1) To analyze the spatial synchrony of Norwegian gray-sided vole populations, we set up a study in the Porsanger region of Norway, sampling from 19 stations along a climate/habitat gradient of 170 km. The different stations could be sorted into three distinct landscape/ecologically-defined regions: coastal ( $R_1$ ), fjord ( $R_2$ ) and inland forest ( $R_3$ ).
- (2) Seasonally-varying time series for log-abundance were obtained as

a result of the long-term study. These were corrected to account for the observation process using the method from paper 1. As it was impossible to collect precise weather data directly at the trapping stations, we derived proxy weather variables to represent mild winter weather conditions, particularly snow melt/ice conditions. These are the most relevant environmental factors affecting vole populations (e.g. Hansson and Henttonen (1985) and Stien et al. (2012)). The proxy variables were *zero crosses*, representing mean temperature crosses above and below 0 degrees (Celsius), and *winter rainfall*, corresponding to the amount of precipitation on positive temperature days.

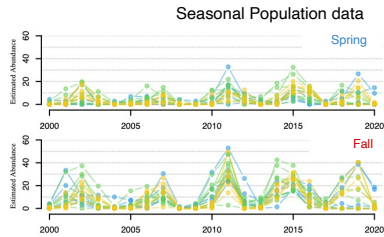
- (3) The total observed synchrony is a product of a multitude of contributing factors, deterministic (density-dependence) and stochastic (environment). To isolate the effects of the environment, it is important to first remove the density-dependence structure of the population from the synchrony estimates. For this, we model (I) the log-abundances obtained in the spring  $X_t$  and in the fall  $Y_t$  using different density-dependent models  $f(\cdot)$ , where: (II) is a general autoregressive model of order  $p = 2$  (AR(2)), regulated by a single population parameter  $\Theta$ ; (III) is an AR(2) model with spatial terms  $\Theta_R$  to account for regional differences in the density-dependence; (IV) a bivariate AR(2) model with a spatial term, addressing  $X_t$  and  $Y_t$  as separate variables (similar to a Vectorial Autoregressive Model (VAR)). The spatial correlations in either (I) or the residuals from (II–IV) represent the measures of synchrony.
- (4) Correlograms can then be used to display the extent and shape of population synchrony (separate by season) using the different measures, as well as the spatial synchrony in the weather variables.
- (5) Finally, we can relate the decomposed synchrony in either spring or fall to the spatial correlations in the environmental variables. If population synchrony is (partially) driven by a weather variable, a positive association is expected.



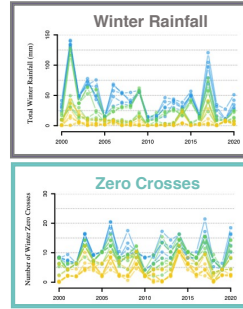
### 1. Sampling design



### 2. Time series



### Relevant weather variables



### 3. Density dependence structure

(I)  $X_t$  Spring log-abundance

Residuals $_X = X_t - f(\cdot)$

(II)  $X_t = f(\mathbf{X}^{(p)}, \Theta)$

(III)  $X_t = f(\mathbf{X}^{(p)}, \Theta_{R_X})$

(IV)  $X_t = f(\mathbf{X}^{(p)}, \mathbf{Y}^{(p)}, \Theta_{R_X}, \Theta_{R_Y})$

$Y_t$  Fall log-abundance

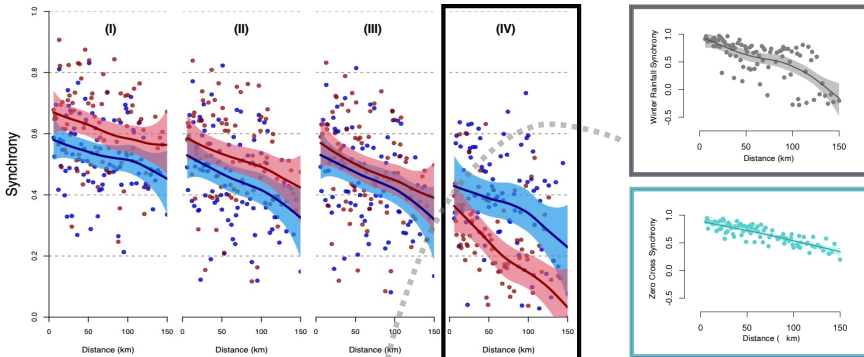
Residuals $_Y = Y_t - f(\cdot)$

$Y_t = f(\mathbf{Y}^{(p)}, \Theta)$

$Y_t = f(\mathbf{Y}^{(p)}, \Theta_{R_X})$

$Y_t = f(\mathbf{X}^{(p)}, \mathbf{Y}^{(p)}, \Theta_{R_Y}, \Theta_{R_X})$

### 4. Scale and Decomposition of Synchrony



### 5. Meteorological synchrony driver

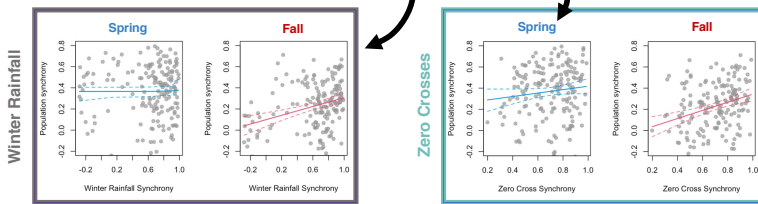


FIGURE 4.3. Schematic visualization of protocol devised in paper 3, applied to our gray-sided vole case study. Specifics are detailed in the text.

Applying our protocol to our case study clearly highlighted the importance of accounting for seasonal density-dependence when estimating stochastic effects of the environment. This is well noted when comparing correlograms (III) and (IV) in Fig. 4.3, where both the strength and shape of synchrony differ markedly between spring and fall. It thus becomes clear how important seasonality is in determining the extent of spatial synchrony. This is especially evident for the fall abundances, for which the synchrony was reduced and with a steeper slope after accounting for seasonal density-dependence. The nature of these season-specific effects was further found to be linked to the relative magnitude of the noise term in the different seasons, being larger in the spring compared to the fall.

Using our protocol allowed us to isolate contributions of mild winter weather to spatial synchrony, namely winter rainfall and the frequency of winter mild-spells. Additionally, we were able to recognize a time-lagged effect of winter weather on fall population synchrony. Interestingly, lagged effects in fall abundances had been previously noted by Moran (1953), and in the case of voles they might be explained by a delay in the onset of reproduction and consequent reduced population growth during summer (Ergon et al., 2001). As rain-on-snow events are likely to become increasingly frequent as a result of climate change (AMAP, 2017), the strength and scale of spatial synchrony of boreal rodent populations (and other taxa) might change accordingly (Hansen et al., 2020).

## CHAPTER 5

### Discussion

For this thesis, we sought to improve and assess methodologies to monitor population dynamics of small rodents, applying it to vole data collected within the COAT program. We focused on two key parts of population monitoring. On one hand, the observation process, concentrating on abundance estimation using both capture-recapture and camera trap methods. On the other, modeling two population processes relevant for rodents – density-dependence and spatial synchrony.

In the context of the observation process, we worked to develop a method which allowed for fast and efficient estimation of the capture probabilities of voles, modeling both observed heterogeneity in the form of covariates, as well as unobserved information as random effects. This was possible by resorting to INLA, which provides a Bayesian alternative to computationally intensive MCMC, commonly employed in state-space modeling approaches (Newman et al., 2022). Consequently, it was possible to implement a comprehensive simulation study (still taking 150 hours to run) to assess accuracy of estimating density-dependence parameters after accounting for capture heterogeneity, for different parameter scenarios. From this study we were able to understand how the AR(2) parameters intrinsically affected parameter estimation. We further realized that even when knowing the true abundances, there were very obvious systematic biases in the estimation of the parameters, given the short length of the time series. A side project to this thesis helps understand these biases and how to correct them, as well as obtaining uncertainty estimates (Sørbye et al., 2021). This has been made available in the R-package `ARbiascorrect`, accessible at the Github repository `pedrognicolau/ARbiascorrect-v1`. We realized that when the process variance is high, allied to relatively high capture probabilities (the case of gray-sided vole populations), accounting for the observation process

becomes less important when estimating density-dependence. This may be relevant practical information when monitoring rodent population cycles using camera trap methodologies, where accounting for the observation process is still very challenging (Gilbert et al., 2021).

Camera traps show great promise for the monitoring of small mammals, and within COAT they are already being put in place to monitor populations (Mölle et al., 2021). It became a prime goal of this thesis to understand how abundance estimates, obtained from capture-recapture, related to the activity measures recorded by the camera traps. The second project focused on this relationship, performing a standard calibration study for two vole species with different habitats, space use, trappability and monitoring schemes. This study further confirmed the great potential of camera traps to replace capture-recapture as the standard monitoring method for small mammals, showing that, for voles, abundance is closely linked to camera activity. Moreover, the added possibilities to expand temporal and spatial resolution, while monitoring the whole small mammal community, are very positive news for long-term monitoring programs such as COAT. Still, our study reinforces the importance of using camera replicates for the same spatial locations to help circumvent the differential space use of distinct species/individuals. It further remains challenging to validate/calibrate the data collected for other species sampled using this methodology, but with no reliable ground-truthing estimates of abundance.

Finally, for the third project we focused on population synchrony – a key process which can provide meta-population scale information on regulatory mechanisms, as well as help predict the challenges that populations will face in the light of climate change. This is a complex phenomenon that several arctic and boreal species can display, to which different factors contribute. In fact, when studying drivers of population synchrony, it is often impossible to isolate the contributions of every single driver, given the interplay between the effects of dispersal and predation, on top of complex environmental interactions (Liebhold et al., 2004; Lottig et al., 2017). Therefore, we developed a methodological protocol which allows the separation of environmental and stochastic contributions to spatial synchrony. By removing density-dependence contributions from the total observed synchrony, we indirectly tackle contributions from both predation and dispersal, which are

---

known to be strongly density-dependent. By analyzing the population synchrony results from sub-arctic gray-sided voles, we noticed that a big part of the observed synchrony could be indeed explained by density-dependence processes. It was then possible to confirm winter snow/ice conditions as an important driver of population synchrony for these small rodents. We believe our methodological framework has wide applicability to analyze synchrony patterns in both multivoltine and univoltine species revealing to season-specific demographic processes, especially relevant in environments like the Arctic. This represents a methodological advancement as the importance of seasonality, despite being widely recognized as a key part of density-dependent processes, has been vastly overlooked in ecological dynamics studies (White and Hastings, 2020). A main limitation for the real case study analysis was the lack of quality/precise weather data, which was not available at each trapping station. To obtain weather information we had to resort to meteorological model estimates which, for such remote areas, can be prone to biases, particularly in the case of the precipitation (Lussana et al., 2019). We were thus limited to rather uncertain weather variables, and were prevented from exploring more complex relationships between the environment and the species population dynamics.

The CR-INLA methodology, developed in the first manuscript, served as the framework to estimate capture-recapture-based abundance in the following papers. In this context, it is important to add a note. When estimating the capture probabilities, we used the observation model  $M_{th}$  (Otis et al., 1978), assuming independent capture probabilities for a given animal on each day. We are aware that this model is not the most accurately representative of the capture process, as it is likely that some behavioral effects ("trap-happy") may be present (and thus,  $M_{tbh}$ ) (Brehm and Mortelliti, 2018). However, the capture-recapture data used throughout the thesis related to two days of trapping, providing capture histories with length equaling two. This makes the parameter estimation of both behavior and temporal effects dependent on forcing constraints (Yee et al., 2015). Hence, we find a temporal model to be more realistic than a simple behavioral model  $M_{bh}$ , which would assume equal probabilities of capture on different days, only affected in case an animal had been trapped before. Interestingly, across our studies, we noticed a clear temporal effect for the

gray-sided vole, with a larger proportion of capture histories “01” compared to “10” and “11” summed together. This suggests animals were more likely to be captured on the second day, independently of having been captured or not on the first day. With this in mind, model  $M_{th}$  appeared the most reasonable.

## CHAPTER 6

### Future Outlook

While there have been decades of intense study and debate surrounding the population dynamics of rodents, it is still surprising how many gaps there are in our knowledge of the drivers and interactants that affect the multi-annual population cycles. New methods and approaches, including those developed during this project, will contribute to tackling the unanswered questions. It remains important to precisely understand which factors determine the rate and timing that lead to population increase, as up to now studies have greatly focused on the crash phase, with several unexplored hypotheses and mechanisms behind population growth (Hein and Jacob, 2015). However, even if the down phase of rodent cycles has been thoroughly studied, there is still no consensus on which exact factors cause populations to crash, particularly in regards to physiological constraints and demographic structure which have been overlooked (Andreassen et al., 2021). Ultimately, disentangling the causes and drivers of rodent population cycles will be required to properly clarify the role of these species in the ecosystems, as well as to predict and act upon the effects of climate change, not only for the rodents themselves, but for the entire system in which they play such a key role. For this, we must first dissect the interplay between factors such as seasonality, environment, predation, diseases and food resources (Oli, 2019; Andreassen et al., 2021).

To help answer many of the outstanding ecological questions surrounding population dynamics of arctic/boreal rodents, it is critical to continue development of new methodologies. This is true both from the perspective of field sampling methods, to increase the quality, quantity and resolution of the data, but also on the statistical side, to correctly account for biases and properly model the ecological parameters of interest. A particular concern of this thesis was understanding how well the new methodology of

camera traps for small mammal monitoring depicted the true abundance state of our populations of interest. Our results support the gradual methodological transition into new camera-based alternatives, which enable an important increase in both temporal and spatial data resolution. However, as we transition into the future, different questions arise, particularly on how to properly analyze continuous-time data. For species with distinctive features in their appearance, it can be possible to combine capture-recapture with camera trap data, and this may be partially possible for certain species in arctic and boreal environments at certain times of the year, with subtle moult changes (Dorning and Harris, 2019). But for most small mammals with no recognizable features, there is still a lack of methodological tools to validate camera trap data and model the error in the observation process (Sollmann, 2018; Gilbert et al., 2021). Nevertheless, the potential to monitor new populations, or parts of population cycles about which we were previously in the dark, together with the possibility to study entire community-level dynamics and interactions (e.g., predator-prey synchrony patterns; Qi et al., 2021), is incredibly promising for ecological theory going forward.

Finally, it is important to reinforce the value of long-term monitoring projects such as COAT. Studying ecological processes is not only very time consuming from a resource perspective, but also given the time scales of ecological events. For this thesis, we needed 20 years of data to even be able to get a grasp of gray-sided vole population dynamics and study some of their intrinsic population parameters. For other species, such as lemmings, 20 years might not be enough. Moreover, it is essential to obtain quality resolved environmental data from weather and landcover variables to be able to explore ecological relationships (Mollenhauer et al., 2018). In fact, many lines of data/evidence are required to perform short-term forecasting, even more so in the face of climate change and for environments as dynamic as the arctic (Dietze et al., 2018). Long-term continuous monitoring is therefore essential to recognize, predict and adapt to change.



---

## Closing Note

As a closing paragraph, I would like to leave a light-hearted consideration regarding the work in statistical ecology. Statistical ecology is a compromise between two worlds – ecological rigor and statistical feasibility. On the statistical side, we usually want the models to be as simple, straightforward and parsimonious as possible. The simplest models are always the best! We cannot simply add an interaction term at every single variable of the model. How good would it be if the data fitted the model instead? We are often forced to make assumptions, which will hopefully not have any practical consequences, and we hope to find justifications for every outlier. And in terms of data? We want loads of it! Long-time series, like hundreds of years long – is that too much to ask for? Also, clean, well formatted datasets, with no insertion typos, and with useful and detailed covariates only. Would it be possible to have weather stations at each individual trapping location? Strange field notes written with indecipherable abbreviations in possibly foreign languages? Maybe just ignore that column for now! From an ecological perspective, it is important to be thorough, account for uncertainty in every possible variable. We want to make the most out of missing data, censored data as well as easily combine data from different sources and formats. And we want those field notes to somehow count into the model, “surely the lack of animals must be due to the loud thunderstorms in the distance!”. We would like to be able to estimate a 5 year cycle using one summer’s worth of data. Essentially, we want 1001 answers from a dataset with 101 rows, that took so much sweat, blood, (money) and tears to collect.

The world is complicated and layered, and statistical ecology has the arduous but beautiful task of deciphering each layer, making the perfect compromise between ecological theory and statistical practice. In the end, we may be told that all models are wrong, with some being useful. Well, at least the useless models will always have our emotional attachment.



## Bibliography

- Abbott, K. C. (2011). A dispersal-induced paradox: synchrony and stability in stochastic metapopulations. *Ecology Letters*, 14(11), 1158–1169. DOI: 10.1111/j.1461-0248.2011.01670.x.
- Agrell, J., S. Erlinge, J. Nelson, C. Nilsson and I. Persson (1995). Delayed density-dependence in a small-rodent population. *Proceedings of the Royal Society B. Biological Sciences*, 262(1363), 65–70. DOI: 10.1098/rspb.1995.0177.
- Allstadt, A. J., A. M. Liebhold, D. M. Johnson, R. E. Davis and K. J. Haynes (2015). Temporal variation in the synchrony of weather and its consequences for spatiotemporal population dynamics. *Ecology*, 96(11), 2935–2946. DOI: 10.1890/14-1497.1.
- AMAP (2017). Snow, Water, Ice and Permafrost in the Arctic (SWIPA) 2017. Arctic Monitoring and Assessment Programme (AMAP), Oslo, Norway. xiv + 269 pp.
- Andreassen, H. P., J. Sundell, F. Ecke, S. Halle, M. Haapakoski, H. Henttonen, O. Huitu, J. Jacob, K. Johnsen, E. Koskela, J. J. Luque-Larena, N. Lecomte, H. Leirs, J. Mariën, M. Neby, O. Rätti, T. Sievert, G. R. Singleton, J. van Cann, B. V. Broecke and H. Ylönen (2021). Population cycles and outbreaks of small rodents: ten essential questions we still need to solve. *Oecologia*, 195(3), 601–622. DOI: 10.1007/s00442-020-04810-w.
- Batzli, G. O., R. G. White, S. F. MacLean, F. A. Pitelka and B. D. Collier (1980). The herbivore-based trophic system. *An Arctic Ecosystem: The Coastal Tundra at Barrow, Alaska*. Ed. by J. Brown, P. C. Miller, L. L. Tieszen and F. L. Bunnell. Dowden, Hutchinson and Ross, Stroudsburg, PA, pp. 335–410.

## BIBLIOGRAPHY

---

- Bjørnstad, O. N., W. Falck and N. C. Stenseth (1995). A geographic gradient in small rodent density fluctuations: a statistical modelling approach. *Proceedings of the Royal Society B. Biological Sciences*, 262(1364), 127–133. DOI: 10.1098/rspb.1995.0186.
- Bjørnstad, O. N., R. A. Ims and X. Lambin (1999a). Spatial population dynamics: analyzing patterns and processes of population synchrony. *Trends in Ecology & Evolution*, 14(11), 427–432. DOI: 10.1016/s0169-5347(99)01677-8.
- Bjørnstad, O. N., N. C. Stenseth and T. Saitoh (1999b). Synchrony and scaling in dynamics of voles and mice in northern Japan. *Ecology*, 80(2), 622. DOI: 10.2307/176640.
- Bliss, L. (1991). Arctic Ecosystems: Patterns of Change in Response to Disturbance. *The Earth in Transition: Patterns and Processes of Biotic Impoverishment*. Ed. by G. M. Woodwell. Cambridge University Press, pp. 347–366. DOI: 10.1017/CB09780511529917.018.
- Boonstra, R. and C. J. Krebs (1978). Pitfall trapping of *Microtus townsendii*. *Journal of Mammalogy*, 59(1), 136–148. DOI: 10.2307/1379883.
- Box, J. E., W. T. Colgan, T. R. Christensen, N. M. Schmidt, M. Lund, F.-J. W. Parmentier, R. Brown, U. S. Bhatt, E. S. Euskirchen, V. E. Romanovsky, J. E. Walsh, J. E. Overland, M. Wang, R. W. Corell, W. N. Meier, B. Wouters, S. Mernild, J. Mård, J. Pawlak and M. S. Olsen (2019). Key indicators of Arctic climate change: 1971–2017. *Environmental Research Letters*, 14(4), 045010. DOI: 10.1088/1748-9326/aafc1b.
- Brehm, A. M. and A. Mortelliti (2018). Mind the trap: large-scale field experiment shows that trappability is not a proxy for personality. *Animal Behaviour*, 142, 101–112. DOI: 10.1016/j.anbehav.2018.06.009.
- Briggs, C. J. and M. F. Hoopes (2004). Stabilizing effects in spatial parasitoid–host and predator–prey models: a review. *Theoretical Population Biology*, 65(3), 299–315. DOI: 10.1016/j.tpb.2003.11.001.
- Buonaccorsi, J. P., J. S. Elkinton, S. R. Evans and A. M. Liebhold (2001). Measuring and testing for spatial synchrony. *Ecology*, 82(6), 1668–1679. DOI: 10.1890/0012-9658(2001)082[1668:matfss]2.0.co;2.
- Burton, A. C., E. Neilson, D. Moreira, A. Ladle, R. Steenweg, J. T. Fisher, E. Bayne and S. Boutin (2015). Wildlife camera trapping: a review and

## BIBLIOGRAPHY

---

- recommendations for linking surveys to ecological processes. *Journal of Applied Ecology*, 52(3), 675–685. DOI: 10.1111/1365-2664.12432.
- Chao, A. (2001). An overview of closed capture-recapture models. *Journal of Agricultural, Biological, and Environmental Statistics*, 6(2), 158–175. DOI: 10.1198/108571101750524670.
- Corell, R. W. (2006). Challenges of climate change: An Arctic perspective. *AMBIO: A Journal of the Human Environment*, 35(4), 148–152. DOI: 10.1579/0044-7447(2006)35[148:coccaa]2.0.co;2.
- Cornulier, T., N. G. Yoccoz, V. Bretagnolle, J. E. Brommer, A. Butet, F. Ecke, D. A. Elston, E. Framstad, H. Henttonen, B. Hörnfeldt, O. Huitu, C. Imholt, R. A. Ims, J. Jacob, B. Jędrzejewska, A. Millon, S. J. Petty, H. Pietiäinen, E. Tkadlec, K. Zub and X. Lambin (2013). Europe-Wide dampening of population cycles in keystone herbivores. *Science*, 340(6128), 63–66. DOI: 10.1126/science.1228992.
- Dahlgren, J., L. Oksanen, T. Oksanen, J. Olofsson, P. Hambäck and Å. Lindgren (2009). Plant defences to no avail? Responses of plants of varying edibility to food web manipulations in a low arctic scrubland. *Evolutionary ecology research*, 11, 1189–1203.
- Dahlgren, J., L. Oksanen, M. Sjödin and J. Olofsson (2007). Interactions between gray-sided voles (*Clethrionomys rufocanus*) and bilberry (*Vaccinium myrtillus*), their main winter food plant. *Oecologia*, 152(3), 525–532. DOI: 10.1007/s00442-007-0664-8.
- Dennis, B., J. M. Ponciano, S. R. Lele, M. L. Taper and D. F. Staples (2006). Estimating density dependence, process noise, and observation error. *Ecological Monographs*, 76(3), 323–341. DOI: 10.1890/0012-9615(2006)76[323:eddpna]2.0.co;2.
- Dietze, M. C., A. Fox, L. M. Beck-Johnson, J. L. Betancourt, M. B. Hooten, C. S. Jarnevich, T. H. Keitt, M. A. Kenney, C. M. Laney, L. G. Larsen, H. W. Loescher, C. K. Lunch, B. C. Pijanowski, J. T. Randerson, E. K. Read, A. T. Tredennick, R. Vargas, K. C. Weathers and E. P. White (2018). Iterative near-term ecological forecasting: Needs, opportunities, and challenges. *Proceedings of the National Academy of Sciences*, 115(7), 1424–1432. DOI: 10.1073/pnas.1710231115.
- Dorning, J. and S. Harris (2019). The challenges of recognising individuals with few distinguishing features: Identifying red foxes *Vulpes vulpes*

## BIBLIOGRAPHY

---

- from camera-trap photos. *PLOS ONE*, 14(5). Ed. by A. M. Ionica, e0216531. DOI: 10.1371/journal.pone.0216531.
- Efford, M. (2004). Density estimation in live-trapping studies. *Oikos*, 106(3), 598–610. DOI: 10.1111/j.0030-1299.2004.13043.x.
- Elton, C. S. (1924). Periodic fluctuations in the numbers of animals: Their causes and effects. *Journal of Experimental Biology*, 2(1), 119–163.
- Engen, S. and B.-E. Sæther (2005). Generalizations of the Moran Effect explaining spatial synchrony in population fluctuations. *The American Naturalist*, 166(5), 603–612. DOI: 10.1086/491690.
- Ergon, T., X. Lambin and N. C. Stenseth (2001). Life-history traits of voles in a fluctuating population respond to the immediate environment. *Nature*, 411(6841), 1043–1045.
- Fauteux, D., A. Stien, N. G. Yoccoz, E. Fuglei and R. A. Ims (2021). Climate variability and density-dependent population dynamics: Lessons from a simple High Arctic ecosystem. *Proceedings of the National Academy of Sciences*, 118(37), e2106635118. DOI: 10.1073/pnas.2106635118.
- Fay, R., S. Michler, J. Laesser, J. Jeanmonod and M. Schaub (2020). Large-scale vole population synchrony in central Europe revealed by kestrel breeding performance. *Frontiers in Ecology and Evolution*, 7(512). DOI: 10.3389/fevo.2019.00512.
- Gilbert, N. A., J. D. J. Clare, J. L. Stenglein and B. Zuckerberg (2021). Abundance estimation of unmarked animals based on camera-trap data. *Conservation biology*, 35(1), 88–100. DOI: 10.1111/cobi.13517.
- Gilg, O. and N. G. Yoccoz (2010). Explaining bird migration. *Science*, 327(5963), 276–277. DOI: 10.1126/science.1184964.
- Gimenez, O., E. Cam and J.-M. Gaillard (2017). Individual heterogeneity and capture-recapture models: what, why and how? *Oikos*, 127(5), 664–686. DOI: 10.1111/oik.04532.
- Gopalaswamy, A. M., M. Delampady, K. U. Karanth, N. S. Kumar and D. W. Macdonald (2015). An examination of index-calibration experiments: counting tigers at macroecological scales. *Methods in Ecology and Evolution*, 6(9). Ed. by N. Yoccoz, 1055–1066. DOI: 10.1111/2041-210x.12351.

## BIBLIOGRAPHY

---

- Gouhier, T. C. and F. Guichard (2014). Synchrony: quantifying variability in space and time. *Methods in Ecology and Evolution*, 5(6). Ed. by S. Dray, 524–533. DOI: 10.1111/2041-210x.12188.
- Gouveia, A. R., O. N. Bjørnstad and E. Tkadlec (2015). Dissecting geographic variation in population synchrony using the common vole in central Europe as a test bed. *Ecology and Evolution*, 6(1), 212–218. DOI: 10.1002/ece3.1863.
- Hansen, B. B., V. Grøtan, I. Herfindal and A. M. Lee (2020). The Moran effect revisited: spatial population synchrony under global warming. *Ecography*, 43(11), 1591–1602. DOI: 10.1111/ecog.04962.
- Hansen, T. F., N. C. Stenseth and H. Henttonen (1999). Multiannual vole cycles and population regulation during long winters: an analysis of seasonal density dependence. *The American Naturalist*, 154(2). PMID: 29578785, 129–139. DOI: 10.1086/303229.
- Hanski, I., L. Hansson and H. Henttonen (1991). Specialist predators, generalist predators, and the Microtine rodent cycle. *The Journal of Animal Ecology*, 60(1), 353. DOI: 10.2307/5465.
- Hansson, L. and H. Henttonen (1985). Gradients in density variations of small rodents: the importance of latitude and snow cover. *Oecologia*, 67(3), 394–402. DOI: 10.1007/bf00384946.
- (1988). Rodent dynamics as community processes. *Trends in Ecology & Evolution*, 3(8), 195–200. DOI: 10.1016/0169-5347(88)90006-7.
- Haynes, K. J., A. M. Liebhold, T. M. Fearer, G. Wang, G. W. Norman and D. M. Johnson (2009). Spatial synchrony propagates through a forest food web via consumer–resource interactions. *Ecology*, 90(11), 2974–2983. DOI: 10.1890/08-1709.1.
- Hein, S. and J. Jacob (2015). Recovery of small rodent populations after population collapse. *Wildlife Research*, 42(2), 108. DOI: 10.1071/wr14165.
- Heino, M., V. Kaitala, E. Ranta and J. Lindström (1997). Synchronous dynamics and rates of extinction in spatially structured populations. *Proceedings of the Royal Society B. Biological Sciences*, 264(1381), 481–486. DOI: 10.1098/rspb.1997.0069.
- Henden, J.-A., R. A. Ims, N. G. Yoccoz, E. J. Asbjørnsen, A. Stien, J. P. Mellard, T. Tveraa, F. Marolla and J. U. Jepsen (2020). End-user involvement to improve predictions and management of populations with

## BIBLIOGRAPHY

---

- complex dynamics and multiple drivers. *Ecological Applications*, 30(6). DOI: 10.1002/eap.2120.
- Henttonen, H., L. Hansson and T. Saitoh (1992). Rodent dynamics and community structure: *Clethrionomys rufocanus* in northern Fennoscandia and Hokkaido. *Annales Zoologici Fennici*, 29(1), 1–6.
- Herliansyah, R., R. King and S. King (2022). Laplace approximations for capture–recapture models in the presence of individual heterogeneity. *Journal of Agricultural, Biological and Environmental Statistics*. DOI: 10.1007/s13253-022-00486-2.
- Hixon, M. A. and D. W. Johnson (2006). Density Dependence and Independence. *Encyclopedia of Life Sciences*. Chichester: John Wiley & Sons Ltd., pp. 1–6. DOI: 10.1002/9780470015902.a0021219.
- Hofgaard, A., K. A. Harper and E. Golubeva (2012). The role of the circumarctic forest–tundra ecotone for Arctic biodiversity. *Biodiversity*, 13(3-4), 174–181. DOI: 10.1080/14888386.2012.700560.
- Horvitz, D. G. and D. J. Thompson (1952). A generalization of sampling without replacement from a finite universe. *Journal of the American Statistical Association*, 47(260), 663–685. DOI: 10.1080/01621459.1952.10483446.
- Huggins, R. and W.-H. Hwang (2011). A review of the use of conditional likelihood in capture-recapture experiments. *International Statistical Review*, 79(3), 385–400. DOI: 10.1111/j.1751-5823.2011.00157.x.
- Hugueny, B. (2006). Spatial synchrony in population fluctuations: extending the Moran theorem to cope with spatially heterogeneous dynamics. *Oikos*, 115(1), 3–14. DOI: 10.1111/j.2006.0030-1299.14686.x.
- Ims, R. A. and H. P. Andreassen (2000). Spatial synchronization of vole population dynamics by predatory birds. *Nature*, 408(6809), 194–196. DOI: 10.1038/35041562.
- Ims, R. A. and E. Fuglei (2005). Trophic interaction cycles in tundra ecosystems and the impact of climate change. *BioScience*, 55(4), 311–322. DOI: 10.1641/0006-3568(2005)055[0311:tcite]2.0.co;2.
- Ims, R. A., J.-A. Henden, A. V. Thingnes and S. T. Killengreen (2013a). Indirect food web interactions mediated by predator–rodent dynamics: relative roles of lemmings and voles. *Biology Letters*, 9(6), 20130802. DOI: 10.1098/rsbl.2013.0802.



## BIBLIOGRAPHY

---

- Ims, R. A., J. U. Jepsen, A. Stien and N. G. Yoccoz (2013b). *Science plan for COAT: Climate-ecological Observatory for Arctic Tundra*. Fram Centre, Tromsø.
- Jareño, D., J. Viñuela, J. J. Luque-Larena, L. Arroyo, B. Arroyo and F. Mougeot (2014). A comparison of methods for estimating common vole (*Microtus arvalis*) abundance in agricultural habitats. *Ecological Indicators*, 36, 111–119. DOI: 10.1016/j.ecolind.2013.07.019.
- Jennelle, C. S., M. C. Runge and D. I. MacKenzie (2002). The use of photographic rates to estimate densities of tigers and other cryptic mammals: a comment on misleading conclusions. *Animal Conservation*, 5(2), 119–120. DOI: 10.1017/S1367943002002160.
- Jensen, P., N. Stenseth and F. E. (1993). Trappability of the Norwegian lemming (*Lemmus lemmus*). *The Biology of Lemmings*. Ed. by N. Stenseth and I. R.A. London: Academic Press, pp. 547–554.
- Kaneko, Y., K. Nakata, T. Saitoh, N. C. Stenseth and O. N. Bjørnstad (1998). The biology of the vole *Clethrionomys rufocanus*: A review. *Researches on Population Ecology*, 40(1), 21–37. DOI: 10.1007/bf02765219.
- King, R. and R. McCrea (2019). Capture–recapture methods and models: estimating population size. *Handbook of Statistics*. Elsevier, pp. 33–83. DOI: 10.1016/bs.host.2018.09.006.
- Kleiven, E. F., J.-A. Henden, R. A. Ims and N. G. Yoccoz (2018). Seasonal difference in temporal transferability of an ecological model: near-term predictions of lemming outbreak abundances. *Scientific Reports*, 8(1), 15252. DOI: 10.1038/s41598-018-33443-6.
- Knape, J. and P. de Valpine (2011). Are patterns of density dependence in the Global Population Dynamics Database driven by uncertainty about population abundance? *Ecology Letters*, 15(1), 17–23. DOI: 10.1111/j.1461-0248.2011.01702.x.
- Koenig, W. D. (1999). Spatial autocorrelation of ecological phenomena. *Trends in Ecology & Evolution*, 14(1), 22–26. DOI: 10.1016/s0169-5347(98)01533-x.
- Koenig, W. D. and A. M. Liebhold (2016). Temporally increasing spatial synchrony of North American temperature and bird populations. *Nature Climate Change*, 6(6), 614–617. DOI: 10.1038/nclimate2933.

## BIBLIOGRAPHY

---

- Kolowski, J. M., J. Oley and W. J. McShea (2021). High-density camera trap grid reveals lack of consistency in detection and capture rates across space and time. *Ecosphere*, 12(2), e03350. DOI: 10.1002/ecs2.3350.
- Korpela, K., M. Delgado, H. Henttonen, E. Korpimäki, E. Koskela, O. Ovaskainen, H. Pietiäinen, J. Sundell, N. G. Yoccoz and O. Huitu (2013). Nonlinear effects of climate on boreal rodent dynamics: mild winters do not negate high-amplitude cycles. *Global Change Biology*, 19(3), 697–710. DOI: 10.1111/gcb.12099.
- Korpela, K., P. Helle, H. Henttonen, E. Korpimäki, E. Koskela, O. Ovaskainen, H. Pietiäinen, J. Sundell, J. Valkama and O. Huitu (2014). Predator–vole interactions in northern Europe: the role of small mustelids revised. *Proceedings of the Royal Society B: Biological Sciences*, 281(1797), 20142119. DOI: 10.1098/rspb.2014.2119.
- Krebs, C. J. (2013). *Population Fluctuations in Rodents*. University of Chicago Press.
- Krebs, C. J., R. Boonstra, S. Gilbert, D. Reid, A. J. Kenney and E. J. Hofer (2011). Density estimation for small mammals from livetrapping grids: rodents in northern Canada. *Journal of Mammalogy*, 92(5), 974–981. DOI: 10.1644/10-MAMM-A-313.1.
- Lande, R., S. Engen and B. Sæther (2002). Estimating density dependence in time-series of age-structured populations. *sophical Transactions of the Royal B. Biological Sciences*, 357(1425). Ed. by R. M. Sibly, J. Hone and T. H. Clutton–Brock, 1179–1184. DOI: 10.1098/rstb.2002.1120.
- Lebreton, J.-D. and O. Gimenez (2012). Detecting and estimating density dependence in wildlife populations. *The Journal of Wildlife Management*, 77(1), 12–23. DOI: 10.1002/jwmg.425.
- Liebholt, A., W. D. Koenig and O. N. Bjørnstad (2004). Spatial synchrony in population dynamics. *Annual Review of Ecology, Evolution, and Systematics*, 35(1), 467–490. DOI: 10.1146/annurev.ecolsys.34.011802.132516.
- Littlewood, N. A., M. H. Hancock, S. Newey, G. Shackelford and R. Toney (2021). Use of a novel camera trapping approach to measure small mammal responses to peatland restoration. *European Journal of Wildlife Research*, 67(1). DOI: 10.1007/s10344-020-01449-z.

## BIBLIOGRAPHY

---

- Lottig, N. R., P.-N. Tan, T. Wagner, K. S. Cheruvilil, P. A. Soranno, E. H. Stanley, C. E. Scott, C. A. Stow and S. Yuan (2017). Macroscale patterns of synchrony identify complex relationships among spatial and temporal ecosystem drivers. *Ecosphere*, 8(12). DOI: 10.1002/ecs2.2024.
- Lussana, C., O. E. Tveito, A. Dobler and K. Tunheim (2019). seNorge\_2018, daily precipitation, and temperature datasets over Norway. *Earth System Science Data*, 11(4), 1531–1551. DOI: 10.5194/essd-11-1531-2019.
- Malhi, Y., J. Franklin, N. Seddon, M. Solan, M. G. Turner, C. B. Field and N. Knowlton (2020). Climate change and ecosystems: threats, opportunities and solutions. *Philosophical Transactions of the Royal Society B: Biological Sciences*, 375(1794), 20190104. DOI: 10.1098/rstb.2019.0104.
- Mölle, J. P., E. F. Kleiven, R. A. Ims and E. M. Soininen (2021). Using subnivean camera traps to study Arctic small mammal community dynamics during winter. *Arctic Science*, 1–17. DOI: 10.1139/as-2021-0006.
- Mollenhauer, H., M. Kasner, P. Haase, J. Peterseil, C. Wohner, M. Frenzel, M. Mirtl, R. Schima, J. Bumberger and S. Zacharias (2018). Long-term environmental monitoring infrastructures in Europe: observations, measurements, scales, and socio-ecological representativeness. *Science of The Total Environment*, 624, 968–978. DOI: 10.1016/j.scitotenv.2017.12.095.
- Moran, P. (1953). The statistical analysis of the Canadian Lynx cycle. 2. Synchronization and meteorology. *Australian Journal of Zoology*, 1(3), 291. DOI: 10.1071/zo9530291.
- Mossberg, B., L. Stenberg and S. Moen (2012). *Gyldendals store nordiske Flora*. Gyldendal. ISBN: 9788205424852.
- Nakashima, Y., K. Fukasawa and H. Samejima (2017). Estimating animal density without individual recognition using information derivable exclusively from camera traps. *Journal of Applied Ecology*, 55(2). Ed. by P. Stephens, 735–744. DOI: 10.1111/1365-2664.13059.
- Nakata, K. (1984). Factors affecting litter size in the red-backed vole, *Clethrionomys rufocanus bedfordiae*, with special emphasis on population phase. *Researches on Population Ecology*, 26(2), 221–234. DOI: 10.1007/bf02515491.

## BIBLIOGRAPHY

---

- Newman, K., R. King, V. Elvira, P. de Valpine, R. S. McCrea and B. J. T. Morgan (2022). State-space Models for ecological time series data: practical model-fitting. *Methods in Ecology and Evolution*. DOI: 10.1111/2041-210x.13833.
- Oli, M. K. (2019). Population cycles in voles and lemmings: state of the science and future directions. *Mammal Review*, 49(3), 226–239. DOI: 10.1111/mam.12156.
- Ono, K., Ø. Langangen and N. C. Stenseth (2019). Improving risk assessments in conservation ecology. *Nature Communications*, 10(1). DOI: 10.1038/s41467-019-10700-4.
- Otis, D. L., K. P. Burnham, G. C. White and D. R. Anderson (1978). Statistical inference from capture data on closed animal populations. *Wildlife Monographs*(62), 3–135.
- Palencia, P., J. M. Rowcliffe, J. Vicente and P. Acevedo (2021). Assessing the camera trap methodologies used to estimate density of unmarked populations. *Journal of Applied Ecology*, 58(8), 1583–1592. DOI: 10.1111/1365-2664.13913.
- Parsons, M. A., A. E. Orloff and L. R. Prugh (2021). Evaluating livetrapping and camera-based indices of small-mammal density. *Canadian Journal of Zoology*, 99(6), 521–530. DOI: 10.1139/cjz-2020-0298.
- Post, E. and M. C. Forchhammer (2004). From the cover: Spatial synchrony of local populations has increased in association with the recent northern hemisphere climate trend. *Proceedings of the National Academy of Sciences*, 101(25), 9286–9290. DOI: 10.1073/pnas.0305029101.
- Powell, L. and G. Gale (2015). *Estimation of Parameters for Animal Populations: a primer for the rest of us*. Caught Napping Publications. ISBN: 9781329061514.
- Qi, J., M. Holyoak, M. T. Dobbins, C. Huang, Q. Li, W. She, Y. Ning, Q. Sun, G. Jiang and X. Wang (2021). Wavelet methods reveal big cat activity patterns and synchrony of activity with preys. *Integrative Zoology*, 17(2), 246–260. DOI: 10.1111/1749-4877.12526.
- Rendall, A. R., D. R. Sutherland, R. Cooke and J. White (2014). Camera trapping: A contemporary approach to monitoring invasive rodents in high conservation priority ecosystems. *PLoS ONE*, 9(3). Ed. by B. Boldgiv, e86592. DOI: 10.1371/journal.pone.0086592.

## BIBLIOGRAPHY

---

- Ripa, J. (2000). Analysing the Moran effect and dispersal: their significance and interaction in synchronous population dynamics. *Oikos*, 89(1), 175–187. DOI: 10.1034/j.1600-0706.2000.890119.x.
- Rodríguez-Pastor, R., R. Escudero, X. Lambin, M. D. Vidal, H. Gil, I. Jado, M. Rodríguez-Vargas, J. J. Luque-Larena and F. Mougeot (2018). Zoonotic pathogens in fluctuating common vole (*Microtus arvalis*) populations: occurrence and dynamics. *Parasitology*, 146(3), 389–398. DOI: 10.1017/s0031182018001543.
- Romairone, J., J. Jiménez, J. J. Luque-Larena and F. Mougeot (2018). Spatial capture-recapture design and modelling for the study of small mammals. *PLOS ONE*, 13(6). Ed. by A. Margalida, e0198766. DOI: 10.1371/journal.pone.0198766.
- Rowcliffe, J. M., J. Field, S. T. Turvey and C. Carbone (2008). Estimating animal density using camera traps without the need for individual recognition. *Journal of Applied Ecology*, 45(4), 1228–1236. DOI: 10.1111/j.1365-2664.2008.01473.x.
- Royama, T. (2005). Moran effect on nonlinear population processes. *Ecological Monographs*, 75(2), 277–293. DOI: 10.1890/04-0770.
- Rue, H., A. Riebler, S. H. Sørbye, J. B. Illian, D. P. Simpson and F. K. Lindgren (2017). Bayesian computing with INLA: A review. *Annual Review of Statistics and its Application*, 4, 395–421. DOI: 10.1146/annurev-statistics-060116-054045.
- Santin-Janin, H., B. Hugueny, P. Aubry, D. Fouchet, O. Gimenez and D. Pontier (2014). Accounting for sampling error when inferring population synchrony from time-series data: A Bayesian state-space modelling approach with applications. *PLoS ONE*, 9(1). Ed. by D. Coppola, e87084. DOI: 10.1371/journal.pone.0087084.
- Seber, G. A. F. (1986). A review of estimating animal abundance. *Biometrics*, 42(2), 267. DOI: 10.2307/2531049.
- Serreze, M. C. and R. G. Barry (2011). Processes and impacts of Arctic amplification: A research synthesis. *Global and Planetary Change*, 77(1-2), 85–96. DOI: 10.1016/j.gloplacha.2011.03.004.
- Sheppard, L. W., J. R. Bell, R. Harrington and D. C. Reuman (2015). Changes in large-scale climate alter spatial synchrony of aphid pests. *Nature Climate Change*, 6(6), 610–613. DOI: 10.1038/nclimate2881.

## BIBLIOGRAPHY

---

- Sirois, L. (1992). The transition between boreal forest and tundra. *A Systems Analysis of the Global Boreal Forest*. Ed. by H. Shugart, R. Leemans and G. Bonan. Cambridge University Press Cambridge, UK, pp. 196–215. DOI: 10.1017/CB09780511565489.009.
- Slade, N. A. (1977). Statistical detection of density dependence from a series of sequential censuses. *Ecology*, 58(5), 1094–1102. DOI: 10.2307/1936929.
- Soininen, E. M., I. Jensvoll, S. T. Killengreen and R. A. Ims (2015). Under the snow: a new camera trap opens the white box of subnivean ecology. *Remote Sensing in Ecology and Conservation*, 1(1), 29–38. DOI: 10.1002/rse2.2.
- Sollmann, R. (2018). A gentle introduction to camera-trap data analysis. *African Journal of Ecology*, 56(4), 740–749. DOI: 10.1111/aje.12557.
- Sørbye, S. H., P. G. Nicolau and H. Rue (2021). Finite-sample properties of estimators for first and second order autoregressive processes. *Statistical Inference for Stochastic Processes*. DOI: 10.1007/s11203-021-09262-4.
- Stenseth, N. C., K. Chan, E. Framstad and H. Tong (1998). Phase- and density-dependent population dynamics in Norwegian lemmings: interaction between deterministic and stochastic processes. *Proceedings of the Royal Society B. Biological Sciences*, 265(1409), 1957–1968. DOI: 10.1098/rspb.1998.0526.
- Stenseth, N. C., H. Viljugrein, T. Saitoh, T. F. Hansen, M. O. Kittilsen, E. Bolviken and F. Glockner (2003). Seasonality, density dependence, and population cycles in Hokkaido voles. *Proceedings of the National Academy of Sciences*, 100(20), 11478–11483. DOI: 10.1073/pnas.1935306100.
- Stenseth, N. C. (1999). Population cycles in voles and lemmings: density dependence and phase dependence in a stochastic world. *Oikos*, 87(3), 427. DOI: 10.2307/3546809.
- Stenseth, N. C., M. O. Kittilsen, D. Ø. Hjernann, H. Viljugrein and T. Saitoh (2002). Interaction between seasonal density-dependence structures and length of the seasons explain the geographical structure of the dynamics of voles in Hokkaido: an example of seasonal forcing. *Proceedings of the Royal Society B. Biological Sciences*, 269(1503), 1853–1863. DOI: 10.1098/rspb.2002.2099.

## BIBLIOGRAPHY

---

- Stephens, R. B. and E. M. Anderson (2014). Effects of trap type on small mammal richness, diversity, and mortality. *Wildlife Society Bulletin*, 38(3), 619–627. DOI: 10.1002/wsb.418.
- Stien, A., R. A. Ims, S. D. Albon, E. Fuglei, R. J. Irvine, E. Ropstad, O. Halvorsen, R. Langvatn, L. E. Loe, V. Veiberg and N. G. Yoccoz (2012). Congruent responses to weather variability in high arctic herbivores. *Biology Letters*, 8(6), 1002–1005. DOI: 10.1098/rsbl.2012.0764.
- Tabak, M. A., M. S. Norouzzadeh, D. W. Wolfson, S. J. Sweeney, K. C. Vercauteren, N. P. Snow, J. M. Halseth, P. A. Di Salvo, J. S. Lewis, M. D. White, B. Teton, J. C. Beasley, P. E. Schlichting, R. K. Boughton, B. Wight, E. S. Newkirk, J. S. Ivan, E. A. Odell, R. K. Brook, P. M. Lukacs, A. K. Moeller, E. G. Mandeville, J. Clune and R. S. Miller (2019). Machine learning to classify animal species in camera trap images: applications in ecology. *Methods in Ecology and Evolution*, 10(4), 585–590. DOI: 10.1111/2041-210X.13120.
- Tast, J. (1966). The root vole, *Microtus oeconomus* (Pallas), as an inhabitant of seasonally flooded land. *Annales Zoologici Fennici*. Vol. 3. 3. JSTOR, pp. 127–171.
- Thorson, J. T., H. J. Skaug, K. Kristensen, A. O. Shelton, E. J. Ward, J. H. Harms and J. A. Benante (2015). The importance of spatial models for estimating the strength of density dependence. *Ecology*, 96(5), 1202–1212. DOI: 10.1890/14-0739.1.
- Trollet, F., C. Vermeulen, M.-C. Huynen and A. Hambuckers (2014). Use of camera traps for wildlife studies: a review. *Biotechnologie, Agronomie, Société et Environnement*, 18(3).
- Turkia, T., J. Jousimo, J. Tiainen, P. Helle, J. Rintala, T. Hokkanen, J. Valkama and V. Selonen (2020). Large-scale spatial synchrony in red squirrel populations driven by a bottom-up effect. *Oecologia*, 192(2), 425–437. DOI: 10.1007/s00442-019-04589-5.
- Ulrich, W., R. Puchalka, M. Koprowski, G. Strona and N. J. Gotelli (2019). Ecological drift and competitive interactions predict unique patterns in temporal fluctuations of population size. *Ecology*, 100(4). DOI: 10.1002/ecy.2623.
- Villette, P., C. J. Krebs, T. S. Jung and R. Boonstra (2015). Can camera trapping provide accurate estimates of small mammal (*Myodes rutilus*

## BIBLIOGRAPHY

---

- and *Peromyscus maniculatus*) density in the boreal forest? *Journal of Mammalogy*, 97(1), 32–40. DOI: 10.1093/jmammal/gyv150.
- Vogwill, T., A. Fenton and M. A. Brockhurst (2009). Dispersal and natural enemies interact to drive spatial synchrony and decrease stability in patchy populations. *Ecology Letters*, 12(11), 1194–1200. DOI: 10.1111/j.1461-0248.2009.01374.x.
- Wall, E., F. Guichard and A. R. Humphries (2013). Synchronization in ecological systems by weak dispersal coupling with time delay. *Theoretical Ecology*, 6(4), 405–418. DOI: 10.1007/s12080-013-0176-6.
- Wearn, O. R. and P. Glover-Kapfer (2019). Snap happy: camera traps are an effective sampling tool when compared with alternative methods. *Royal Society Open Science*, 6(3), 181748. DOI: 10.1098/rsos.181748.
- White, E. R. and A. Hastings (2020). Seasonality in ecology: progress and prospects in theory. *Ecological Complexity*, 44, 100867. DOI: 10.1016/j.ecocom.2020.100867.
- Xu, L., R. B. Myneni, F. S. C. III, T. V. Callaghan, J. E. Pinzon, C. J. Tucker, Z. Zhu, J. Bi, P. Ciais, H. Tømmervik, E. S. Euskirchen, B. C. Forbes, S. L. Piao, B. T. Anderson, S. Ganguly, R. R. Nemani, S. J. Goetz, P. S. A. Beck, A. G. Bunn, C. Cao and J. C. Stroeve (2013). Temperature and vegetation seasonality diminishment over northern lands. *Nature Climate Change*, 3(6), 581–586. DOI: 10.1038/nclimate1836.
- Yee, T. W., J. Stoklosa and R. M. Huggins (2015). The VGAM Package for capture-recapture data using the conditional likelihood. *Journal of Statistical Software*, 65(5). DOI: 10.18637/jss.v065.i05.
- Yoccoz, N. G. and R. A. Ims (2004). Spatial population dynamics of small mammals: some methodological and practical issues. *Animal Biodiversity and Conservation*, 27(1), 427–435.
- Young, L. J. and J. H. Young (1998). Capture—recapture: open populations. *Statistical Ecology*. Springer US, pp. 357–389. DOI: 10.1007/978-1-4757-2829-3\_10.
- Zhang, Y., F. Lutscher and F. Guichard (2015). How robust is dispersal-induced spatial synchrony? *Chaos: An Interdisciplinary Journal of Non-linear Science*, 25(3), 036402. DOI: 10.1063/1.4906951.






## Paper I

**Incorporating capture heterogeneity in the estimation of autoregressive coefficients of animal population dynamics using capture–recapture data.**

*Ecology & Evolution*, **10**,(23), 12710-12726, 2020.



# Incorporating capture heterogeneity in the estimation of autoregressive coefficients of animal population dynamics using capture–recapture data

Pedro G. Nicolau<sup>1</sup>  | Sigrunn H. Sørbye<sup>1</sup>  | Nigel G. Yoccoz<sup>2</sup> 

<sup>1</sup>Department of Mathematics and Statistics, Faculty of Science and Technology, UiT The Arctic University of Norway, Tromsø, Norway

<sup>2</sup>Department of Arctic and Marine Biology, Faculty of Biosciences, Fisheries and Economics, UiT The Arctic University of Norway, Tromsø, Norway

## Correspondence

Pedro G. Nicolau, Department of Mathematics and Statistics, UiT The Arctic University of Norway, PO Box 6050 Langnes, N-9037 Tromsø, Norway.  
Email: pedro.nicolau@uit.no

[Correction Statement: Correction added on 15 October 2020 after first online publication: Table 1 and 2 headers and supporting information have been corrected in this version]

## Abstract

Population dynamic models combine density dependence and environmental effects. Ignoring sampling uncertainty might lead to biased estimation of the strength of density dependence. This is typically addressed using state-space model approaches, which integrate sampling error and population process estimates. Such models seldom include an explicit link between the sampling procedures and the true abundance, which is common in capture–recapture settings. However, many of the models proposed to estimate abundance in the presence of capture heterogeneity lead to incomplete likelihood functions and cannot be straightforwardly included in state-space models. We assessed the importance of estimating sampling error explicitly by taking an intermediate approach between ignoring uncertainty in abundance estimates and fully specified state-space models for density-dependence estimation based on autoregressive processes. First, we estimated individual capture probabilities based on a heterogeneity model for a closed population, using a conditional multinomial likelihood, followed by a Horvitz–Thompson estimate for abundance. Second, we estimated coefficients of autoregressive models for the log abundance. Inference was performed using the methodology of integrated nested Laplace approximation (INLA). We performed an extensive simulation study to compare our approach with estimates disregarding capture history information, and using R-package VGAM, for different parameter specifications. The methods were then applied to a real data set of gray-sided voles *Myodes rufocanus* from Northern Norway. We found that density-dependence estimation was improved when explicitly modeling sampling error in scenarios with low process variances, in which differences in coverage reached up to 8% in estimating the coefficients of the autoregressive processes. In this case, the bias also increased assuming a Poisson distribution in the observational model. For high process variances, the differences between methods were small and it appeared less important to model heterogeneity.

This is an open access article under the terms of the Creative Commons Attribution License, which permits use, distribution and reproduction in any medium, provided the original work is properly cited.

© 2020 The Authors. *Ecology and Evolution* published by John Wiley & Sons Ltd

## KEYWORDS

abundance, capture probability, closed population models, density dependence, INLA, process variance

## 1 | INTRODUCTION

Models used to analyze population dynamics include a combination of density dependence and environmental effects. Ignoring the uncertainty in abundance estimates biases estimates of the strength of density dependence, and different approaches exist to achieve better accuracy (see Lebreton & Gimenez, 2012 for a review). In particular, state-space models combining an observation model—linking the observations such as counts to the true abundance—and a process model—describing the processes driving population dynamics—have become a standard approach in many analyses (Dennis & Taper, 1994). However, these models rarely include an explicit model of the link between how counts were obtained and true abundance, often relying on a nonspecific observation model such as log normal or Poisson distribution (for instance, Ono, Langangen, & Chr. Stenseth, 2019, but see below).

Capture–recapture methods have been extensively used to estimate abundance and density dependence, and many methods have been developed to incorporate different sources of variability into capture probability estimation, such as environmental information, survival, or trophic interactions (Barker, Fletcher, & Scofield, 2002; Lebreton & Gimenez, 2012; Schofield & Barker, 2008; Yackulic, Korman, Yard, & Dzul, 2018). Estimating abundance is a challenging statistical problem (Link, 2003), and heterogeneity in capture probabilities can lead to large biases in abundance estimates when using models assuming no heterogeneity (Carothers, 1973; Otis, Burnham, White, & Anderson, 1978). However, many of the models that have been proposed to estimate abundance in the presence of heterogeneity do not lead to observation models that can be included in state-space models as they do not lead to likelihood functions in a closed form (Chao & Huggins, 2006; Huggins & Hwang, 2011).

Many studies investigating density dependence have used simple process models such as the Gompertz model—that is, a model which is a first-order autoregressive model on a log scale (Ono et al., 2019; Thibaut & Connolly, 2019). However, ecological processes such as trophic interactions (Bjørnstad, Falck, & Stenseth, 1995) or intrinsic ecological properties such as age structure (Lande, Engen, & Sæther, 2002) may lead to more complex process models such as a second-order autoregressive model (AR(2)). An important case is the population cycles observed in many small mammal populations, particularly in northern environments (Bjørnstad & Chr. Stenseth, 1999; Elton, 1924; Stenseth, 1999). These quasi-periodic fluctuations are quite well approximated by AR(2) models on a logarithmic scale (Bjørnstad et al., 1995). Whereas most analyses have ignored the uncertainty in abundance estimates (Bjørnstad et al., 1995), some have used state-space models (Cornulier et al., 2013; Ims, Yoccoz, & Killengreen, 2011; Kleiven, Henden, Ims, & Yoccoz, 2018; Stenseth et al., 2003). However, approaches using a capture–recapture

framework and including capture heterogeneity have relied on integrating out random effects describing capture heterogeneity (King, Brooks, & Coulson, 2008; Schofield & Barker, 2013) and using superpopulation data augmentation (Royle, 2008); these approaches did not consider the conditional likelihood approach to estimating population size, which can easily handle, for example, individual covariates (Huggins & Hwang, 2011). Moreover, a fully MCMC-based Bayesian approach is computationally intensive on large data sets and requires that careful considerations are given to choices of priors and superpopulation sizes for data augmentation (Royle, Dorazio, & Link, 2007).

Here, we investigated the performance of an intermediate approach between ignoring uncertainty in abundance estimates (i.e., using the raw population counts) and fully specified state-space models. Specifically, we first used a multinomial observation model to estimate capture probabilities followed by estimating abundance at each time point using the Horvitz–Thompson estimator (Horvitz & Thompson, 1952). Second, we fitted an AR(2) process model to the log abundance to estimate direct and delayed density dependence given by the first and second coefficients of the AR(2) model, respectively. Both estimation steps were performed in a unified way, incorporating the models within the general class of latent Gaussian models (Rue, Martino, & Chopin, 2009). Full Bayesian inference was then obtained using the methodology of integrated nested Laplace approximation (INLA) (Rue et al., 2009, 2017).

We based our analyses on a large-scale study of population dynamics of the dominant small mammal species in northern Fennoscandia, the gray-sided vole *Myodes rufocanus* (Ims et al., 2011). This species shows large fluctuations with a 4- to 5-year periodicity (Ims et al., 2011; Marolla et al., 2019). We monitored populations of gray-sided voles along a 155-km gradient from coast to inland, using live capture–recapture methods, starting in 2000. Previous analyses have shown that there was large heterogeneity in capture probabilities (Yoccoz & Ims, 2004). In this rodent study, the goal was to understand spatial patterns of population dynamics, assessing potential seasonal effects on the density-dependence estimates. For this, we first needed to assess the robustness of using an approach based on estimated abundances but without implementing a full state-space model. In this paper, we therefore use a simulation study built around the case study (adaptable to other situations from the code provided) to assess the estimation accuracy of the density dependence, both including and excluding capture history information.

The structure of this paper is as follows. Section 2 provides our methodological background to analyze capture–recapture data and describes the Bayesian framework to perform parameter estimation. This includes using INLA to estimate individual capture probabilities and the direct and delayed density dependence given by the

coefficients of AR(2) models. Section 3 contains an extensive simulation study, investigating how density-dependence estimates are influenced when individual capture probabilities are taken into account. In Section 4, we study the population cycles of gray-sided voles. We first compare different observation models in estimating individual capture probabilities and then assess whether incorporation of individual capture probabilities influences density-dependence estimates. A summary and concluding remarks are given in Section 5.

## 2 | METHODOLOGY

Capture–recapture experiments are important to assess heterogeneity in individual capture probabilities. This section describes our approach to incorporate capture–recapture information in the estimation of density dependence. First, we define an observation model in which capture probabilities are modeled in terms of individual features and then used to estimate abundance. Second, we fit an AR(2) process model to the estimated log abundance to assess density dependence. When using state-space approaches, the parameters of the observation and process model are estimated simultaneously. This is not possible in our case as the capture probabilities are estimated based on a conditional multinomial likelihood, due to individuals that were not observed. Instead, we apply a sequential approach, first estimating the capture probabilities and then the AR(2) coefficients. This allows us to use an explicit sampling model to estimate capture probabilities, instead of assuming that the observed counts have a Poisson or log normal distribution. The given sequential approach is computationally efficient using the R-INLA package which is freely available at [www.r-inla.org](http://www.r-inla.org).

### 2.1 | Statistical background on capture–recapture data

Assume a closed population with a total of  $N$  individuals and a capture–recapture experiment with  $\tau$  capture sessions. Let

$$\mathbf{w}_i = (w_{i1}, \dots, w_{i\tau}), \quad i = 1, \dots, N,$$

denote the capture history for the  $i$ th individual. If  $w_{ij} = 1$ , the individual was captured at the  $j$ th capture session, while  $w_{ij} = 0$  otherwise, that is,  $w_{ij} \sim \text{Bernoulli}(p_{ij})$ ,  $j = 1, \dots, \tau$ . For each individual, the probability of a given capture history is then

$$p_{w_i} = \prod_{j=1}^{\tau} p_{ij}^{w_{ij}} (1-p_{ij})^{1-w_{ij}}, \quad i = 1, \dots, N.$$

Assuming that all individuals are captured independently, the complete likelihood becomes

$$L(N, \{p_{ij}\} | \{w_{ij}\}) = \prod_{i=1}^N \prod_{j=1}^{\tau} p_{ij}^{w_{ij}} (1-p_{ij})^{1-w_{ij}},$$

where both  $N$  and the set of probabilities  $\{p_{ij}\}$  are unknown. Due to the unknown number of noncaptured individuals, computation of the likelihood is unfeasible. This is a well-known problem (Huggins & Hwang, 2011) and requires alternative strategies to perform parameter estimation.

A commonly applied approach is to maximize the conditional likelihood for the  $n$  individuals that were captured at least once. Let  $c_{ik}$ ,  $k = 0, \dots, 2^{\tau} - 1$ , denotes the probability that the capture history of individual  $i$  is equal to category  $k$ . The different categories are defined by all possible permutations of the capture session vector, giving a total of  $m = 2^{\tau} - 1$  categories for the captured individuals.

From here onwards, we will refer to data sets with only two capture events, in which mortality and emigration are disregarded considering capture events on adjacent days. The event that an individual is never captured is then defined as category 0, while the categories 1, 2, and 3 refer to the capture histories (1,0), (0,1), and (1,1), respectively. To perform parameter estimation, we need to make realistic assumptions on the capture probabilities for different capture sessions. Otis et al. (1978) propose a total of eight different models characterizing capture probabilities for different sessions depending on time, behavior, and homogeneity of the individuals, also including combinations of these three factors. Here, we consider a heterogeneity model including a temporal effect, Mth. This implies that the capture probabilities depend on different features of the individuals. Further, we assume that the capture probability on the first and second capture sessions is independent. The probabilities for the different categories are then specified as

$$c_{i0} = (1-p_{i1})(1-p_{i2}), \quad c_{i1} = p_{i1}(1-p_{i2}), \quad c_{i2} = (1-p_{i1})p_{i2}, \quad c_{i3} = p_{i1}p_{i2}, \quad i = 1, \dots, N. \quad (1)$$

To estimate abundance based on individuals that were captured, we use the Horvitz–Thompson estimator (Horvitz & Thompson, 1952)

$$\hat{N} = \sum_{i=1}^n (1-\hat{c}_{i0})^{-1}, \quad (2)$$

where  $\hat{c}_{i0}$  denotes the estimated probability that individual  $i$  was not captured. This probability is estimated using a regression model as explained in the next section.

### 2.2 | A multinomial capture–recapture regression model including a Poisson transformation

An important question in analyzing population processes from capture–recapture data is whether features of the captured individuals give valuable information in further analysis of density dependence. To estimate the probabilities in (2), it is natural to assume a multinomial regression model for the captured individuals, incorporating covariate information which helps to separate different capture categories. We define the vector  $\mathbf{Y}_i' = (Y_{i1}, \dots, Y_{im})$ , where  $Y_{ik} = 1$  for an individual classified to category  $k$ , while the remaining elements of  $\mathbf{Y}_i$  are 0. Each of the vectors  $\mathbf{Y}_1, \dots, \mathbf{Y}_n$  has a multinomial distribution.

Based on (1), probabilities for the  $m = 3$  observed categories are defined by  $\tilde{c}_{ik} = c_{ik} / (1 - c_{i0})$ ,  $k = 1, \dots, m$ , ensuring that the probabilities sum to 1. These probabilities can then be modeled in terms of observed individual features such as weight, sex, and age.

We denote the individual features or covariates by  $\mathbf{z}'_i = (\mathbf{z}_{1r}, \dots, \mathbf{z}_{nr})$ . Further, we define the linear predictor

$$V_{ik} = \sum_{r=1}^v \gamma_{kr} z_{ir}, \quad i = 1, \dots, n, \quad k = 1, \dots, m, \quad (3)$$

where the coefficient  $\gamma_{kr}$  is specific for category  $k$  and covariate  $r$ , while  $v$  is the number of covariates. The scaled probabilities for the captured individuals are then expressed as

$$\tilde{c}_{ik} = \frac{e^{V_{ik}}}{\sum_{k=1}^m e^{V_{ik}}}, \quad i = 1, \dots, n, \quad k = 1, \dots, m. \quad (4)$$

The resulting multinomial likelihood is

$$L_M(\boldsymbol{\gamma}_1, \dots, \boldsymbol{\gamma}_v | \mathbf{y}_1, \dots, \mathbf{y}_n) \propto \prod_{i=1}^n \prod_{k=1}^m (\tilde{c}_{ik})^{y_{ik}}, \quad (5)$$

where  $\boldsymbol{\gamma}'_i = (\gamma_{1r}, \dots, \gamma_{mr})$ ,  $r = 1, \dots, v$ . Notice that in maximizing (5), the denominator of  $\tilde{c}_{ik}$  does not simplify using the ordinary logarithmic transformation. It is therefore common to apply the well-known multinomial Poisson transformation (Baker, 1994) in which the likelihood is rewritten as

$$L_P(\boldsymbol{\gamma}_1, \dots, \boldsymbol{\gamma}_v, \boldsymbol{\beta} | \mathbf{y}_1, \dots, \mathbf{y}_n) \propto \prod_{i=1}^n \prod_{k=1}^m e^{-\mu_{ik}} \mu_{ik}^{y_{ik}}.$$

Here,  $\mu_{ik} = e^{V_{ik} + \beta_i}$  represents the rate of a Poisson distributed random variable  $Y_{ik}$ . The given transformation from a multinomial likelihood to the Poisson likelihood introduces auxiliary parameters  $\boldsymbol{\beta}' = (\beta_1, \dots, \beta_m)$ , in which  $\beta_i$  is proportional to  $\ln(\sum_{k=1}^m e^{V_{ik}})$ . This is just a technical detail to make the approximation work correctly. The likelihood  $L_P(\cdot)$  is proportional to  $L_M(\cdot)$  and gives the same maximum-likelihood estimates for the coefficient vectors  $\boldsymbol{\gamma}_r$ . The resulting regression model is then summarized in terms of linking the expectation of the Poisson variables to the linear predictor using the log transform, that is,

$$\ln(E(Y_{ik})) = \ln(\mu_{ik}) = \sum_{r=1}^v \gamma_{kr} z_{ir} + \beta_i + \epsilon_i, \quad i = 1, \dots, n, \quad k = 1, \dots, m, \quad (6)$$

where  $\epsilon_i \sim N(0, \kappa^{-1})$  denotes small independent random error terms.

In fitting the given model to a data set, the vectors  $\{\boldsymbol{\gamma}_r\}_{r=1}^v$  will not be identifiable. However, in our case we only need estimates of the differences in these coefficients as these represent ratios of log probabilities between the different categories. For categories  $k$  and  $l$ , we notice that

$$\ln\left(\frac{\tilde{c}_{ik}}{\tilde{c}_{il}}\right) = V_{ik} - V_{il} = \sum_{r=1}^v (\gamma_{kr} - \gamma_{lr}) z_{ir}.$$

In estimating the parameters of the model, this implies that the auxiliary parameters and error terms disappear, but these are still included in fitting (6) to a data set. In the case of assuming (1), the estimated individual probabilities are then given by

$$\ln\left(\frac{\hat{\rho}_{i1}}{1 - \hat{\rho}_{i1}}\right) = \sum_{r=1}^v (\hat{\gamma}_{3r} - \hat{\gamma}_{2r}) z_{ir}, \quad (7)$$

$$\ln\left(\frac{\hat{\rho}_{i2}}{1 - \hat{\rho}_{i2}}\right) = \sum_{r=1}^v (\hat{\gamma}_{3r} - \hat{\gamma}_{1r}) z_{ir}, \quad (8)$$

or equivalently

$$\hat{\rho}_{i1} = \frac{e^{\sum_{r=1}^v (\hat{\gamma}_{3r} - \hat{\gamma}_{2r}) z_{ir}}}{1 + e^{\sum_{r=1}^v (\hat{\gamma}_{3r} - \hat{\gamma}_{2r}) z_{ir}}}, \quad (9)$$

$$\hat{\rho}_{i2} = \frac{e^{\sum_{r=1}^v (\hat{\gamma}_{3r} - \hat{\gamma}_{1r}) z_{ir}}}{1 + e^{\sum_{r=1}^v (\hat{\gamma}_{3r} - \hat{\gamma}_{1r}) z_{ir}}}. \quad (10)$$

These probabilities are then used to estimate  $\hat{c}_{i0}$  in (2).

### 2.3 | Implementation using a Bayesian framework

To fit (6) to a data set and estimate the capture probabilities, we choose to apply a Bayesian approach. This implies that all parameters in (6) are viewed as random variables. Specifically, the resulting regression model can be incorporated within the computational framework of latent Gaussian models. This is a flexible class of three-stage hierarchical models, which can be analyzed in a unified way using INLA. Subsequently, the model in (6) is reformulated in terms of having conditionally independent observations, given a latent field and hyperparameters.

The three stages of a latent Gaussian model are expressed as follows, where  $\pi(\cdot)$  is generic notation for probability densities:

1. The first stage specifies the likelihood where the observations are assumed conditionally independent given a latent field  $\mathbf{x}$  and hyperparameters  $\boldsymbol{\theta}$ . In our case, let  $\mathbf{y}' = (\mathbf{y}'_1, \dots, \mathbf{y}'_n)$  denote the stacked vector of the  $m$  categories for the  $n$  individuals. The likelihood is then expressed as

$$L(\mathbf{x}, \boldsymbol{\theta} | \mathbf{y}) = \prod_{i=1}^{nm} \pi(y_i | x_i, \boldsymbol{\theta}).$$

2. The latent field  $\mathbf{x}$  collects all random variables of the linear predictor

$$\mathbf{x} = \{\boldsymbol{\gamma}_1, \dots, \boldsymbol{\gamma}_v, \boldsymbol{\beta}, \boldsymbol{\epsilon}\} \quad (11)$$

where we could also include the predictor itself. The latent field models the dependency structure of the observations and is assigned a multivariate Gaussian prior

$$\pi(\mathbf{x}|\boldsymbol{\theta}) \sim N(\mathbf{0}, \mathbf{Q}^{-1}(\boldsymbol{\theta})).$$

The precision (inverse covariance) matrix  $\mathbf{Q}$  is typically sparse such that  $\mathbf{x}$  has Markov properties and is then referred to as a Gaussian Markov random field.

3. The hyperparameters  $\boldsymbol{\theta}$  of a latent Gaussian model are usually assigned non-Gaussian priors. Here, we only have one hyperparameter being the precision parameter of the random error terms,  $\theta = \kappa$ . This parameter is assigned a penalized complexity prior (Simpson, Rue, Riebler, Martins, & Sørbye, 2017), implying that  $\kappa^{-1/2}$  has an exponential density.

The joint posterior for all elements of the latent field and the additional hyperparameter is then described as

$$\pi(\mathbf{x}, \theta | \mathbf{y}) \propto \prod_{i=1}^{nm} \pi(y_i | x_i, \theta) \pi(\mathbf{x} | \theta) \pi(\theta).$$

The main interest is to calculate the marginal posteriors for each of the latent field components and each of the hyperparameters.

For the multinomial model, INLA is used to estimate the marginal posteriors for all the coefficients

$$\pi(y_{kr} | \mathbf{y}), \quad k = 1, \dots, m, \quad r = 1, \dots, v.$$

These provide posterior mean estimates of the differences  $\gamma_{kr} - \gamma_{lr}$ , which are used to estimate the individual capture probabilities and the abundance by (2).

## 2.4 | Estimating density dependence

Our final step is to fit a process model to study population dynamics of a species. Specifically, we focus on estimating density dependence by fitting an AR(2) model to a given time series, reflecting the population cycle for the relevant species. Let  $\ln(N_t)$  denote the true log abundance at time  $t$ . The AR(2) model is then defined by

$$\ln(N_t) = \ln(\eta) + \phi_1 \ln(N_{t-1}) + \phi_2 \ln(N_{t-2}) + \epsilon_t, \quad t = 1, \dots, T, \quad (12)$$

where  $\ln(\eta)$  denotes an offset, while the noise terms are independent Gaussian variables,  $\epsilon_t \sim N(0, \sigma_\epsilon^2)$ .  $T$  denotes the length of the time series, while the coefficients  $\phi_1$  and  $\phi_2$  characterize the direct and delayed density dependence of the series. The given process is stationary when  $-1 \leq \phi_2 \leq 1 - |\phi_1| < 1$  and has pseudoperiodic behavior when  $\phi_1^2 + 4\phi_2 \leq 0$ . Estimation of the coefficients of AR(2) is

not influenced by the offset  $\ln(\eta)$ . This implies that if the number of captured individuals at different time points is proportional to the underlying true abundance, we would get identical parameter estimates.

The AR(2) model is fitted within the framework of latent Gaussian models using INLA. In this case, the model has three hyperparameters, including  $\kappa = \sigma_\epsilon^{-2}$  and the coefficients  $\phi_1$  and  $\phi_2$ . These parameters are all assigned PC priors (Simpson et al., 2017; Sørbye & Rue, 2017). Of main interest is to study how the estimates of  $\phi_1$  and  $\phi_2$  vary when capture heterogeneity is accounted for using the multinomial observational model.

Often, simplifying assumptions regarding the data generating process are made, for example, by assuming a Poisson process (Stenseth et al., 2003) or a log-normal distribution (Santin-Janin et al., 2014) for the observed counts. These assumptions can be implicit while defining the observation models in state-space approaches. We study the Poisson distribution assumption in an additional step also fitted using INLA. The log rate of the assumed underlying Poisson process for the abundance is expressed in terms of the linear predictor

$$\lambda_t = \ln(E(N_t)) = \beta_0 + \epsilon_t, \quad t = 1, \dots, T. \quad (13)$$

Here,  $\beta_0$  denotes an intercept, while  $\epsilon_1, \dots, \epsilon_T$  denotes independent and identically distributed random variables,  $\epsilon_t \sim N(0, \kappa_\epsilon^{-1})$ . These error terms are included to model random variation as a function of time. As detailed in the next section, the AR(2) model will be fitted either to the estimated log abundance  $\ln(\hat{N}_1), \dots, \ln(\hat{N}_T)$  or to the posterior means of the log rates of the corresponding Poisson process, denoted  $\hat{\lambda}_1, \dots, \hat{\lambda}_T$ .

## 3 | SIMULATION STUDY COMPARING METHODS TO ESTIMATE DENSITY DEPENDENCE

This section provides an extensive simulation study to assess how the inclusion of capture history information influences estimation of density dependence. We start by simulating data to approximate a realistic capture–recapture sampling scenario. The underlying log population of the sampled species is generated as an AR(2) process in time, using different fixed combinations of the coefficients ( $\phi_1, \phi_2$ ) and the innovation variance  $\sigma_\epsilon^2$ , from here onwards referred to as the (population) process variance. Each resulting individual is then assigned a random weight, and a two-day capture history according to a multinomial model with probabilities defined by (1). We then fit an AR(2) process model to the estimates of log abundance or log rates obtained by different methods. These different methods are described in Section 3.1, while Section 3.2 specifies the simulation procedure and the method performance criteria used. Finally, Section 3.3 provides simulation results and an evaluation of the different methods.

### 3.1 | Estimation methods

An overview of the different estimation methods used in the simulation study is given in Figure 1. The left-hand side of the figure shows the additional steps needed to implement the observation model, incorporating sampling error in terms of capture history information. We employ two methods of estimating individual capture probabilities. The first is described in Sections 2.2 using INLA (method: CR-INLA) and corresponds to our suggested approach. The second, for comparison, estimates individual capture probabilities using the R-package VGAM (Yee, 2019). Among other utilities, the VGAM (vector generalized additive model) framework can be used to analyze closed population capture–recapture data, allowing the incorporation of individual covariates while using the conditional likelihood (Yee, Stoklosa, & Huggins, 2015). This application of VGAM allows for a flexible and efficient estimation of capture probabilities for all of the eight heterogeneity models given by Otis et al. (1978) (method: CR-VGAM). From the estimated capture probabilities from either of the two methods, we proceed to estimate the true log abundance using the Horvitz–Thompson estimator in (2). At this point, we have two possible variants in estimating density dependence: We either fit the AR(2) model to the times series of estimated log abundance  $\{\ln(\hat{N}_t)\}_{t=1}^T$

(A variant), or we fit the AR(2) model to the corresponding estimated log rate of a Poisson process,  $\{\hat{\lambda}_t\}_{t=1}^T$  (P variant). The right-hand side of Figure 1 illustrates the approach disregarding capture history, fitting the AR(2) model directly to the observed log counts, or to the log rate of the corresponding Poisson process (method: ObsCount). Finally, the performance of the different estimation methods is compared with the results fitting the AR(2) model to the true generated log abundance or estimated log rate (method: Baseline).

### 3.2 | Simulation procedure

For each combination of AR(2) coefficients,  $(\phi_1, \phi_2)$ , we generated  $M = 200$  time series. Specifically, we chose  $\phi_1 \in (-1, -0.5, 0, 0.5, 1)$  and  $\phi_2 \in (-0.8, -0.5, -0.2)$ , giving a total of fifteen combinations of the coefficients. These combinations ensure that the resulting generated time series were stationary, also having pseudoperiodic behavior. To investigate the effect of varying the process variance of the AR(2) process, we further compared density-dependence estimates for the values  $\sigma_\epsilon^2 \in (0.04, 0.08, 0.16, 0.32, 0.64)$ . The details of the simulation procedure can be described in the following steps:

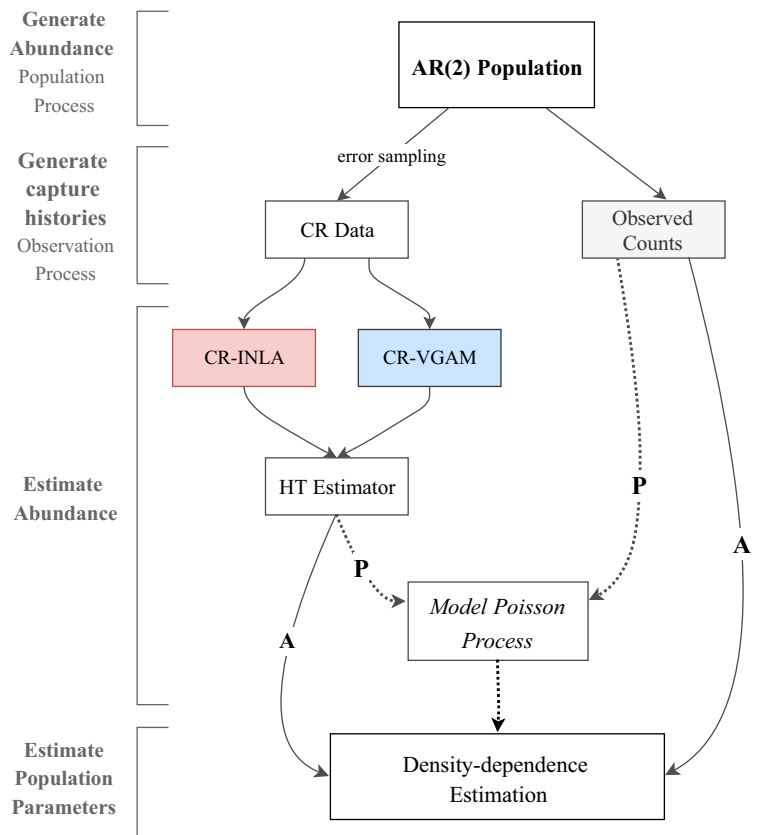


FIGURE 1 Methodological flowchart



Method	$\sigma_\epsilon^2$	Coverage				RMSE			
		$\phi_1$		$\phi_2$		$\phi_1$		$\phi_2$	
		A	P	A	P	A	P	A	P
Baseline	0.04	0.91	0.85	0.88	0.86	0.21	0.40	0.20	0.36
CR-INLA	0.04	0.83	0.87	0.80	0.85	0.27	0.38	0.27	0.35
CR-VGAM	0.04	0.80	0.83	0.77	0.83	0.29	0.40	0.28	0.37
ObsCount	0.04	0.77	0.81	0.75	0.82	0.31	0.42	0.29	0.38
Baseline	0.08	0.91	0.92	0.89	0.90	0.20	0.26	0.20	0.25
CR-INLA	0.08	0.87	0.89	0.85	0.87	0.25	0.27	0.24	0.26
CR-VGAM	0.08	0.86	0.88	0.84	0.86	0.26	0.29	0.25	0.27
ObsCount	0.08	0.84	0.87	0.82	0.85	0.27	0.31	0.26	0.29
Baseline	0.16	0.92	0.91	0.88	0.88	0.20	0.22	0.20	0.21
CR-INLA	0.16	0.89	0.89	0.86	0.86	0.23	0.24	0.22	0.23
CR-VGAM	0.16	0.88	0.88	0.86	0.85	0.24	0.25	0.23	0.24
ObsCount	0.16	0.87	0.88	0.85	0.85	0.24	0.25	0.23	0.24
Baseline	0.32	0.91	0.91	0.88	0.88	0.21	0.21	0.20	0.21
CR-INLA	0.32	0.89	0.89	0.86	0.87	0.23	0.23	0.22	0.22
CR-VGAM	0.32	0.88	0.88	0.87	0.86	0.23	0.23	0.22	0.23
ObsCount	0.32	0.88	0.88	0.86	0.86	0.23	0.24	0.23	0.23
Baseline	0.64	0.91	0.90	0.89	0.87	0.21	0.22	0.20	0.21
CR-INLA	0.64	0.88	0.88	0.85	0.85	0.23	0.23	0.22	0.22
CR-VGAM	0.64	0.88	0.87	0.84	0.84	0.23	0.23	0.23	0.23
ObsCount	0.64	0.87	0.87	0.84	0.84	0.23	0.24	0.23	0.23

**TABLE 1** The estimated average coverage and RMSE for all combinations of  $(\phi_1, \phi_2)$  in the four methods, using five levels of  $\sigma_\epsilon^2$ . The AR(2) process was either fitted to the log abundance (A) or the log rate of the corresponding Poisson process (P)

1. Generate the series  $\{\ln(N_t)\}_{t=1}^T$  according to (12) where  $T = 20$ , using different fixed combinations of  $(\phi_1, \phi_2)$ . To remove the effect of sample size on the estimation of capture probability, we assumed that  $E(N_t) = 20$  by using an offset  $\ln(\eta) = \ln(20) - \frac{1}{2}\text{Var}(\ln(N_t))$ . The series was rounded to give integer values for  $\{N_t\}_{t=1}^T$ , representing the abundance of an animal population. The total number of individuals generated for one simulated AR(2) process was then  $\tilde{N} = \sum_{t=1}^T N_t$ .
2. For each of the  $\tilde{N}$  individuals, we generated a random weight

$$z_{it} | \mu_t \sim \text{Log normal}(\ln(\mu_t), \ln(\sigma_w)),$$

where  $\sigma_w = 1.2$ , while  $\mu_t \sim \text{Log normal}(\ln(30), \ln(5))$ . The weight was then scaled by the sample standard deviation of the generated weights to make it dimensionless. The resulting variable was used as an individual-specific covariate in (3). In this context, weight is a proxy for detectability. We varied the expected value of weight with time to model varying detectability, reflecting changes in the composition of the population at different time points. Thus, the varying mean reflects biological variation which we considered more realistic than assuming constant capture probabilities for different time points. The parameters relating to the weight distribution were here chosen to illustrate this biological variation.

3. Assume a temporal effect  $M_{th}$  for the capture–recapture process with  $\tau = 2$ . To assign a capture history to each individual, we first assumed that the capture probabilities for days 1 and 2 were  $p_{11} \equiv p_1 = 0.55$  and  $p_{12} \equiv p_2 = 0.75$  for the total generated population. These probabilities were used to find reasonable values for the specific coefficients for the observed categories in terms of

$$\gamma_{31} - \gamma_{21} = \ln\left(\frac{p_1}{1-p_1}\right) \text{ and } \gamma_{31} - \gamma_{11} = \ln\left(\frac{p_2}{1-p_2}\right).$$

The final individual capture probabilities were then computed according to (9)–(10) including the generated random weight as a covariate, implying  $v = 1$ .

4. Remove individuals with capture history according to category 0 (undetected).
5. Estimate abundance using each of the methods described in Section 3.1 and fit an AR(2) model to the resulting time series including both the A and P variants.

The choices made in this simulation study intended to approximate the characteristics of a real ecological data set. Specifically,

we have chosen to simulate rather short time series, having similar length as the real data set used in Section 4. Also, the initial capture probabilities for day 1 and day 2 were close to the proportions of captured individuals in the real data set (being 0.55 and 0.77, respectively).

Our next step was to apply INLA and fit the AR(2) process model to the generated time series. This provided estimates of the marginal posterior distributions for the two AR coefficients  $\phi_1$  and  $\phi_2$ , for all approaches. Based on the posterior distributions, we could then calculate summary statistics, including the posterior mean of the coefficients, the standard deviations, and credible intervals. To evaluate and compare the quality of the different density-dependence estimates, we computed the estimated root mean-squared error (RMSE), defined by

$$\text{RMSE}(\hat{\phi}_k) = \sqrt{\frac{1}{M} \sum_{i=1}^M (\hat{\phi}_k - \phi_k)^2}, \quad k = 1, 2.$$

Here,  $\hat{\phi}_k$  denotes the posterior mean estimate of the  $k$ th AR coefficient and  $\phi_k$  denotes the true value of that coefficient, while  $M$  is the number of simulations. We also compared the frequentist coverage properties using the different approaches. This corresponded to finding the proportion of times the true AR coefficient was inside the  $M$  estimated 95% credible intervals. This means we would expect a coverage of 0.95 for an unbiased AR coefficient estimator.

### 3.3 | Simulation results

Table 1 displays the average performance in terms of coverage and RMSE for the different methods used to estimate density dependence, including the two variants A and P. The averages were computed across all the given combinations of  $(\phi_1, \phi_2)$  and for each of the five fixed values of  $\sigma_e^2$ . Due to the short time-series length, coverage using the Baseline method will not achieve the nominal level of 0.95 (only nominal for the A variant). It is well known that estimators for the coefficients of AR processes are biased for small sample sizes (Shaman & Stine, 1988). Furthermore, the Baseline method for the P variant is not optimal considering it is based on the true log counts rather than alternatively generating true log rates of a Poisson process.

The differences for the different methods were rather small, except for the two lowest process variance levels where there was a clear benefit from including capture history. CR-INLA provided the highest coverage, followed by CR-VGAM and ObsCount. Using CR-INLA, the coverage was within the range (0.83–0.89) for  $\phi_1$  and within the range (0.80–0.86) for  $\phi_2$ . Further, the results indicated that fitting the AR(2) model to the log rate of a Poisson process (P variant) provided generally higher coverage than using the A variants. When comparing the different methods using RMSE, which considers both bias and variance, we see that CR-INLA had the smallest error in all cases, while the method ObsCount had the largest error. Again, the

differences between the methods were very small except for the lowest levels of the process variance. In general, RMSE was reduced for all methods as the process variance increased. Moreover, RMSE was higher for the P variants compared with the A variants at the two lowest process variance levels, using all methods. This was due to both an increased variance and bias, which explains why the P variants had higher coverage.

The estimation bias of the different methods can be assessed explicitly in Figure 2, containing the posterior mean estimates ( $\hat{\phi}_1, \hat{\phi}_2$ ) for each of the fixed combinations. The figure includes point estimates both using the A variant (left-hand side) and P variant (right-hand side) of the different methods. Here, the results refer to  $\sigma_e^2 = 0.08$  (upper panels) and  $\sigma_e^2 = 0.32$  (lower panels). The corresponding results using the other variance levels are given in the supplementary material (Figures S1–S9). For the two lowest levels of process variance, the estimation bias using CR-INLA was slightly lower than using the other methods for all combinations of  $(\phi_1, \phi_2)$ . When the process variance was increased, the different methods gave approximately the same point estimates. The bias was slightly larger using the P variants compared with the A variants. This was in correspondence with the higher averages of the RMSE values for the P variants, as already observed.

To further study coverage and RMSE for each of the 15 combinations, we computed a joint coverage being the proportion of times both of the estimated 95% credible intervals contained  $\phi_1$  and  $\phi_2$ , respectively. We also computed a joint RMSE for both parameters, defined by

$$\text{RMSE}(\hat{\phi}_1, \hat{\phi}_2) = \sqrt{\frac{1}{M} \sum_{i=1}^M \sum_{k=1}^2 (\hat{\phi}_k - \phi_k)^2}.$$

The results for coverage and RMSE are shown in Figures 3 and 4, respectively. Our results showed that the coverage was smallest and RMSE is largest when  $|\phi_1| = 1$  in most combinations of the AR coefficients. CR-INLA was seen to give the highest coverage and lowest RMSE for most of the combinations when  $\sigma_e^2 = 0.08$ , at least for the A variants. When  $\sigma_e^2 = 0.32$ , the results were very similar for all methods.

In summary, we can conclude that including capture history information improved the estimation of density dependence in process models having low process variance. Out of the tested methods, our suggested approach CR-INLA performed best, followed by CR-VGAM. For the given simulated data, the additional step of estimating log rates of a Poisson process resulted in larger RMSE.

Finally, we notice that both of the two AR coefficients were underestimated, and this bias increased with the absolute values of the coefficients.

The given simulation study was based on certain choices to illustrate a capture–recapture scenario using an AR(2) process model. Here, we have assumed independent capture probabilities for the two capture sessions. The given approach could have easily been adapted to other models given by Otis et al. (1978), such as to also include a behavioral effect. Longer time series would have improved the estimation results using all of the suggested methods, albeit being less realistic from an ecological point of view.

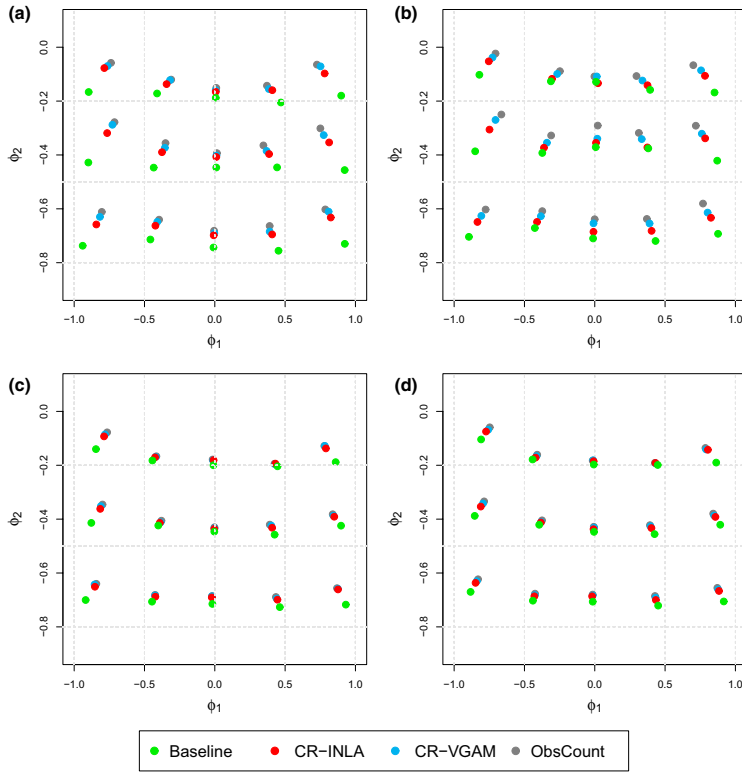


**FIGURE 2** Posterior mean estimates of  $\phi_1$  and  $\phi_2$ , for the A variants on the left (panels a and c) and P variants on the right (panels b and d). The points of intersection of the dotted gray lines correspond to the true parameter values. The intersections, at which each set of dots lean to, correspond to the true value of that given set. Panels a and b show results when  $\sigma_c^2 = 0.08$ , whereas c and d correspond to  $\sigma_c^2 = 0.32$

## 4 | ESTIMATING DENSITY DEPENDENCE USING A REAL DATA SET

In this section, we estimated density dependence for a real capture–recapture data set of small mammals, collected at 20 different spatial locations over a period of 18 years. Our main focus was to assess density-dependence estimates, studying how inclusion of capture history influenced the estimation. Using the CR-INLA approach, we estimated capture probabilities by the regression model in (6), including individual-specific covariate information and random effects. We proceeded to estimate the true abundances at each time point for each spatial location using (2). Finally, we fitted the AR(2) model to estimate density dependence and compared the results with using the methods CR-VGAM and ObsCount. For all three methods, we assessed both the A and P variants.

### 4.1 | Data description

The data included a total of 3,090 gray-sided voles, captured alive in the Porsanger region (latitude 70°N), in Northern Norway. The data were collected at 20 different stations, spaced evenly along 155 km of road (see Figure 5), in the period 2000–2017. Sampling was conducted twice a year, in spring and fall, and each capture session

consisted of two visits. Two individual-specific variables were recorded, including *weight* and *sex*. Animals captured dead during the first trapping session were excluded from the analysis.

### 4.2 | Observation model selection, estimating capture probabilities

To estimate individual capture probabilities, we used the whole data set across time points and stations. Our first step was to select a reasonable observation model. Fitting the regression model in (6), we considered inclusion of the following variables

1. *Weight* (continuous standardized variable);
2. *Sex* (categorical variable for male or female);
3. *Season* (categorical variable for spring or fall);
4. *Station* (index variable for the evenly spaced stations);
5. *Time* (index variable for year)

To select which variables should be included, we evaluated different models using various information criteria. When applying CR-INLA, we used the estimates for the deviance information criterion (DIC) (Spiegelhalter, Best, Carlin, & van der Linde, 2002) and Watanabe–Akaike’s information criterion (WAIC) (Watanabe, 2010). When using CR-VGAM, we used the estimates of Akaike’s

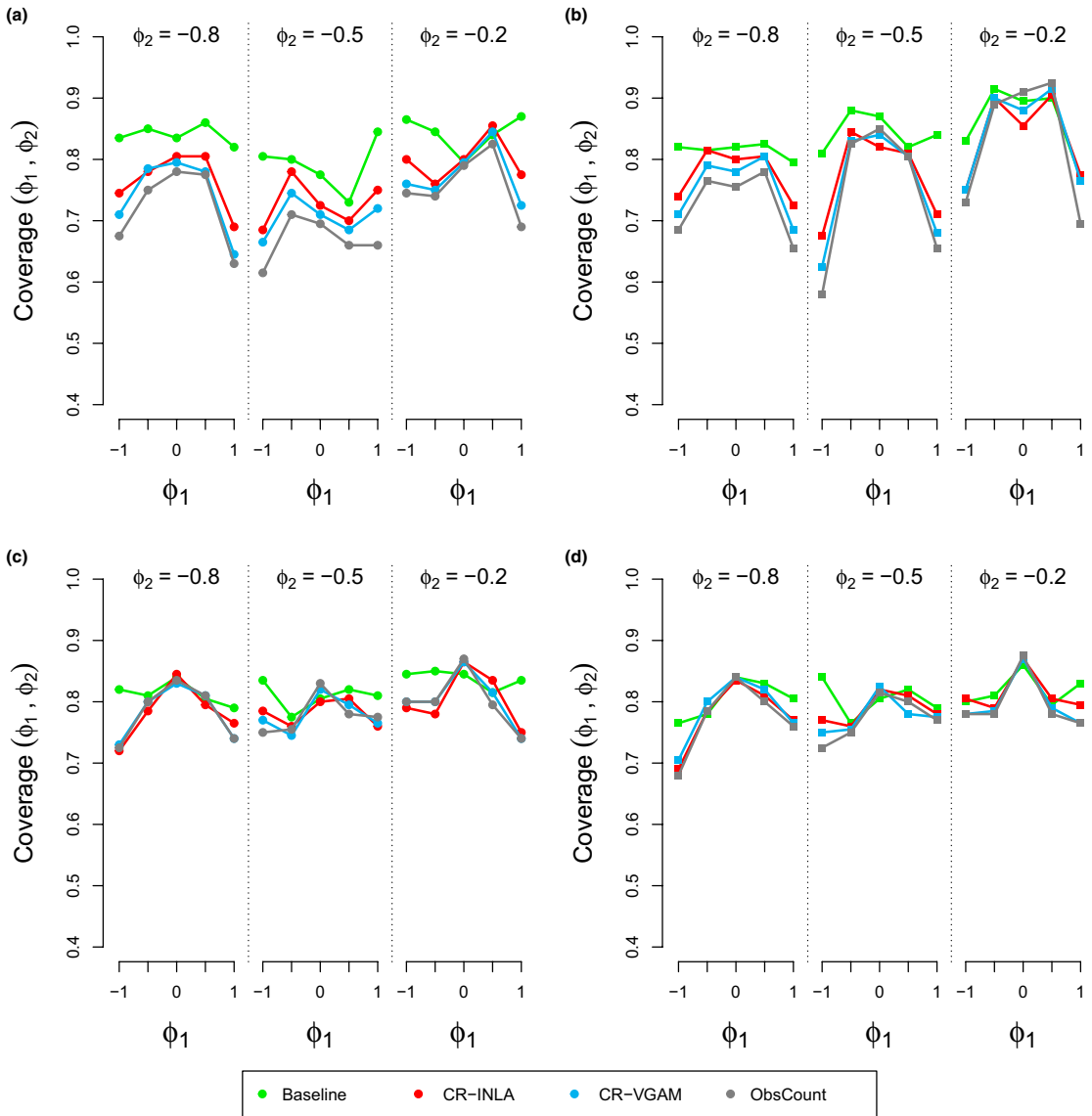


**FIGURE 3** Joint coverage for different combinations of  $(\phi_1, \phi_2)$  for  $\sigma_e^2=0.08$  (panels a and b) and  $\sigma_e^2=0.32$  (panels c and d). A variants are represented on the left (panels a and c) and P variants on the right (panels b and d). The results were split into 3 sets ( $\phi_2 \in (-0.8, -0.5, -0.2)$ ), where each set includes the coverage results for  $\phi_1 \in (-1, -0.5, 0, 0.5, 1)$

information criterion (AIC) (Akaike, 1973) and the Bayesian information criterion (BIC) (Schwarz, 1978).

An overview of the different models and the estimated information criteria is shown in Table 2, comparing the two methods for a total of 8 different models. The VGAM package does not allow for inclusion of random effect terms (Yee et al., 2015), which implies that *Time* could not be included in the CR-VGAM model explicitly. Using INLA, we can straightforwardly include nonlinear effects of covariates. Applying the

method CR-INLA, we chose to model *Time* as a first-order random walk process (rw1) (Rue & Held, 2005; Sørbye & Rue, 2014). Also, we considered to include *season* as a categorical covariate, both using CR-INLA and CR-VGAM. However, using the CR-INLA approach, *season* is not included simultaneously with *time* to avoid confounding.

The resulting optimal observation model for CR-INLA, minimizing both DIC and WAIC, included all variables except *season*. The linear predictor as defined by (6) is here given by

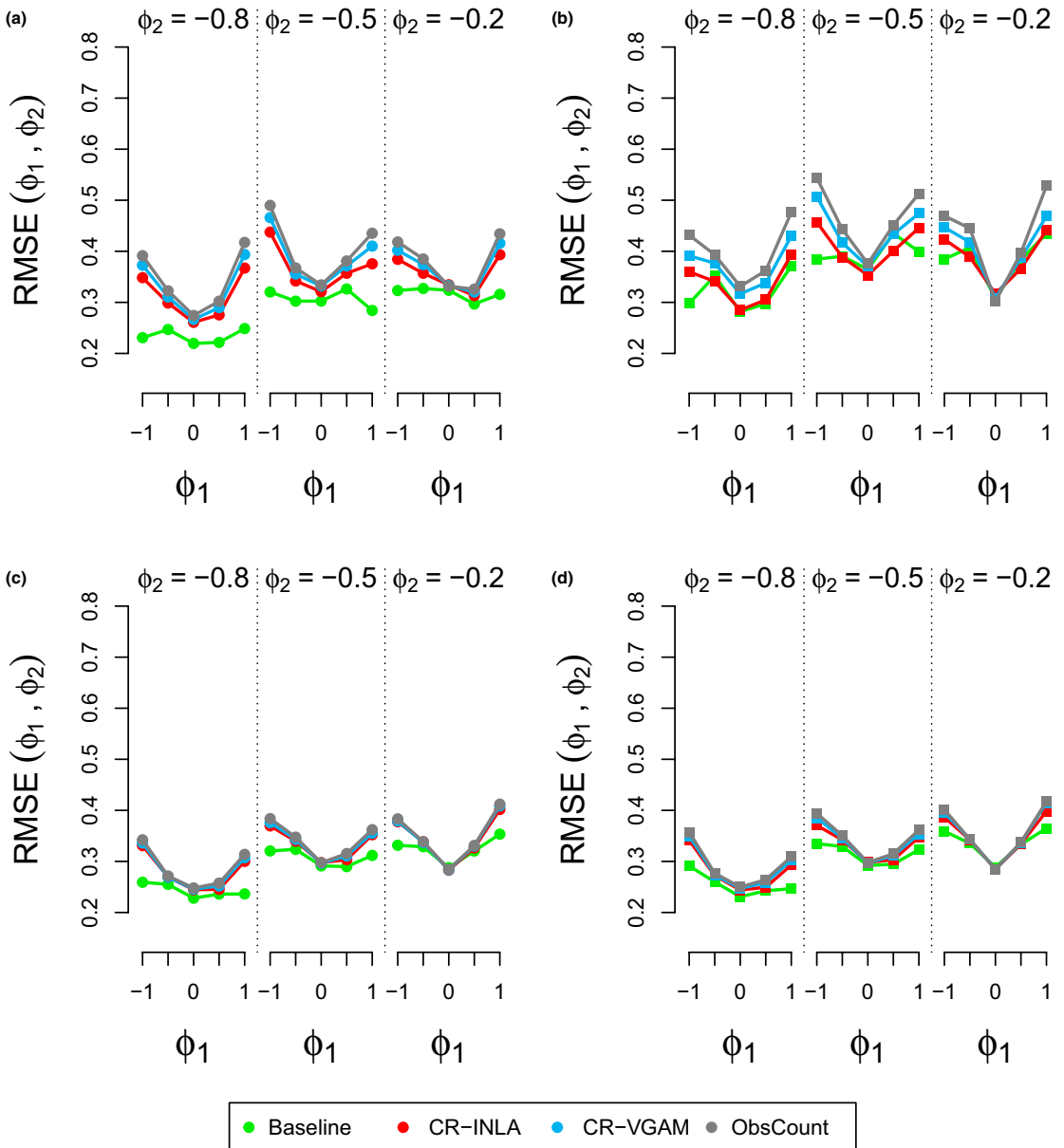


**FIGURE 4** Joint RMSE for different combinations of  $(\phi_1, \phi_2)$  for  $\sigma_\epsilon^2 = 0.08$  (panels a and b) and  $\sigma_\epsilon^2 = 0.32$  (panels c and d). A variants are represented on the left (panels a and c) and P variants on the right (panels b and d). The results were split into 3 sets ( $\phi_2 \in (-0.8, -0.5, -0.2)$ , where each set includes the RMSE results for  $\phi_1 \in (-1, -0.5, 0, 0.5, 1)$ )

$$\ln(E(Y_{ik})) = \ln(\mu_{ik}) = \gamma_{k1} \text{weight}_i + \gamma_{k2} \text{sex}_i + \gamma_{k3} \text{station}_i + f(\text{time}_i) + \beta_i + \epsilon_i, \quad i = 1, \dots, n, \quad k = 1, \dots, 3,$$

where  $f(\text{time}_i)$  denotes the rw1 model, specifying a nonlinear random effect of time. In selecting an observation model for the CR-VGAM approach, we observed rather small differences in the values of the goodness-of-fit criteria for the different models. The optimal observation model according to AIC included *weight* and *sex*, while

BIC was minimized when only *weight* was included. In the case of vole species, *sex* is known to have an effect on detectability (Bryja et al., 2005), so we chose to include both *weight* and *sex* in estimating the capture probabilities.

Figure 6 illustrates the distributions of the estimated capture probabilities for the two capture sessions,  $\{\hat{p}_{i1}\}_{i=1}^n$  and  $\{\hat{p}_{i2}\}_{i=1}^n$ , using both CR-INLA and CR-VGAM. The mean capture probability

**FIGURE 5** Stations distribution in Northern Norway, from Lillefjord to Karasjok. The station numbering goes along the north/south gradient, with station 1 being near Lillefjord and station 20 near Karasjok. This map was obtained from Google Maps

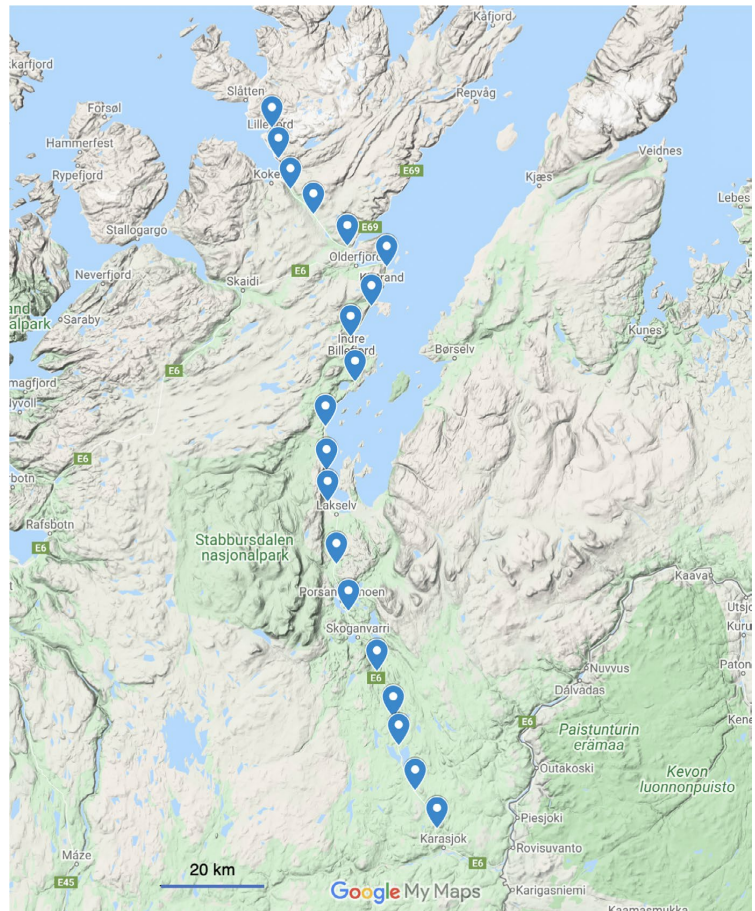


**TABLE 2** Observation model selection for CR-INLA and CR-VGAM, using the selected information criteria. All values are given in comparison with the intercept model (1) for easier visualization. The lowest scores represent the best models, compromising goodness of fit with model complexity

Model	Covariates	CR-INLA		CR-VGAM	
		DIC	WAIC	AIC	BIC
1	Intercept	19,400	19,613	6,568	6,580
2	Weight	-149	-158	-8	-2
3	Weight + sex	-199	-217	-12	0
4	Weight + sex + season	-223	-242	-11	+8
5	Weight + sex + station	-213	-232	-10	+7
6	Weight + sex + time	-254	-278	-	-
7	Weight + sex + season + station	-249	-269	-9	+15
8	Weight + sex + station + time	-275	-300	-	-

is seen to increase on the second day using both methods. CR-VGAM gave higher estimates of the capture probabilities, having a low variance for both days. Using CR-INLA, the estimated individual capture probabilities showed more heterogeneity, having a larger variance for both days. Using the given estimated capture

probabilities for the observed categories, we can estimate the probability that an individual is never captured, corresponding to category  $c_{i0}$  in (1). The resulting 95% percentile interval for  $c_{i0}$  was (0.19–0.32) using CR-INLA. Using CR-VGAM, the corresponding interval was (0.08–0.12).

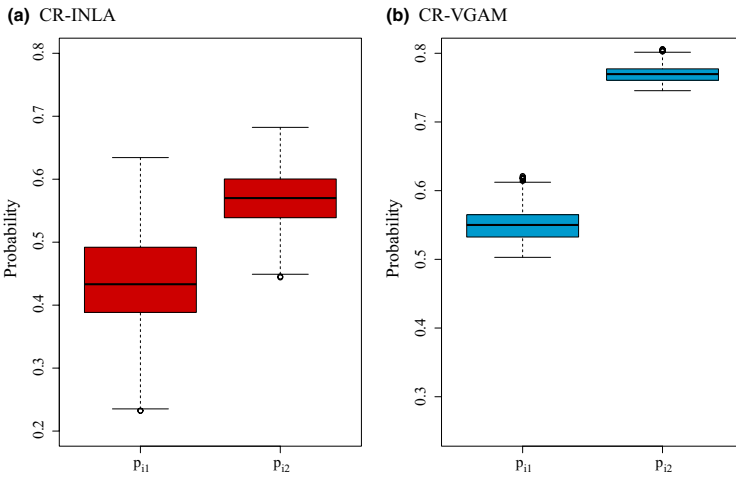


**FIGURE 6** Estimates for  $p_1$  and  $p_2$  for the CR-INLA (panel a) and CR-VGAM (panel b) models

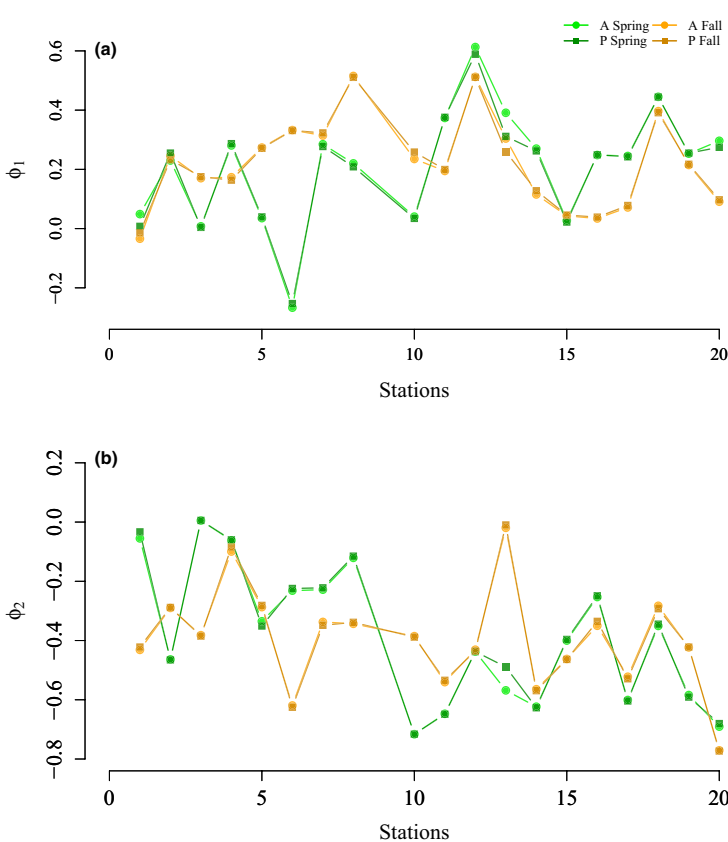


**FIGURE 7** Estimates for  $\phi_1$  (panel a) and  $\phi_2$  (panel b) for the mean coefficients of both A and P variants, for the spring (green hue) and fall (orange hue) seasons separately

#### 4.3 | Fitting the AR(2) process model to estimate density dependence

Given the estimates of the capture probabilities for each individual, we used the Horvitz-Thompson estimator to compute abundance at

each time point for each station. We then fitted the AR(2) model to the resulting estimated log abundance, providing estimates of both direct and delayed density dependence. We split the time series into spring and fall, to account for a possible seasonal influence in the parameter estimation. This resulted in two time series of length

$T = 18$  for each of the 20 stations. The AR(2) model was fitted using the three presented methods (CR-INLA, CR-VGAM, and ObsCount) using both the A and P variants. Station 9 did not have enough observations for the parameters to be estimated and was thus not included in the results.

The main results are displayed in Figure 7, showing the posterior mean estimates of the AR coefficients for the two seasons, for variants A and P. The estimates of both direct and delayed density dependence were very similar using all the given methods and were thus lumped together (see Figures S11 and S12 for detailed values). Interestingly, the differences seen in the capture probability estimates between CR-INLA and CR-VGAM do not seem to have influenced the density-dependence estimates. This is in correspondence with the simulation study in Section 3, as the process variance  $\sigma_\epsilon^2$  for all of the stations was quite high, with the overall estimated average being  $\hat{\sigma}_\epsilon^2 = 0.9$ . This value likely corresponds to an overestimation of  $\sigma_\epsilon^2$ , with the true average being likely significantly lower and closer to 0.6 (see Figure S10 for bias estimates at different variance levels). In both spring and fall, the estimates of  $\phi_1$  varied from around  $-0.25$  to 0.6, whereas the estimates of  $\phi_2$  ranged from around 0 to  $-0.8$ . For all stations, except 3 and 13, the estimated time series showed a semi-periodic behavior. We also notice that the AR(2) coefficients varied with season for the same station, which suggests a seasonal effect in the density dependence. Additionally, during both seasons, the results indicate a decreasing trend in the value of  $\phi_2$  along the given transect (from coast to inland).

## 5 | DISCUSSION

The main goal of this paper was to assess the importance of including capture heterogeneity in the estimation of density dependence, thus incorporating sampling error in the observation model. To investigate this, we performed an extensive simulation study in which we generated AR(2) time series, representing the true log abundance of an animal population, and simulated a CR sampling scenario from that population. We then tested the performance of different methods, both including capture history information and disregarding it. For the first method, CR-INLA, we defined an observation model to estimate individual capture probabilities through a multinomial likelihood and followed it with a Horvitz-Thompson estimate of the true abundance. The second method, CR-VGAM, used the existing VGAM methodology to estimate abundance from CR data, establishing it as a control method. Finally, we compared these two methods with a simple (yet common) approach, disregarding the capture history information (effectively assuming a homogeneous capture process), to estimate the true autoregressive coefficients from the observed counts directly. We further investigated the assumption of using a Poisson distribution for the capture data, fitting the AR(2) process to the estimated log rates. This was chosen as an example of an observation model used in the ubiquitous state-space models, where the observation model typically assumes some type of homogeneous capture process, such as Poisson or log normal.

Based on our simulation study, we found that incorporating capture history information was important in estimating density dependence for AR(2) models with process variance below 0.16. In such scenarios, both methods including capture history outperformed the method disregarding it, with reduced estimation bias and improved parameter coverage (8% higher in CR-INLA (A) compared with ObsCount (A) for the lowest tested process variance; see Table S1). However, in scenarios with a large process variance, the methods that estimated capture probability did not stand out, producing extremely similar results compared with the observed counts approach. Furthermore, parameter estimates for both AR coefficients were generally biased toward 0, using all the methods, increasingly underestimating the absolute values of the parameters. In the context of quasi-periodic dynamics described by an AR(2) process, this means underestimating the strength of direct  $\phi_1$  and delayed  $\phi_2$  density dependence, and overestimating the process variance of the AR(2) model (see Figure S10).

The data collected in Porsanger showcased vole populations with very large fluctuations in abundance, as is typical of such systems (Cornulier et al., 2013; Henttonen & Hanski, 2000). Moreover, the estimated capture probabilities were relatively high, resulting in a relatively small bias when comparing the observed counts and the estimated abundance. This resulted in all methods, and respective variants, producing similar results—this could have been expected given the observation variance is, in that case, only a minor component of the total variance. Other populations, such as large mammals, may show much smaller abundance fluctuations and therefore a larger contribution of the observation error to the total variance (e.g., Besbeas & Morgan, 2019). Moreover, in the case of other animal groups, such as snakes, capture probabilities are often very low (Rose, Wylie, Casazza, & Halstead, 2018), and could potentially lead to a larger bias corrections in density-dependence estimates by accounting for capture heterogeneity (Fletcher et al., 2011), although we do not explicitly test this in this paper.

Extending our approach to other observation process models (e.g., spatial capture–recapture models (Royle, Fuller, & Sutherland, 2017), including individual heterogeneity (Efford & Mowat, 2014), would provide a general approach to reducing biases in population dynamic models. One disadvantage of the CR-INLA method is that it would be cumbersome to apply in CR data sets with more than 3 days, given the data expansion necessary to fit multinomial likelihoods in INLA, where all the category combinations, observed and not, must be present. This could potentially be automatized as in Bayesian fitting of capture–mark–recapture models (McCrea, 2014).

Two limitations of our simulation study were pointed out during the revision process of this manuscript. Given the complex nature of the simulation setup, involving 4 methods in 2 variants, and 75 combinations of parameters, the running time proved to be lengthy. Even when running in parallel, we needed roughly 150 hr to obtain the full results, from running 200 simulations per unique combination of parameters. Time thus became a constraint and prevented us from running a higher number of simulations, such as 500 or even 1,000. Nonetheless, we believe our results show true patterns as we



noticed early convergence in both coverage and RMSE, from around 50 simulations. Moreover, because we decided to split the results by process variance level, our aggregated averages, displayed in Table 1, combine 3,000 simulations for each method. In addition, it was noted that we did not propagate the uncertainty from our first modeling step into the second. We recognize that this would be a definite advantage, working with a Bayesian framework, and we have now investigated this. We first generated 200 posterior samples from the fitted multinomial model, and then, we fitted the AR(2) model to these samples. The resulting variance in estimating the AR coefficients was very small. This can be seen with an example displayed in Figure S13. The upper panels (a and b) show the posterior sampling distributions for the differences in the specific coefficients related to the categories of the multinomial model. These are used to estimate the abundances at each time point (panel c). The resulting distributions for the AR coefficients (panel d and e) are very narrow giving standard deviations smaller than 0.01. This is much smaller than the standard deviation in estimating the coefficients of independently generated AR(2) time series. Therefore, we realized we would not gain much from the uncertainty propagation, also taking into consideration the large amount of additional running time required.

In summary, we have found that capture–recapture information given by two capture events contributes to improve density-dependence estimates of AR(2) models with low process variance. In such cases, we recommended that capture heterogeneity is accounted for in the observation model, as it can constitute an important part of the total sampling error. Further analyses are required to assess how more capture events could impact process estimation.

## ACKNOWLEDGMENTS

This study was supported by the COAT Tools project. We thank Prof. Rolf Ims for taking part in the collection of the field data used to test the studied methods. We thank the anonymous reviewers for their comments that improved the quality of this manuscript.

## CONFLICT OF INTEREST

None declared.

## AUTHOR CONTRIBUTION

**Pedro Guilherme Nicolau:** Conceptualization (equal); Data curation (lead); Formal analysis (equal); Investigation (equal); Methodology (equal); Resources (supporting); Software (supporting); Validation (equal); Visualization (equal); Writing-original draft (lead); Writing-review & editing (equal). **Sigrunn Sørbye:** Conceptualization (equal); Formal analysis (equal); Investigation (equal); Methodology (equal); Project administration (equal); Software (equal); Supervision (lead); Validation (equal); Writing-original draft (equal); Writing-review & editing (equal). **Nigel Yoccoz:** Conceptualization (lead); Funding acquisition (lead); Investigation (equal); Methodology (supporting); Project administration (equal); Resources (lead); Supervision (supporting); Writing-original draft (equal); Writing-review & editing (equal).

## OPEN RESEARCH BADGES



This article has been awarded Open Materials, Open Data Badges. All materials and data are publicly accessible via the Open Science Framework at <https://doi.org/10.5061/dryad.fj6q573rr>.

## DATA AVAILABILITY STATEMENT

The simulation code used to obtain the results in this paper and the real data set used to test the methods have been submitted to Dryad (<https://doi.org/10.5061/dryad.fj6q573rr>).

## ORCID

Pedro G. Nicolau <https://orcid.org/0000-0002-7384-3784>  
Sigrunn H. Sørbye <https://orcid.org/0000-0002-5818-1508>  
Nigel G. Yoccoz <https://orcid.org/0000-0003-2192-1039>

## REFERENCES

- Akaike, H. (1973). Information theory and an extension of the maximum likelihood principle. In *Proc. 2nd Inter. Symposium on Information Theory*, 267–281. Budapest. [https://doi.org/10.1007/978-1-4612-1694-0\\_15](https://doi.org/10.1007/978-1-4612-1694-0_15)
- Baker, S. G. (1994). The multinomial-poisson transformation. *The Statistician*, 43(4), 495–504. <https://doi.org/10.2307/2348134>
- Barker, R., Fletcher, D., & Scofield, P. (2002). Measuring density dependence in survival from mark-recapture data. *Journal of Applied Statistics*, 29(1-4), 305–313. <https://doi.org/10.1080/02664760120108782>
- Besbeas, P., & Morgan, B. J. T. (2019). Exact inference for integrated population modelling. *Biometrics*, 75(2), 475–484. <https://doi.org/10.1111/biom.13045>
- Bjørnstad, O. N., Chr. Stenseth, N., and Saitoh, T. (1999). Synchrony and scaling in dynamics of voles and mice in Northern Japan. *Ecology*, 80(2), 622–637. [https://doi.org/10.1890/0012-9658\(1999\)080\[0622:asid\]2.0.co;2](https://doi.org/10.1890/0012-9658(1999)080[0622:asid]2.0.co;2)
- Bjørnstad, O. N., Falck, W., & Stenseth, N. C. (1995). A geographic gradient in small rodent density fluctuations: A statistical modelling approach. *Proceedings of the Royal Society of London. Series B: Biological Sciences*, 262(1364), 127–133. <https://doi.org/10.1098/rspb.1995.0186>
- Bryja, J., Nesvadbová, J., Heroldová, M., Jánová, E., Losík, J., Trebatická, L., & Tkadlec, E. (2005). Common vole *Microtus arvalis* population sex ratio: Biases and process variation. *Canadian Journal of Zoology-Revue Canadienne De Zoologie*, 83, 1391–1399. <https://doi.org/10.1139/z05-133>
- Carothers, A. D. (1973). The effects of unequal catchability on Jolly-Seber estimates. *Biometrics*, 29(1), 79. <https://doi.org/10.2307/2529678>
- Chao, A., & Huggins, R. M. (2006). Four modern closed-population capture-recapture models. In B. J. Manly, T. L. McDonald, & S. C. Amstrup (Eds.), *Handbook of capture-recapture analysis* (pp. 58–87). NJ: Princeton University Press.
- Cornulier, T., Yoccoz, N. G., Bretagnolle, V., Brommer, J. E., Butet, A., Ecke, F., ... Lambin, X. (2013). Europe-wide dampening of population cycles in keystone herbivores. *Science*, 340(6128), 63–66. <https://doi.org/10.1126/science.1228992>
- Dennis, B., & Taper, M. L. (1994). Density dependence in time series observations of natural populations: Estimation and testing. *Ecological Monographs*, 64(2), 205–224. <https://doi.org/10.2307/2937041>
- Efford, M. G., & Mowat, G. (2014). Compensatory heterogeneity in spatially explicit capture-recapture data. *Ecology*, 95(5), 1341–1348. <https://doi.org/10.1890/13-1497.1>

- Elton, C. S. (1924). Periodic fluctuations in the numbers of animals: Their causes and effects. *Journal of Experimental Biology*, 2(1), 119–163.
- Fletcher, D., Lebreton, J.-D., Marescot, L., Schaub, M., Gimenez, O., Dawson, S., & Slooten, E. (2011). Bias in estimation of adult survival and asymptotic population growth rate caused by undetected capture heterogeneity. *Methods in Ecology and Evolution*, 3(1), 206–216. <https://doi.org/10.1111/j.2041-210x.2011.00137.x>
- Henttonen, H., & Hanski, I. (2000). Population dynamics of small rodents in Northern Fennoscandia. In J. N. Perry, R. H. Smith, I. P. Woiwod, & D. R. Morse (Eds.), *Chaos in real data* (pp. 73–96). Dordrecht, The Netherlands: Springer.
- Horvitz, D. G., & Thompson, D. J. (1952). A generalization of sampling without replacement from a Finite Universe. *Journal of the American Statistical Association*, 47(260), 663–685. <https://doi.org/10.1080/01621459.1952.10483446>
- Huggins, R., & Hwang, W.-H. (2011). A review of the use of conditional likelihood in capture-recapture experiments. *International Statistical Review*, 79(3), 385–400. <https://doi.org/10.1111/j.1751-5823.2011.00157.x>
- Ims, R. A., Yoccoz, N. G., & Killengreen, S. T. (2011). Determinants of lemming outbreaks. *Proceedings of the National Academy of Sciences of the United States of America*, 108(5), 1970–1974. <https://doi.org/10.1073/pnas.1012714108>
- King, R., Brooks, S. P., & Coulson, T. (2008). Analyzing complex capture-recapture data in the presence of individual and temporal covariates and model uncertainty. *Biometrics*, 64(4), 1187–1195. <https://doi.org/10.1111/j.1541-0420.2008.00991.x>
- Kleiven, E. F., Henden, J.-A., Ims, R. A., & Yoccoz, N. G. (2018). Seasonal difference in temporal transferability of an ecological model: Near-term predictions of lemming outbreak abundances. *Scientific Reports*, 8(1). <https://doi.org/10.1038/s41598-018-33443-6>
- Lande, R., Engen, S., & Sæther, B. E. (2002). Estimating density dependence in time-series of age-structured populations. *Philosophical Transactions of the Royal Society of London. Series B: Biological Sciences*, 357(1425), 1179–1184. <https://doi.org/10.1098/rstb.2002.1120>
- Lebreton, J.-D., & Gimenez, O. (2012). Detecting and estimating density dependence in wildlife populations. *The Journal of Wildlife Management*, 77(1), 12–23. <https://doi.org/10.1002/jwmg.425>
- Link, W. A. (2003). Nonidentifiability of population size from capture-recapture data with heterogeneous detection probabilities. *Biometrics*, 59(4), 1123–1130. <https://doi.org/10.1111/j.0006-341x.2003.00129.x>
- Marolla, F., Aarvak, T., Øien, I. J., Mellard, J. P., Henden, J.-A., Hamel, S., ... Ims, R. A. (2019). Assessing the effect of predator control on an endangered goose population subjected to predator-mediated food web dynamics. *Journal of Applied Ecology*, 56(5), 1245–1255. <https://doi.org/10.1111/1365-2664.13346>
- McCrea, R. (2014). *Analysis of capture-recapture data*. Boca Raton, FL: CRC Press/Taylor; Francis Group.
- Ono, K., Langangen, Ø., & Chr. Stenseth, N. (2019). Improving risk assessments in conservation ecology. *Nature Communications*, 10(1). <https://doi.org/10.1038/s41467-019-10700-4>
- Otis, D. L., Burnham, K. P., White, G. C., & Anderson, D. R. (1978). *Statistical inference from capture data on closed animal populations*. Wildlife Monographs, no. 62. [Wiley, Wildlife Society]: 3–135.
- Rose, J. P., Wylie, G. D., Casazza, M. L., & Halstead, B. J. (2018). Integrating growth and capture-mark-recapture models reveals size-dependent survival in an elusive species. *Ecosphere*, 9(8), e02384. <https://doi.org/10.1002/ecs2.2384>
- Royle, J. A. (2008). Analysis of capture-recapture models with individual covariates using data augmentation. *Biometrics*, 65(1), 267–274. <https://doi.org/10.1111/j.1541-0420.2008.01038.x>
- Royle, J. A., Dorazio, R. M., & Link, W. A. (2007). Analysis of multinomial models with unknown index using data augmentation. *Journal of Computational and Graphical Statistics*, 16(1), 67–85. <https://doi.org/10.1198/106186007x181425>
- Royle, J. A., Fuller, A. K., & Sutherland, C. (2017). Unifying population and landscape ecology with spatial capture-recapture. *Ecography*, 41(3), 444–456. <https://doi.org/10.1111/ecog.03170>
- Rue, H., & Held, L. (2005). *Gaussian Markov Random Fields*. Boca Raton: Chapman & Hall/CRC.
- Rue, H., Martino, S., & Chopin, N. (2009). Approximate Bayesian inference for latent Gaussian models by using integrated nested Laplace approximations. *Journal of the Royal Statistical Society: Series B (Statistical Methodology)*, 71(2), 319–392. <https://doi.org/10.1111/j.1467-9868.2008.00700.x>
- Rue, H., Riebler, A., Sørbye, S. H., Illian, J. B., Simpson, D. P., & Lindgren, F. K. (2017). Bayesian computing with INLA: A review. *Annual Review of Statistics and Its Application*, 4, 395–421. <https://doi.org/10.1146/annurev-statistics-060116-054045>
- Santin-Janin, H., Hugueny, B., Aubry, P., Fouchet, D., Gimenez, O., & Pontier, D. (2014). Accounting for sampling error when inferring population synchrony from time-series data: A Bayesian state-space modelling approach with applications. *PLoS One*, 9(1), e87084. <https://doi.org/10.1371/journal.pone.0087084>
- Schofield, M. R., & Barker, R. J. (2008). A unified capture-recapture framework. *Journal of Agricultural, Biological, and Environmental Statistics*, 13(4), 458–477. <https://doi.org/10.1198/108571108x383465>
- Schofield, M. R., & Barker, R. J. (2013). Hierarchical modeling of abundance in closed population capture-recapture models under heterogeneity. *Environmental and Ecological Statistics*, 21(3), 435–451. <https://doi.org/10.1007/s10651-013-0262-3>
- Schwarz, G. (1978). Estimating the dimension of a model. *The Annals of Statistics*, 6(2), 461–464. <https://doi.org/10.1214/aos/1176344136>
- Shaman, P., & Stine, R. A. (1988). The bias of autoregressive coefficient estimators. *Journal of the American Statistical Association*, 83(403), 842–848. <https://doi.org/10.1080/01621459.1988.10478672>
- Simpson, D., Rue, H., Riebler, A., Martins, T. G., & Sørbye, S. H. (2017). Penalising model component complexity: A principled, practical approach to constructing priors. *Statistical Science*, 232(1), 1–28. <https://doi.org/10.1214/16-STS576>
- Sørbye, S. H., & Rue, H. (2014). Scaling intrinsic Gaussian Markov random field priors in spatial modelling. *Spatial Statistics*, 8, 39–51. <https://doi.org/10.1016/j.spa.2013.06.004>
- Sørbye, S. H., & Rue, H. (2017). Penalised complexity priors for stationary autoregressive processes. *Journal of Time Series Analysis*, 38(6), 923–935. <https://doi.org/10.1111/jtsa.12242>
- Spiegelhalter, D. J., Best, N. G., Carlin, B. P., & van der Linde, A. (2002). Bayesian measures of model complexity and fit. *Journal of the Royal Statistical Society: Series B (Statistical Methodology)*, 64(4), 583–639. <https://doi.org/10.1111/1467-9868.00353>
- Stenseth, N. C. (1999). Population cycles in voles and lemmings: Density dependence and phase dependence in a stochastic world. *Oikos*, 87(3), 427. <https://doi.org/10.2307/3546809>
- Stenseth, N. C., Viljugrein, H., Saitoh, T., Hansen, T. F., Kittilsen, M. O., Bolviken, E., & Glockner, F. (2003). Seasonality, density dependence, and population cycles in Hokkaido voles. *Proceedings of the National Academy of Sciences of the United States of America*, 100(20), 11478–11483. <https://doi.org/10.1073/pnas.1935306100>
- Thibaut, L. M., & Connolly, S. R. (2019). Hierarchical modeling strengthens evidence for density dependence in observational time series of population dynamics. *Ecology*, 101(1). <https://doi.org/10.1002/ecy.2893>
- Watanabe, S. (2010). Asymptotic equivalence of bayes cross validation and widely applicable information criterion in singular learning theory. *Journal of Machine Learning Research*, 11, 3571–3594.
- Yackulic, C. B., Korman, J., Yard, M. D., & Dzul, M. (2018). Inferring species interactions through joint mark-recapture analysis. *Ecology*, 99(4), 812–821. <https://doi.org/10.1002/ecy.2166>

- Yee, T. W. (2019). VGAM: Vector generalized linear and additive models. Retrieved from <https://CRAN.R-project.org/package=VGAM>
- Yee, T. W., Stoklosa, J., & Huggins, R. M. (2015). The VGAM package for capture-recapture data using the conditional likelihood. *Journal of Statistical Software*, 65(5). <https://doi.org/10.18637/jss.v065.i05>
- Yoccoz, N. G., & Ims, R. A. (2004). Spatial population dynamics of small mammals: Some methodological and practical issues. *Animal Biodiversity and Conservation*, 27(1), 427–435.

**How to cite this article:** Nicolau PG, Sørbye SH, Yoccoz NG. Incorporating capture heterogeneity in the estimation of autoregressive coefficients of animal population dynamics using capture–recapture data. *Ecol Evol.* 2020;10:12710–12726. <https://doi.org/10.1002/ece3.6642>

#### SUPPORTING INFORMATION

Additional supporting information may be found online in the Supporting Information section.

# Supplementary Material

## A Simulation results

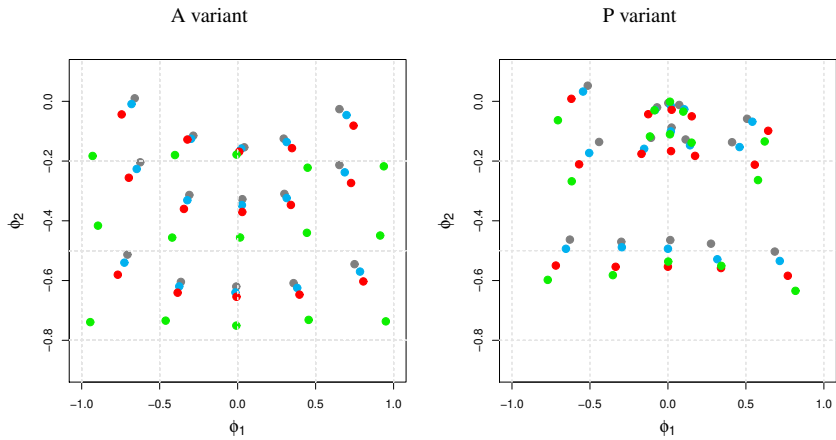


Figure 1: Estimates of the different methods for  $\sigma_\epsilon^2 = 0.04$ .

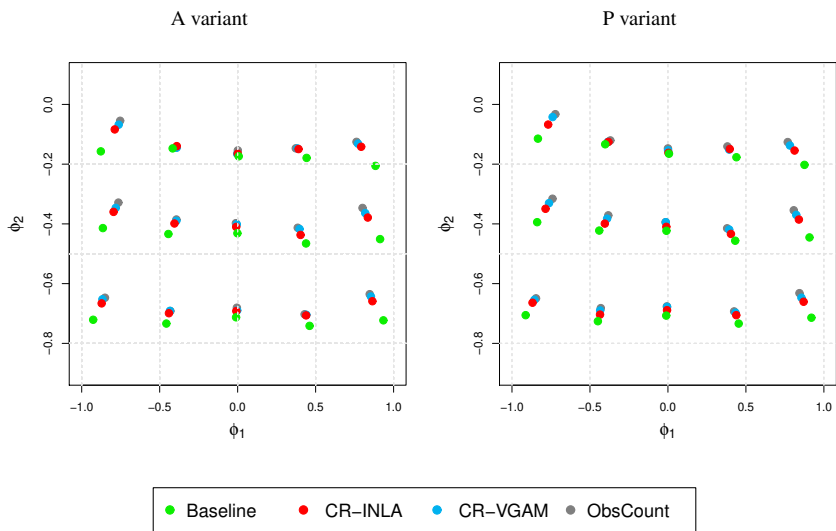


Figure 2: Estimates of the different methods for  $\sigma_\epsilon^2 = 0.16$ .

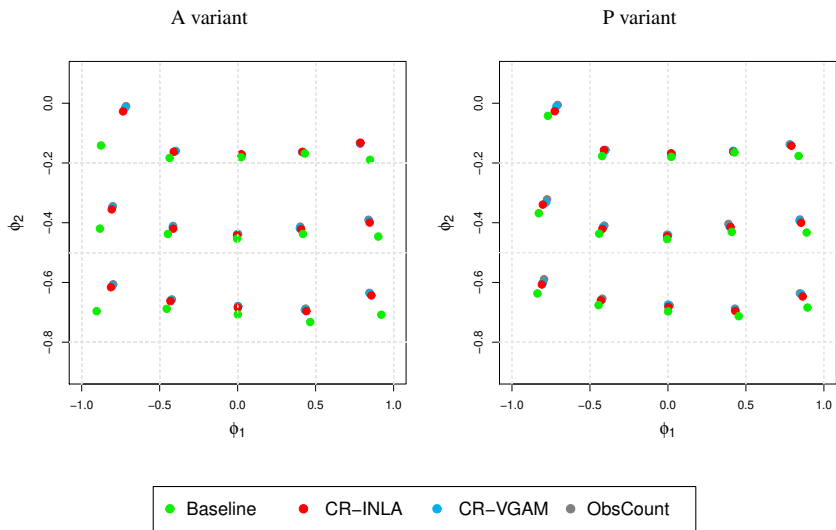


Figure 3: Estimates of the different methods for  $\sigma_\epsilon^2 = 0.64$ .

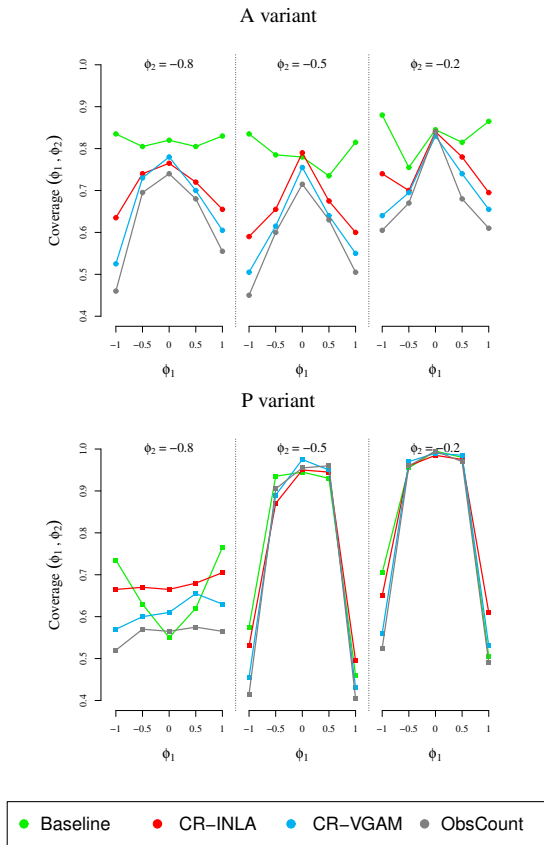


Figure 4: Coverage for different combinations of  $(\phi_1, \phi_2)$  for  $\sigma_\epsilon^2 = 0.04$  in both variants.

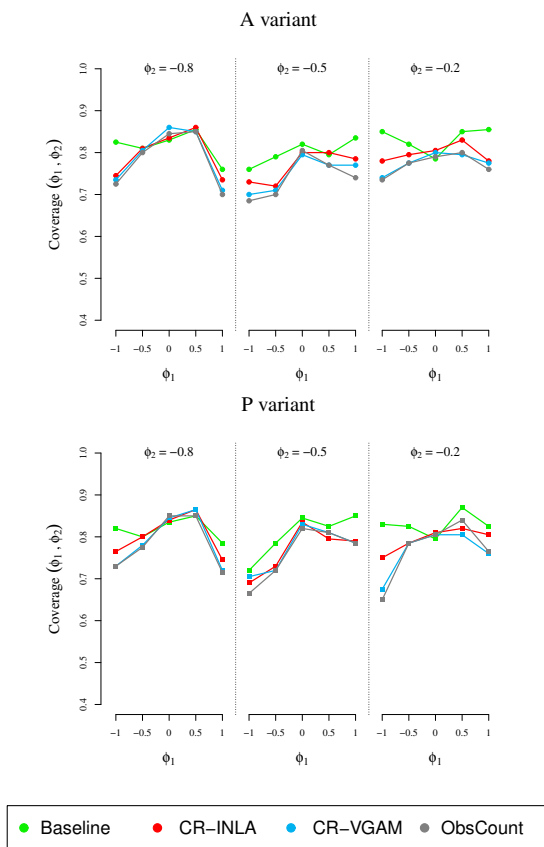


Figure 5: Coverage for different combinations of  $(\phi_1, \phi_2)$  for  $\sigma_\epsilon^2 = 0.16$  in both variants.

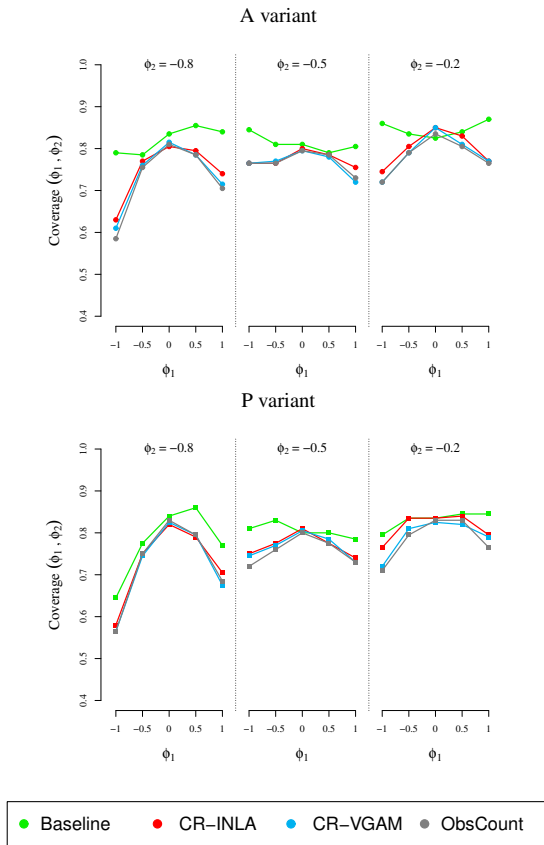


Figure 6: Coverage for different combinations of  $(\phi_1, \phi_2)$  for  $\sigma_\epsilon^2 = 0.64$  in both variants.



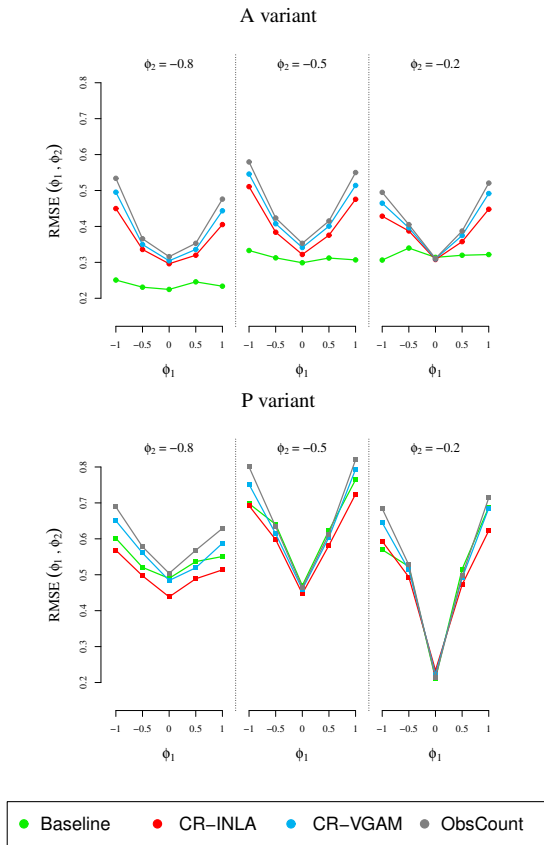


Figure 7: RMSE for different combinations of  $(\phi_1, \phi_2)$  for  $\sigma_\epsilon^2 = 0.04$  in both variants.

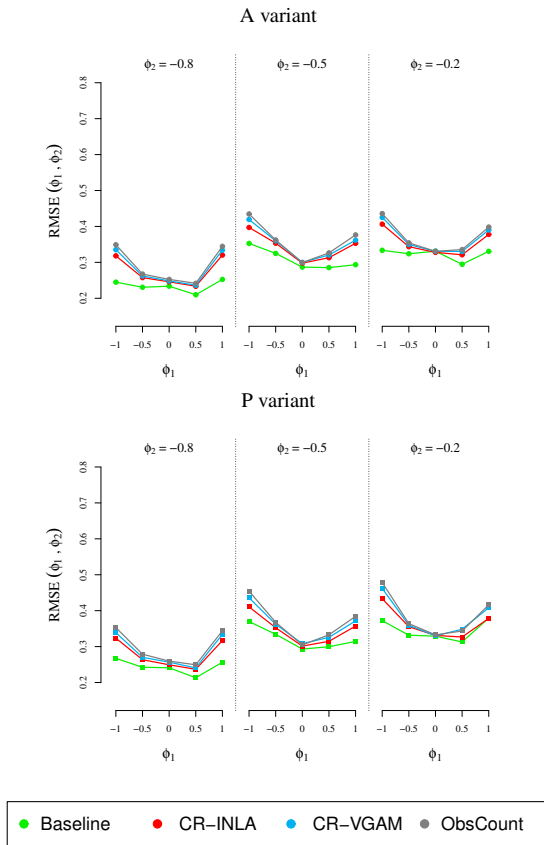


Figure 8: RMSE for different combinations of  $(\phi_1, \phi_2)$  for  $\sigma_\epsilon^2 = 0.16$  in both variants.

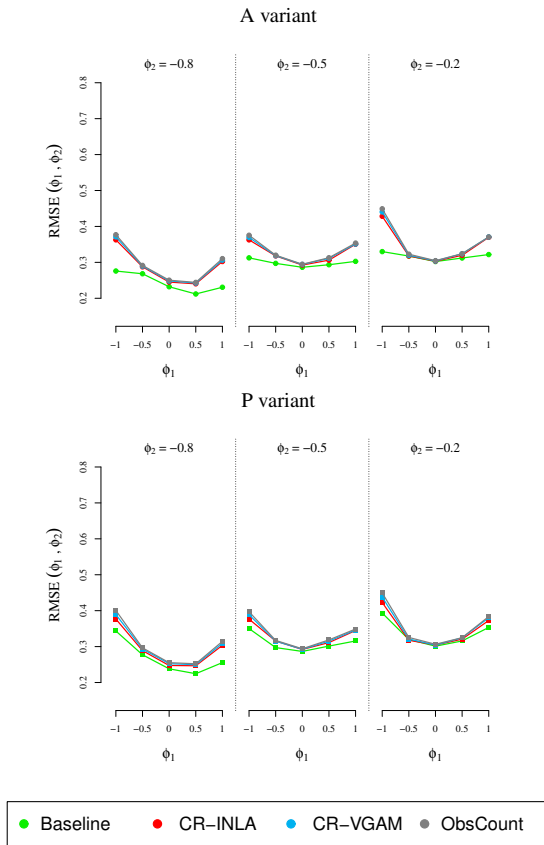


Figure 9: RMSE for different combinations of  $(\phi_1, \phi_2)$  for  $\sigma_\epsilon^2 = 0.64$  in both variants.

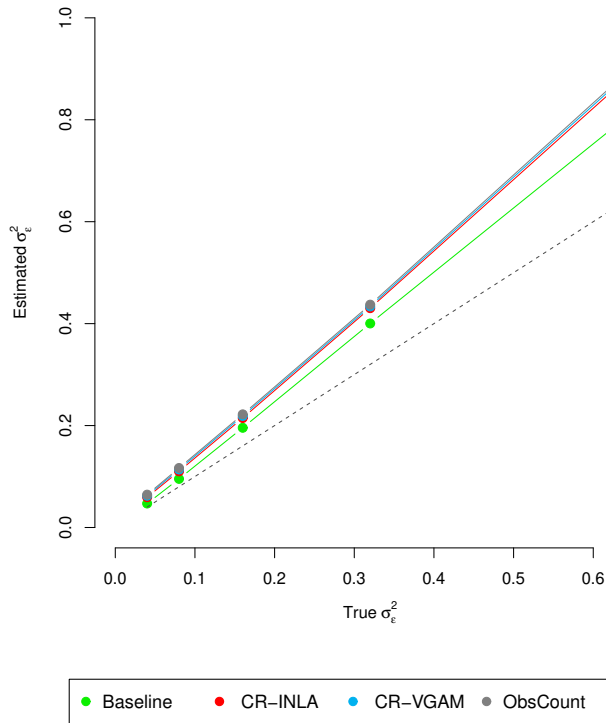


Figure 10: Mean process variance estimate for the A variants in the simulation exercise, across all combinations of parameters. The dashed grey line corresponds to the theoretical optimum. The green line provides the practical optimum. The three methods provide similar estimates of the process variance, increasingly overestimating it for larger  $\sigma_\epsilon^2$  values.

Table 1: Values of average joint coverage and joint RMSE for all combinations of simulations for the four different methods, in 5 levels of variance  $\sigma_\epsilon^2$ . (A) columns represent the log-Abundance variants, while (P) columns show values for the log-Poisson rate variants.

<i>Method</i>	$\sigma_\epsilon^2$	<i>Joint Coverage</i>		<i>Joint RMSE</i>	
		<i>A</i>	<i>P</i>	<i>A</i>	<i>P</i>
Baseline	0.04	0.81	0.75	0.41	0.75
CR-INLA		0.71	0.76	0.54	0.72
CR-VGAM		0.66	0.72	0.58	0.77
ObsCount		0.63	0.69	0.61	0.80
Baseline	0.08	0.82	0.84	0.40	0.51
CR-INLA		0.76	0.80	0.48	0.53
CR-VGAM		0.74	0.78	0.51	0.57
ObsCount		0.72	0.77	0.53	0.60
Baseline	0.16	0.82	0.82	0.41	0.43
CR-INLA		0.79	0.79	0.46	0.46
CR-VGAM		0.77	0.77	0.47	0.48
ObsCount		0.77	0.77	0.48	0.49
Baseline	0.32	0.82	0.81	0.41	0.43
CR-INLA		0.79	0.79	0.45	0.45
CR-VGAM		0.79	0.79	0.45	0.46
ObsCount		0.79	0.78	0.46	0.47
Baseline	0.64	0.83	0.80	0.40	0.43
CR-INLA		0.77	0.77	0.45	0.45
CR-VGAM		0.76	0.76	0.46	0.46
ObsCount		0.76	0.76	0.46	0.47

## B Real data results

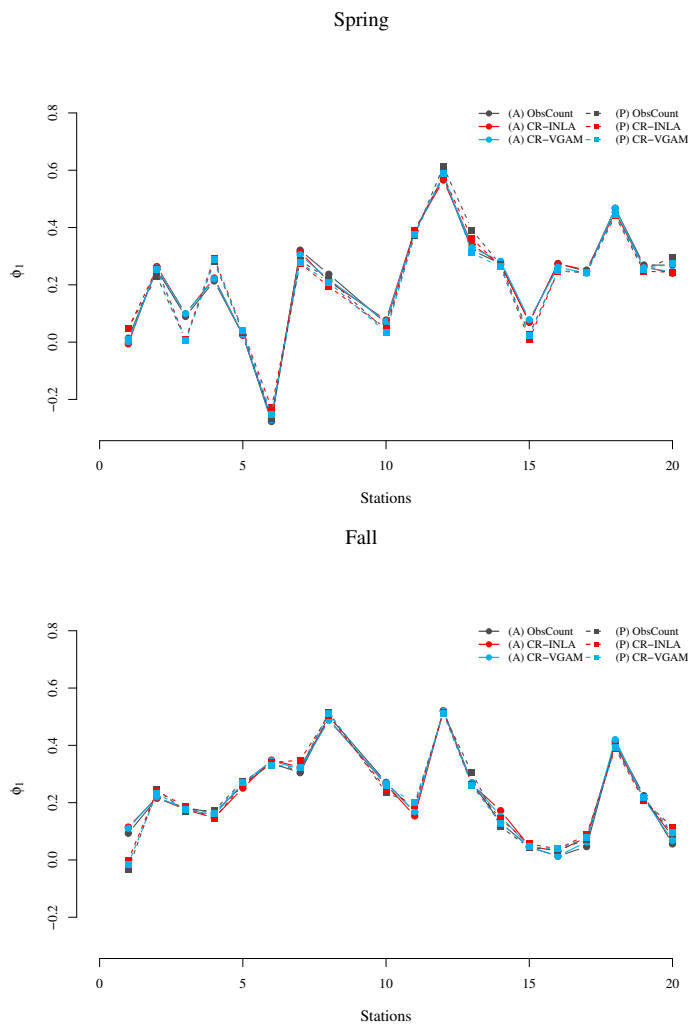
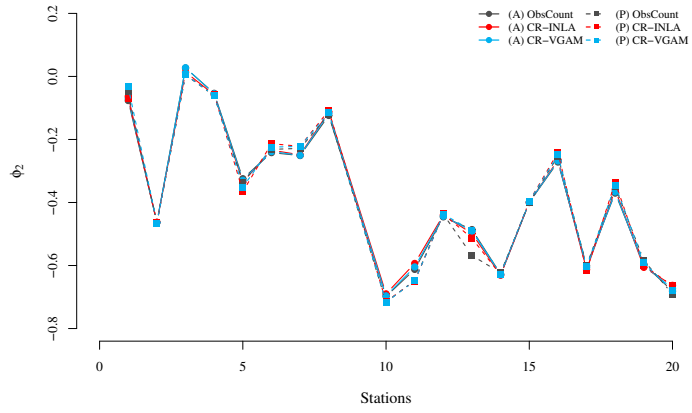


Figure 11: Estimates for  $\phi_1$  for the different methods in both variants, per season.

Spring



Fall

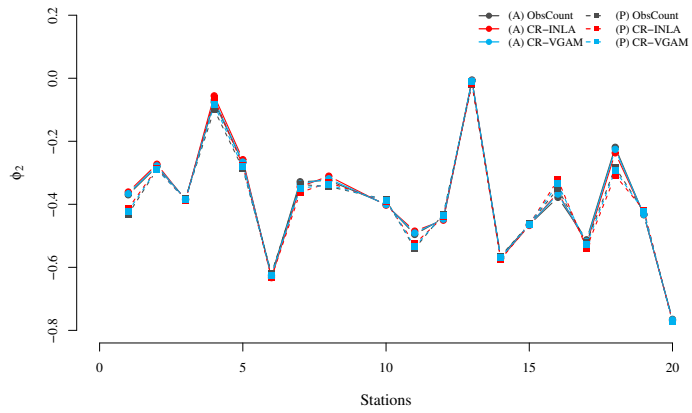


Figure 12: Estimates for  $\phi_2$  for the different methods in both variants, per season.

### C (C) Propagating uncertainty example

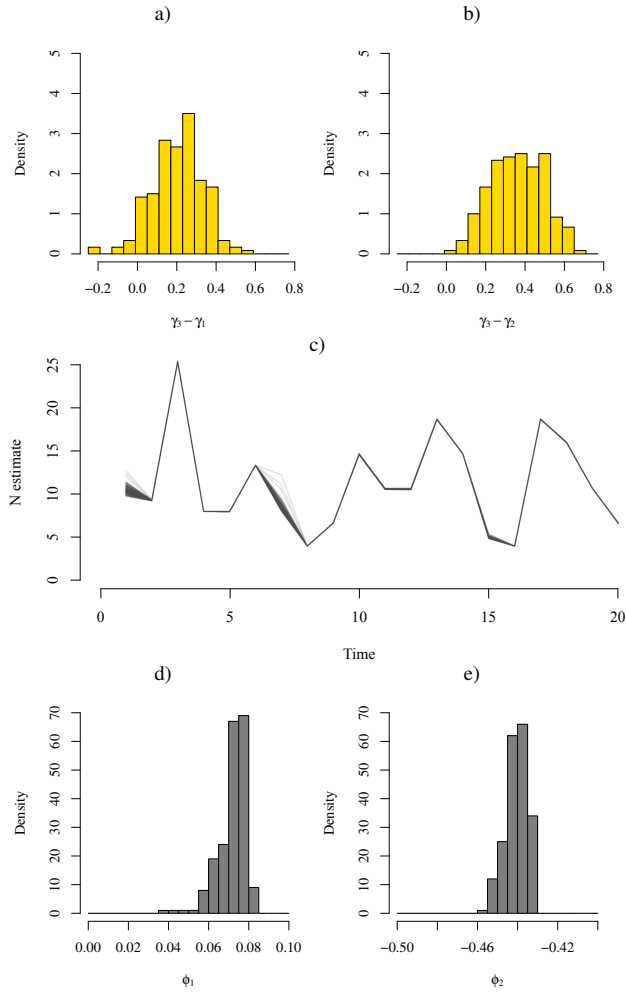


Figure 13: Example of propagating uncertainty from the estimation of the  $\gamma$ -coefficients of the multinomial model (a and b) to the estimation of  $\phi_1$  and  $\phi_2$  with CR-INLA for one simulation setting.



*Figure C1* (cont.) These plots show an example of propagating uncertainty from the estimation of the  $\gamma$ -coefficients, used to estimate the capture probabilities in (??) and (??), to estimating abundance and the AR coefficients. The posterior Monte Carlo samples for the  $\gamma$ -coefficients were obtained using the function `inla.posterior.sample` for the fitted multinomial model. The figure illustrates error propagation for a single simulated dataset with true parameters  $\{\phi_1 = 0.2, \phi_2 = -0.5, \sigma_\epsilon^2 = 0.08\}$ , using 200 Monte Carlo samples. Panels a) and b) show the distribution of the differences between the  $\gamma$ -coefficients. Panel c) shows the resulting overlapped estimates for the abundance  $\hat{N}$ , while panels d) and e) give the resulting distributions for  $\phi_1$  and  $\phi_2$ . These distributions are very narrow, giving standard deviations equal to 0.007 and 0.005 for  $\phi_1$  and  $\phi_2$ , respectively. This is a consequence of the very low variation in the estimated abundance in panel c).



## Paper II

**Using camera traps to monitor voles exhibiting multi-annual population cycles**

Submitted to *Remote Sensing in Ecology and Conservation*.



# Using camera traps to monitor voles exhibiting multi-annual population cycles

Eivind Flittie Kleiven<sup>1,\*</sup>, Pedro Guilherme Nicolau<sup>2,\*</sup>, Sigrunn Holbek Sørbye<sup>2</sup>, Jon Aars<sup>3</sup>, Nigel Gilles Yoccoz<sup>1</sup>, and Rolf Anker Ims<sup>1</sup>

<sup>1</sup>Department of Arctic and Marine Biology, Faculty of Biosciences, Fisheries and Economics, UiT The Arctic University of Norway, N-9037, Tromsø

<sup>2</sup>Department of Mathematics and Statistics, Faculty of Science, UiT The Arctic University of Norway, N-9037, Tromsø

<sup>3</sup>Norwegian Polar Institute, Fram Centre, Tromsø 9296, Norway

\*These authors have contributed equally.

## Abstract

Camera traps have become increasingly popular as a labor-efficient and non-invasive tool to study animal ecology. Despite rodents being the most abundant and speciose order of living mammals, camera trap studies have mainly focused on larger mammals. Here we investigate the suitability of camera-trap-based abundance indices to monitor population cycles of two species of voles with key functions in boreal and Arctic ecosystems. The targeted species — gray-sided vole (*Myodes rufocanus*) and tundra vole (*Microtus oeconomus*) – differ with respect to habitat use and spatial-social organization, which allow us to assess whether such species-traits influence the accuracy of the abundance indices. For both species, multiple live-trapping grids yielding capture-mark-recapture (CMR) abundance estimates, were matched with single tunnel-based camera traps (CT) intended to yield abundance indices. The study encompassed three years with contrasting abundances and phases of the population cycle. First, we used lin-

ear regressions to calibrate CT-indices based on photo counts over different time-windows as a function of CMR-derived abundance estimates. Then, we performed inverse regressions to predict CMR-abundances from CT-indices. We found that CT-indices (for windows showing best goodness-of-fit) from single camera traps predicted adequately the CMR-based estimates for the gray-sided vole, whereas such predictions were generally poor for the tundra vole. However, aggregating photo counts over several nearby camera traps yielded also reliable abundance indices for the tundra vole. The two species differed also with respect to the optimal time-window for the CT-indices, which was 1 day for the tundra vole and 5 days for the gray-sided vole. Such species differences imply that the design of camera trap studies of rodent population dynamics should to be adapted to the species in focus. Overall, tunnel-based camera traps yield much more temporally resolved abundance metrics than alternative methods. This gives a potential for revealing new aspects of the multi-annual population cycles of voles as well as other small mammal species they interact with in boreal and Arctic ecosystems.

Key words: Rodents, Index-calibration regression, inverse prediction, camera trap, population monitoring

## 1 Introduction

2 During the last decade, the use of camera traps has increased drastically in animal ecology as this  
3 provides a non-invasive and cost efficient alternative to traditional census methods (Wearn and  
4 Glover-Kapfer, 2019). In studies of mammals, the use of camera traps has so far largely focused  
5 on large-sized species (Burton et al., 2015). Nonetheless, smaller-sized rodents represent the most  
6 abundant and specious order of mammals (Wilson and Reeder, 2005). Many rodent species are  
7 cryptic, and hence resource-demanding, or otherwise difficult to study by means of conventional  
8 methods. Hence, camera traps specifically adapted to study small rodents may advance our abil-  
9 ity to investigate their ecology (Rendall et al., 2014). Studying the population dynamics of small

10 rodents is important for several reasons (Krebs, 2013). Many rodent species pose risks to humans  
11 as vectors of zoonoses (Meerburg et al., 2009a; Capizzi et al., 2014) or by damaging crops (Meer-  
12 burg et al., 2009b; Andreassen et al., 2021). Moreover, voles and lemmings exert key ecosystem  
13 functions, especially in northern biomes where they exhibit multi-annual population cycles (Ims  
14 and Fuglei, 2005). Therefore, accurate monitoring of boreal and Arctic small rodent populations is  
15 fundamental to studies of ecosystem dynamics (Legagneux et al., 2014; Boonstra et al., 2016) and  
16 to the successful conservation of endangered species that are directly (Ims et al., 2018) or indirectly  
17 affected by their population dynamics (Marolla et al., 2019; Henden et al., 2021). Many boreal and  
18 Arctic rodent monitoring programs are still based on kill-traps (snap-traps), providing counts as  
19 indices of abundance (Turchin et al., 2000; Hörnfeldt et al., 2005; Korpela et al., 2013; Cornulier  
20 et al., 2013; Kleiven et al., 2018; Ehrich et al., 2019). However, kill-trapping is fraught with both  
21 ethical issues (Powell and Proulx, 2003) and questionable assumptions regarding sampling errors  
22 (Hanski et al., 1994). Live-trap-based, capture-mark-recapture (CMR) monitoring is less invasive  
23 and allows to account for sampling errors (Krebs et al., 2011). However, live-trapping requires  
24 much effort from qualified personnel and is therefore rarely sufficiently long-term and spatially  
25 extensive to support monitoring programs. In addition, several species display very low trappabil-  
26 ity in live-traps and are thus inadequately monitored by capture-recapture methods (Boonstra and  
27 Krebs, 1978; Jensen et al., 1993). In general, existing monitoring programs of rodent populations  
28 are logistically limited in terms of their coarse temporal resolution. In northern ecosystems such  
29 monitoring is usually restricted to two trapping sessions per year (Cornulier et al., 2013). This  
30 implies an important limitation due to the multivoltine life histories and the fast population dynam-  
31 ics of voles and lemmings. Camera traps may potentially resolve such constraints by providing  
32 means for spatially extensive and continuous year-round monitoring, even in climatically harsh and  
33 remote boreal and Arctic regions (Soininen et al., 2015; Mölle et al., 2021).

34 Camera traps are today most commonly used to analyze presence-absence dynamics (i.e. oc-  
35 cupancy probability) (MacKenzie et al., 2002; Bailey et al., 2014). However, presence-absence

36 is a less informative population state variable than abundance, especially when density-dependent  
37 population regulatory mechanisms are of concern. Hence, the use of camera traps to estimate  
38 abundance is increasing. Most of these studies have however focused on marked (or otherwise  
39 distinguishable) individuals (Gilbert et al., 2021; Palencia et al., 2021). For many species, such  
40 as small rodents, it is not feasible to either mark or distinguish individuals by clues that are visi-  
41 ble in camera trap images. Moreover, design constraints make presence-absence-based abundance  
42 estimators less applicable in the case of unmarked small mammals.

43 If the aim is to study population dynamics, for instance by means of time series analyses  
44 (Stenseth, 1999; Cornulier et al., 2013; Barraquand et al., 2017), simple indices of abundance  
45 can be used if there is a proportionate relationship between true abundance and the abundance  
46 index (Hanski et al., 1994; Lambin et al., 2000; Yoccoz et al., 2001; Gilbert et al., 2021). Counts  
47 of motion triggered photos appear to be a promising abundance index for large- to medium-sized  
48 mammals (Palmer et al., 2018). Recent studies suggest that this may also be the case for some small  
49 rodent species (Villette et al., 2015; Parsons et al., 2021). However, as of yet, such camera-based  
50 abundance indices have not been validated for rodent species that exhibit multi-annual popula-  
51 tion cycles, for instance, boreal and Arctic voles. Furthermore, previous works have been limited  
52 in scope and have not assessed the uncertainty associated with using camera-trap indices to esti-  
53 mate population abundance. A potential challenge in the case of such population dynamics is that  
54 there may be density- and/or cyclic phase-dependent aspects of their performance (sensu Stenseth  
55 (1999)) that may influence the reliability of camera-trap (CT) indices.

56 Proper calibration of CT-based abundance indices as a function of CMR-based abundance esti-  
57 mates is challenging. Generally, calibration consists of modelling the measurable response variable  
58 (e.g. a population index) as a function of a ground-truthing variable that typically is assumed to be  
59 measured accurately (e.g. a population state variable measured without error). Once a calibration  
60 function is established, it can be used in inverse regression to predict the state variable for a given  
61 value of the response variable (Eisenhart, 1939). The goodness of the fit of the regression may be



62 assessed using the ordinary coefficient of determination ( $R^2$ ). In most ecological studies, the true  
63 state of a population is not known and must be estimated with some error, for instance, based on  
64 CMR trapping. As the error of the population state estimate (i.e. the ground-truth variable) may not  
65 be negligible, this becomes a more difficult calibration problem because the uncertainty of the true  
66 abundance can bias the estimation of the population state (Gopaldaswamy et al., 2015). Thus it is  
67 important to assess the accuracy of prediction after establishing a calibration function (Diefenbach  
68 et al., 1994), to ensure high precision of the abundance predictions, which can sometimes be too  
69 low (Jennelle et al., 2002). Furthermore, camera trap-based abundance indices have been criticized  
70 for not being generalizable to other species or sampling sites (Jennelle et al., 2002). It is there-  
71 fore important to investigate potential differences in the performance of the abundance index for  
72 different species, i.e., to assess out-of-sample predictive ability of the index-calibration models.

73 In this study, we assess the suitability of camera-trap-based abundance indices for studying  
74 population dynamics of the gray-sided vole (*Myodes rufocanus*) and the tundra vole (*Microtus*  
75 *oeconomus*). Both species are renowned for their multi-annual cycles (Hansen et al., 1999; Turchin  
76 et al., 2000; Cornulier et al., 2013) and key roles in boreal and sub-arctic ecosystems (Ims and  
77 Fuglei, 2005; Boonstra et al., 2016). The two vole species are also known to differ profoundly  
78 in their habitat use and spatial-social organization (Ims, 1987a; Bondrup-Nielsen and Ims, 1990),  
79 which provides a case for assessing whether such species-specific traits influence camera trap-  
80 based abundance indices (CT-indices). For both species, we used time series of spatio-temporally  
81 matched CT-indices and CMR-estimates, spanning a wide range of abundances and different phases  
82 of the population cycle. We followed a two-step calibration approach. First, we fitted calibration  
83 regressions, with the CT-indices, based on photo counts from single camera traps, as the exposure  
84 variable and CMR-based abundance estimates as the ground-truthing variable. In the case of tundra  
85 vole, for which several camera traps were used within the same local population, we also assessed to  
86 what extent aggregating data over several camera traps improved the fit of the calibration regression,  
87 i.e., treating the cameras as spatial replicates. As the camera traps provide continuous-time data,

88 we assessed which temporal resolution (i.e. time-window) of the camera trap data was optimal,  
89 in the sense of providing the best goodness-of-fit calibration regression (i.e, maximized the  $R^2$ ).  
90 As the second step, we performed inverse prediction to estimate vole abundance using the optimal  
91 CT-index, and evaluated the predictive performance of the model using k-fold cross-validation, bias  
92 and a classification metric for three abundance classes.

## 93 **2 Methods**

### 94 ***2.1 Study areas and species***

95 The data were obtained from two study areas in sub-arctic Norway (Figure 1), where long-term  
96 monitoring of vole population is ongoing by means of CMR-trapping. Regional-scale population  
97 dynamics of gray-sided vole were monitored in Porsanger (N 70.05°, E 24.97°) with multiple trap-  
98 ping stations spaced along a 170 km transect (Nicolau et al., 2020). The sampling was conducted in  
99 mountain birch forest, where the gray-sided vole is the most common species within a community  
100 with four other rodent species (Yoccoz and Ims, 2004). The phases of the 4-year population cycle  
101 exhibit a great deal of spatial synchrony across the sampled region In case of the tundra vole, local  
102 population dynamics were monitored within an area of  $1km^2$  on the small oceanic island Håkøya  
103 (N 69.67°, E 18.83°). The tundra vole is here the only rodent species present. The population is  
104 distributed on patches of coastal meadows (Soininen et al., 2015), which is the preferred habitat for  
105 this species in Arctic and boreal ecosystem (Tast, 1966; Soininen et al., 2018).

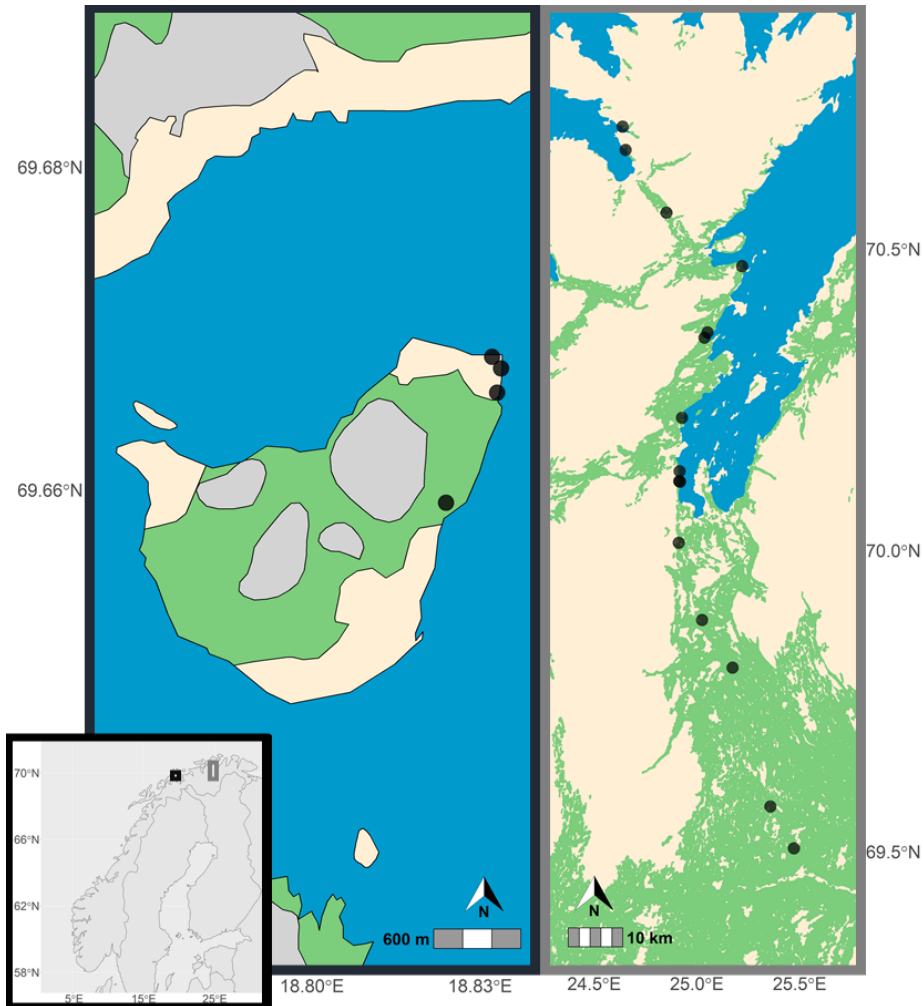


Figure 1: Maps of the study areas. Bottom left: regional map of Fennoscandia with the two study areas marked with different colored rectangles (Håkøya in black and Porsanger in gray). Left: Håkøya study area for the tundra vole. Right: Porsanger study area for the gray-sided vole. Black dots denote sampling stations, green hue is forest, light yellow corresponds to non-forested areas on dry ground (e.g. alpine or coastal heaths), gray is mire and the blue is sea. Notice the different scale of the two study area maps.

## 106 **2.2 Sampling design**

### 107 **2.2.1 CMR-trapping**

108 CMR-trapping was conducted with baited Ugglan No. 2 live traps during the snow-free seasons  
109 in the years 2018-2020. Unless previously marked, trapped animals were marked with a passive  
110 induced transponder (PIT)-tag, and the individual covariates *weight* and *sex* were recorded.

111 For the gray-sided vole monitoring, the trapping was conducted on 15 trapping stations spaced  
112 along the study transect (Figure 1). Each trapping station consisted of a standardized grid with  
113 16 live traps, covering an area of about 0.5 ha (Ehrich et al., 2009). In each of the three years,  
114 trapping was conducted in three sessions: middle of June, beginning of August and middle of  
115 September. During each session, the trapping was conducted over two consecutive days trapping  
116 days, following a trap-setting day (see Ehrich et al. (2009) for more details).

117 For the tundra vole monitoring, trapping was conducted in variably shaped and sized coastal  
118 meadow patches. For the purpose of the present study, we defined 4 sampling stations with sizes  
119 (approximately 0.5) and trapping grids (10-20 live traps) that were comparable to the sampling  
120 stations of the gray-sided vole monitoring. However, in contrast to the widely spaced trapping  
121 stations in the regional-scale monitoring of the gray-sided vole, the adjacent tundra vole trapping  
122 stations were considered to cover the same local population. CMR-trapping of tundra voles was  
123 conducted monthly from June to October (i.e., five trapping sessions) in each of the three years. As  
124 the trappability of tundra voles is lower than that of gray-sided voles (Øvrejorde, 2007), the tundra  
125 vole trapping was conducted over three consecutive days per session. Trappability was further  
126 enhanced by pre-baiting the live-traps one day prior to the first trap-night.

## 127 **2.2.2 CMR-based abundance estimation**

128 To address the sampling error associated with capture heterogeneity, abundances were estimated  
129 using the capture histories of each of the trapped individuals. Specifically, individual capture prob-  
130 abilities were assumed to have a temporal effect (model  $M_{th}$  in Otis et al. (1978)). We then fitted  
131 a multinomial regression model, where the logit-transformed probabilities of the capture histo-  
132 ries were modelled in terms of the individual variables *weight* and *sex*. In addition, the predictor  
133 included independent random effects for stations, to account for spatially-varying capture hetero-  
134 geneity. Finally, the CMR-based abundances ( $N_{s,t}$ ) were estimated using the Horvitz-Thompson  
135 estimator (Horvitz and Thompson, 1952), for each station  $s$  and trap season  $t$  (Huggins and Hwang,  
136 2011). This corresponds to the CR-INLA framework presented in Nicolau et al. (2020). Finally, we  
137 standardized the abundance estimates according to the number of live traps per trapping location.

## 138 **2.2.3 Camera trapping and abundance indices**

139 In November 2017 (tundra vole) and June 2018 (gray-sided vole), a single camera trap was placed  
140 within each of the CMR-grids, for a total of 15 camera traps in Porsanger and 4 in Håkkøya. We used  
141 the tunnel trap developed by (Soininen et al., 2015) and with the specific camera settings described  
142 in Mölle et al. (2021) and Appendix A.2.

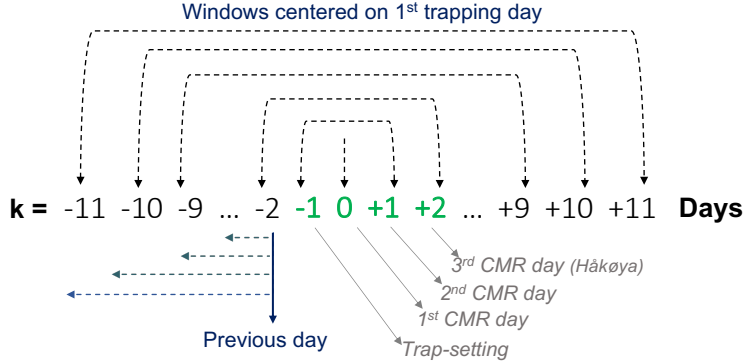


Figure 2: Schematic representation of the time-windows used to aggregate photo counts for the camera trap-based abundance indices. Days related to the CMR-trapping are presented in green, with day 0 corresponding to the first capture day (following trap-setting on the previous day; day -1), followed by one (gray-sided vole) or two (tundra vole) capture days. Two types/groups of time-windows are defined: CMR-encompassing, centered on first CMR day and thus including all days with activated live traps, shown by the upper set of vertical arrows; and CMR-preceding, for the days preceding the trap-setting day, shown by the set of bottom left vertical arrows.

143 We use a range of time-windows of daily photo counts to derive CT-indices (Figure 1). Let  $X_k$ ,  
 144  $k = -11, \dots, 11$ , denote the number of photos counted at day  $k$  relative to the first day of CMR-  
 145 trapping ( $k = 0$ ). The different temporal windows  $I$  denote intervals of  $d$  days. Each CT-index is  
 146 then defined as the average CT-counts per day for a given  $I$ , given by  $Y_I = \frac{1}{d} \sum_{k \in I} X_k$ .

147 We define two types/groups of time-windows, depending on whether the window encompassed  
 148 the CMR-trapping or preceded it. We make this distinction to account for the potential confounding  
 149 effect of entrapment of animals during CMR-trapping (i.e. considering that animals in live traps  
 150 cannot be camera trapped). For the CMR-preceding intervals, we assessed the windows  $I = [k, -2]$ ,  
 151 where  $k = -11, \dots, -2$ . For the CMR-encompassing intervals, we used the windows  $I = [-k, k]$ ,  
 152 where  $k = 0, \dots, 11$ .

## 2.3 Calibration analysis

For each time-window, we calibrated the CT-indices from the single camera trap per sampling station against the temporally matching CMR-based abundances estimates for the same station. For gray-sided voles, the dataset includes in total 115 calibration points, while there are 60 calibration points for the tundra voles (see Appendix A.1). As the 4 trapping stations for the tundra vole covered the same local population, we additionally perform a calibration analysis with the abundance indices and estimates averaged over all stations, which yields 15 calibration points.

### 2.3.1 Calibration Regression

Let  $Y_{I,s,t}$  denote the CT-index for a given temporal window  $I$ , measured at station  $s$  and trap season  $t$ . A linear relationship between the CT-index and the CMR-abundance ( $N_{s,t}$ ) is best fitted on a log-scale. A linear regression model is thus formulated by

$$\log(Y_{I,s,t} + 1) = \beta_0 + \beta_1 \log(N_{I,s,t} + 1) + \varepsilon_{I,s,t}, \quad (1)$$

where  $\beta_0$  and  $\beta_1$  are coefficients to be estimated to define the calibration line for each temporal window  $I$ . The set  $\{\varepsilon_{I,s,t}\}$  denotes error terms that are assumed to be independent and normally distributed with homogeneous variance. The number 1 was added to ensure positive arguments of the log-function. The ordinary coefficient of determination  $R^2$  is used as a measure of the goodness-of-fit.

### 2.3.2 Inverse prediction and model validation

For a simple linear regression model, the prediction interval for the explanatory variable can be calculated by inverting the corresponding prediction interval for the response variable. Here, we

169 used the R-package `investr` (Greenwell and Schubert Kabban, 2014) to compute the Wald 95%  
170 prediction interval for a new observation,  $\hat{x}_0 = \frac{\hat{y}_0 + \hat{\beta}_0}{\hat{\beta}_1}$ , where  $\hat{x}_0$  is the CMR-abundance estimate  
171 using the observed CT-index  $\hat{y}_0$ , and  $\hat{\beta}_0$  and  $\hat{\beta}_1$  denote estimates of the coefficients.

172 To assess the predictive performance of the calibration model with the time-window with the  
173 highest  $R^2$  value, we employ a k-fold cross-validation approach. Specifically, we remove all cali-  
174 bration points for a given station and estimate the coefficients of (1) using the remaining stations.  
175 We then predict the CMR-abundances given the corresponding CT-index of the excluded station.  
176 This is repeated for all stations, thus being equivalent to a 15-fold cross-validation approach for  
177 the gray-sided vole and a 4-fold cross-validation approach for tundra voles. For the spatially aggre-  
178 gated tundra vole calibration, performing cross-validation is not feasible (only 15 calibration points  
179 at a single spatial location).

180 Different measures of predictive performance are computed. These include coverage of the 95%  
181 prediction interval for the explanatory variables log CMR-abundances, the mean absolute error and  
182 the root mean squared error. Additionally, we define an ecological classification metric (ECM)  
183 which intends to provide qualitative information on predictions that are functionally relevant for  
184 a cyclic populations (i.e. cycle phases). We define the following three population density cate-  
185 gories: low-abundances (low phase of the cycle), intermediate abundances and high abundances  
186 (high phase). The high and low abundances are defined as the 25% and 75% quantiles of the re-  
187 spective sample distributions for each species. The ECM is thus defined as the proportion of times  
188 the true observed log-abundance value and the predicted value belong to the same category. The  
189 analysis was conducted in R 4.0.3 (R Core Team 2020).



## 3 Results

### 3.1 *Abundance estimates and indices*

Annual means of the CMR-based abundance estimates reveal the phases/years of population increase (2018), peak (2019) and crash (2020) for both vole species (Figure 3). The distributions of the standardized abundance estimates and indices were similar between the species (Table 1). Moreover, neither the overall means nor the variance in the CT-indices differed notably between species or time windows (Table 1 and Figure 4). However, there was a difference in the temporal autocorrelations of daily CT-counts between the two species. While the estimated auto-correlations decreased linearly over time with relatively little scatter for the gray-sided vole, the estimated auto-correlations for the tundra vole showed a steeper decrease over the first 4 days before it leveled off with a large scatter. Furthermore, for the gray-sided vole, there was an increase in the mean number of photos taken the days right after the trapping experiment, which could suggest a possible interaction between the two methodologies.

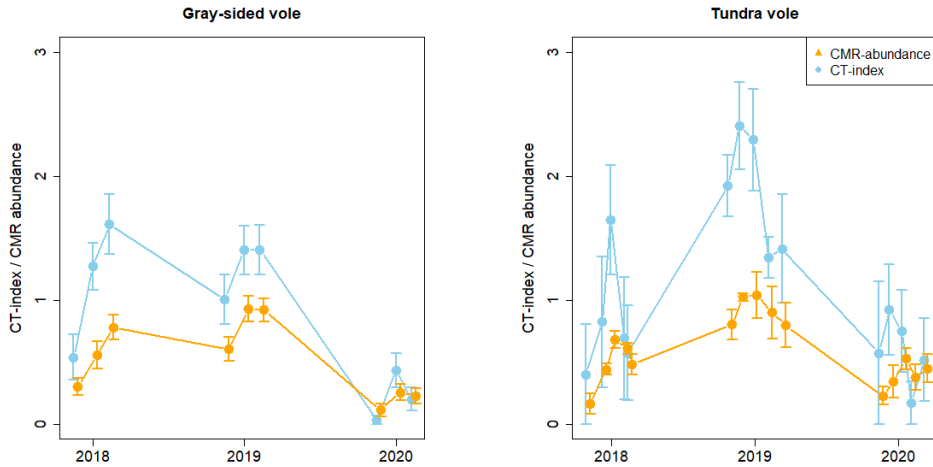


Figure 3: Population dynamics over trapping seasons (within-years) and years based on log-scale CT-abundance indices (blue circles) and log CMR-abundance estimates standardized by number of traps (orange circles). The indices and estimates represent means with standard error bars over all trapping stations for the two species. The optimal time-windows for the CT-index are used for both species (see Figure 5).

Table 1: Distribution statistics (arithmetic mean, standard deviation and range) for the standardized log-transformed abundances estimates (CMR-based;  $\log(\text{abundance}/N \text{ traps})$ ) and CT-indices ( $\log(\text{CT-counts})/(N \text{ days})$ ) used in the calibration regression models. The CT-indices are given for the time-window that provided the best fitting calibration regression (see Figure 5).

Metric	Statistic	Gray-sided vole	Tundra vole
CMR-estimates	Mean	0.54	0.59
	STDev	0.44	0.34
	Range	0-1.63	0-1.59
CT-indices	Mean	0.93	1.13
	STDev	0.84	0.94
	Range	0-3.10	0-3.22

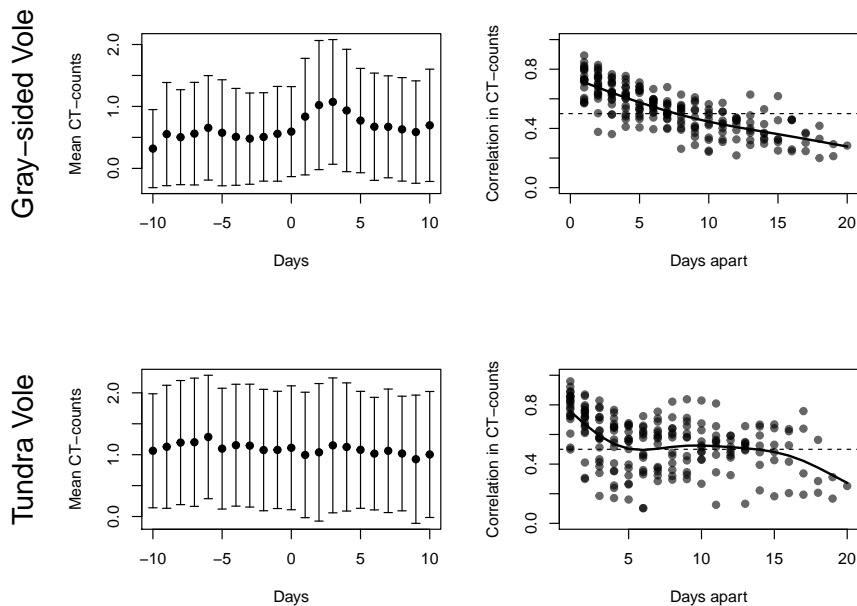


Figure 4: CT-count variation and temporal correlations. Left panels: mean of all the log CT-counts on each day relative to the trapping experiment (according to Fig.2), with standard deviation bars. Right panels: temporal auto-correlations in daily CT-counts per trap and trapping session as a function of temporal distance, i.e., days apart. The solid lines are non-parametric smooth regression lines from the `smooth.spline` function of the `stats` R-package (version 4.0.3).

### 3.2 Linear calibration regression

The linear calibration regressions based on the single camera trap per trapping station yielded  $R^2$ -values that greatly differed between the two species. The  $R^2$ -values for all time-windows are substantially higher for the gray-sided vole than the tundra vole (Figure 5). For the gray-sided vole, all time-windows for the CMR-encompassing group yielded similarly good fits (all  $R^2 > 0.5$  except for  $Y_{[0,0]}$ ). The best fitting calibration model ( $R^2 = 0.58$ , coefficients:  $\beta_0 = 0.15$ ;  $\beta_1 = 1.44$ ) was obtained for the 5-day time-window that encompassed the live-trapping session ( $Y_{[-2,2]}$ ). This regression model fulfilled the assumptions regarding log-scale linearity. For the tundra vole, the

211 best fit ( $R^2 = 0.21$ , coefficients:  $\beta_0 = 0.37$ ;  $\beta_1 = 1.28$ ) was obtained for the CT-index based on the  
 212 single day before the onset of the live-trapping ( $Y_{[-2,-2]}$ ). For the other time-windows (all  $R^2 < 0.2$ )  
 213 the difference between the two groups of time-windows was small. When the data were aggregated  
 214 over four adjacent sampling stations for the tundra vole population, the fit of the calibration function  
 215 improved substantially ( $R^2 = 0.81$ , Coefficients:  $\beta_0 = -0.16$ ;  $\beta_1 = 2.17$ , Figure 6).

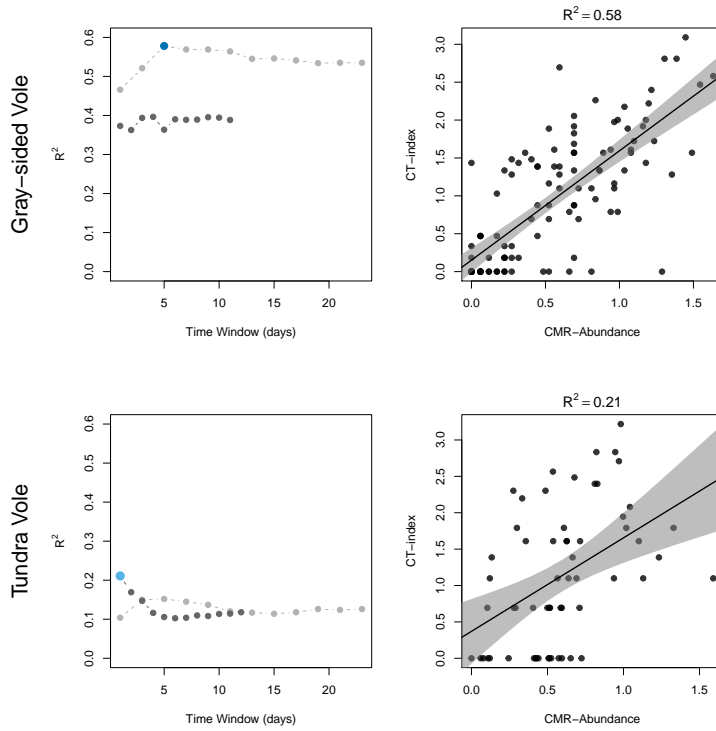


Figure 5: Statistics for linear calibration regressions. Left panels:  $R^2$  values for the calibration linear regressions fitted to the two groups of time-windows (CRM-encompassing: light gray symbols and CMR-preceding: dark gray symbols). The highest  $R^2$  values for each species is marked with an enlarged blue dot. Right panels: Data points and regression lines with 95% confidence intervals for the species-specific linear calibration models that yielded the highest  $R^2$ .

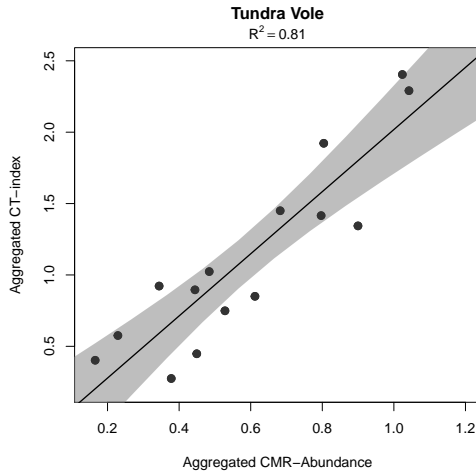


Figure 6: Calibration regression for tundra vole using aggregated data across all stations for the best fitting time-window ( $Y_{[-2,-2]}$ ). Coefficients:  $\beta_0 = -0.16$ ;  $\beta_1 = 2.17$ ; p-value  $< 0.001$ .

### 216 **3.3 Inverse prediction and validation**

217 As could be expected from the differences in the goodness-of-fit of the calibration regression (i.e.  
 218 the  $R^2$  values), the prediction intervals derived by the inverse regression were wider for the tundra  
 219 vole than for the gray-sided vole (Figure 7). The RMSE value (indicating the width of the interval)  
 220 was almost twice as high as for the tundra vole compared to the gray-sided vole, and the bias was  
 221 about three times higher (Table 2). In terms of classifying abundances based on the single camera  
 222 traps with respect to the three abundance classes (cf. ECM metrics in Table 2), two thirds of the  
 223 instances were correctly classified for the gray-sided vole, compared to roughly one third for the  
 224 tundra vole.

Table 2: Prediction metrics for the models with highest  $R^2$  for both the gray-sided Vole ( $Y_{[-2,2]}$ ) and the tundra vole ( $Y_{[-2,-2]}$ ).

Species	Coverage	ECM <sub>A</sub>	Bias	RMSE
Gray-sided vole	0.957	0.661	-0.004	0.385
Tundra vole	0.933	0.350	0.013	0.701

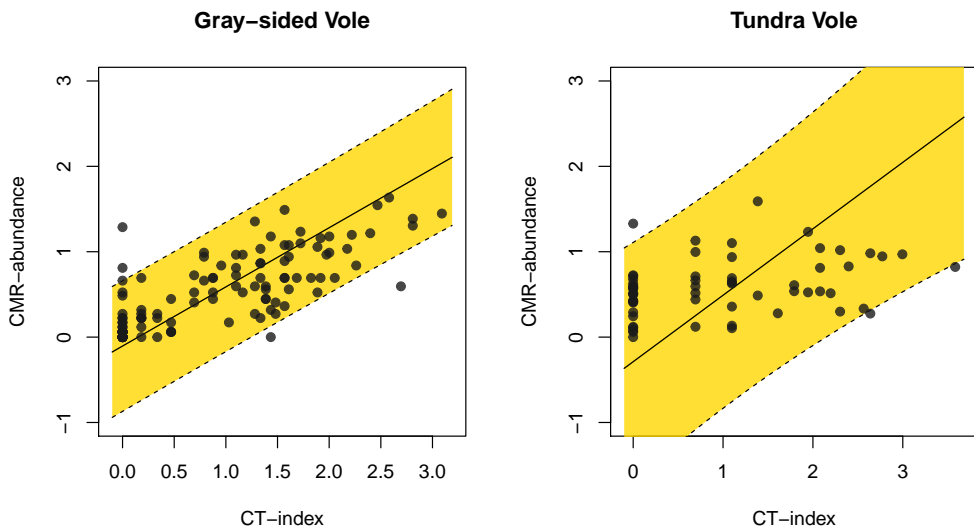


Figure 7: Inverse prediction plots for the CT-index windows yielding the best goodness-of-fit for each region, on the log scale. The Wald 95% confidence intervals are colored in yellow, and the data points are plotted in black dots.

## 4 Discussion

We have here assessed the adequacy of using photo counts, from the tunnel-camera trap developed by Soininen et al. (2015), as abundance metrics to study population dynamics of two ecologically important vole species that exhibit multi-annual cycles in boreal and Arctic ecosystems. Our assessment employed a two-step calibration approach, in which different temporally-scaled CT-indices from single camera traps were used as exposure variables calibrated against CMR-based abundance estimates from local live-trap grids, as the ground-truthing variable. In order to be adequate, abundance indices are required to have proportional (e.g. linear) relationships to the true abundance as well as reasonable precision. Considering that count-based camera trap indices (i.e. the number of motion-triggered animal passages) also reflect animal behavior (e.g. spacing behavior; *sensu* Krebs (1996)), which for long has been known to be density and phase dependent in cyclic vole populations (Chitty, 1960; Krebs, 2013), the assumption regarding proportionality can be violated.

While the proportionality assumption (on the log-scale) appeared to be met for both vole species, the precision of the abundance indices based on single camera traps differed considerably between them. For the gray-sided vole, the CT-indices from the single camera traps correlated well with the CMR-abundance estimates from the matched live-trapping grids, whereas equivalent correlation for the tundra vole was poorer. Accordingly, validation metrics of the inverse regressions showed that the abundance predictions based on single camera traps were substantially better for the gray-sided vole than the tundra vole. Compared with two previous calibration studies of non-cyclic vole populations in boreal America, the goodness of fit of the calibration regression for the cyclic gray-sided vole population ( $R^2 = 0.58$ ) performed equally good (Villette et al., 2015) or better (Parsons et al., 2021). The two American studies employed a different camera trap; i.e. open cameras mounted in front of the entrance of baited live traps. Moreover, these previous studies used aggregated CT-indices over 15-16 (Villette et al., 2015) and 16-20 camera traps (Parsons et al., 2021) per live-trapping grid, which was twice the size of our grids. The fact that we obtained

250 at least an equally good calibration for gray-sided vole with a single camera trap, and an even bet-  
251 ter calibration ( $R^2 = 0.81$ ) for the tundra vole when aggregating the data over only 4 camera traps,  
252 indicates that our unbaited tunnel-based traps are more efficient in capturing voles.

253 The differences in goodness-of-fit of the calibrations (and thus also precision of the abun-  
254 dance predictions) of gray-sided voles and tundra voles are reflected by the different optimal  
255 time-windows and the temporal auto-correlations of CT-counts for the two species. The optimized  
256 time-window for the gray-sided vole was longer (5 days including the live trapping days) and less  
257 temporally distinct (high  $R^2$ -values for wide range of time-windows) than for the tundra voles. The  
258 best time-window for the tundra vole was based on a single day just prior to the onset of the live-  
259 trapping sessions. Accordingly, the auto-correlations of the daily camera counts dropped faster and  
260 had a generally higher scatter for the tundra vole than the gray-sided vole. We believe this can  
261 be explained by the fact that the two vole species differ with respect to how their populations are  
262 spatio-socially organized (Ims, 1987b; Bondrup-Nielsen and Ims, 1990). Due to female territorial-  
263 ity, gray-sided voles are more evenly spaced within their habitat than tundra voles where females  
264 form spatially clustered kin-groups. These local tundra vole kin-groups are temporally unstable  
265 since females frequently shift home ranges (Tast, 1966). Consequently, local-scale abundance dy-  
266 namics of tundra voles is typically characterized with a high turnover (Andreassen and Ims, 2001)  
267 and weak auto-correlations (Ims and Andreassen, 1999). The much improved fit of the tundra vole  
268 calibration regression, when based on 4 instead of 1 camera trap, is most likely due to the effect of  
269 smoothing out the large small-scale spatio-temporal variability. This result underlines the benefit  
270 of spatially replicating camera traps within the same location/local population, which has also been  
271 highlighted by other authors (Kolowski et al., 2021). However, our study also shows that only a few  
272 tunnel-based camera traps may be needed to get adequate abundance indices for both vole species.  
273 In fact, a single camera trap was able to capture the main features of the cyclic dynamics of gray-  
274 sided vole. This indicates there may be a potential for conducting spatially extensive monitoring,  
275 for instance in order to estimate patterns of large-scale spatial population synchrony (Bjørnstad



276 et al., 1999), even with a limited number of camera traps available.

277 We believe that the greatest asset of the tunnel-based camera trap employed in our study is  
278 its ability to yield population metrics year-round, with a finer temporal resolution than any other  
279 presently available method. For small rodents with multi-annual cycles, the transitions between  
280 the different cyclic phases (e.g. between peak and crash) can be very rapid and take place at any  
281 time of the year (Krebs, 2013). By providing reliable abundance indices for time-windows as  
282 short as a few days, camera traps radically enhance our options for identifying the drivers of cyclic  
283 rodent dynamics. Strongly density-dependent interactions and rapid community-level dynamics  
284 have for long been assumed to be driving rodent cycles (Hansson and Henttonen, 1988; Turchin  
285 and Hanski, 2001; Barraquand et al., 2017). Assumed key interactions – such as those between  
286 voles and small mustelids – have been beyond the reach of thorough investigations owing to dif-  
287 ficulty of obtaining adequately scaled data for both interactants simultaneously (King and Powell,  
288 2006). Our tunnel-based camera traps recorded substantial data (i.e. relatively high number of  
289 photo counts) for all members of the small mammal community in both study areas, including  
290 small mustelids (least weasel *Mustela nivalis* and stoat *Mustela erminea*), Norwegian lemmings  
291 (*Lemmus lemmus*) and shrews (*Sorex* spp.) (see also (Möller et al., 2021) and Appendix B.3). While  
292 species-interactions based on camera trap data can be analysed based on absence-presence records  
293 within an occupancy modelling framework ((Rota et al., 2016; Fidino et al., 2019)), abundance met-  
294 rics are more informative as they allow analyses of the density-dependent interactions that appear  
295 to drive population cycles (Stenseth, 1999). New studies are needed to validate camera trap-based  
296 abundance indices for species such as mustelids and lemmings. As true ground-truthing variables  
297 for such species (especially mustelids (King and Powell, 2006)) are extremely difficult to obtain,  
298 there may be alternatives to use other statistical frameworks to obtain detectability corrected abun-  
299 dance indices (Gilbert et al., 2021; Palencia et al., 2021). Such frameworks may also be used derive  
300 unbiased abundance indices from camera-trap data during the boreal and Arctic winter, when deep  
301 snow and harsh climatic condition hinder calibration studies of the kind we have performed in this

302 study. Hence, although our study highlights the potential of tunnel-based camera traps to likely  
303 advance studies of cyclic rodent populations, it also illustrates the need for performing species- and  
304 context-specific validation studies.

## 305 **References**

306 Andreassen, H. P. and Ims, R. A. (2001). Dispersal in patchy vole populations: role of patch  
307 configuration, density dependence, and demography. *Ecology*, 82(10):2911–2926.

308 Andreassen, H. P., Sundell, J., Ecke, F., Halle, S., Haapakoski, M., Henttonen, H., Huitu, O., Jacob,  
309 J., Johnsen, K., Koskela, E., Luque-Larena, J. J., Lecomte, N., Leirs, H., Mariën, J., Neby, M.,  
310 Rätti, O., Sievert, T., Singleton, G. R., van Cann, J., Broecker, B. V., and Ylönen, H. (2021).  
311 Population cycles and outbreaks of small rodents: ten essential questions we still need to solve.  
312 *Oecologia*, 195(3):601–622.

313 Bailey, L. L., MacKenzie, D. I., and Nichols, J. D. (2014). Advances and applications of occupancy  
314 models. *Methods in Ecology and Evolution*, 5(12):1269–1279.

315 Barraquand, F., Louca, S., Abbott, K. C., Cobbold, C. A., Cordoleani, F., DeAngelis, D. L., Elderd,  
316 B. D., Fox, J. W., Greenwood, P., Hilker, F. M., Murray, D. L., Stieha, C. R., Taylor, R. A.,  
317 Vitense, K., Wolkowicz, G. S., and Tyson, R. C. (2017). Moving forward in circles: challenges  
318 and opportunities in modelling population cycles. *Ecology Letters*, 20(8):1074–1092.

319 Bjørnstad, O. N., Ims, R. A., and Lambin, X. (1999). Spatial population dynamics: analyzing  
320 patterns and processes of population synchrony. *Trends in Ecology & Evolution*, 14(11):427–  
321 432.

322 Bondrup-Nielsen, S. and Ims, R. A. (1990). Reversed sexual size dimorphism in microtines: Are

323 females larger than males or are males smaller than females? *Evolutionary Ecology*, 4(3):261–  
324 272.

325 Boonstra, R., Andreassen, H. P., Boutin, S., Hušek, J., Ims, R. A., Krebs, C. J., Skarpe, C., and  
326 Wabakken, P. (2016). Why do the boreal forest ecosystems of northwestern Europe differ from  
327 those of western North America? *BioScience*, 66(9):722–734.

328 Boonstra, R. and Krebs, C. J. (1978). Pitfall trapping of *Microtus townsendii*. *Journal of Mammal-*  
329 *ogy*, 59(1):136–148.

330 Burton, A. C., Neilson, E., Moreira, D., Ladle, A., Steenweg, R., Fisher, J. T., Bayne, E., and  
331 Boutin, S. (2015). Review: Wildlife camera trapping: a review and recommendations for linking  
332 surveys to ecological processes. *Journal of Applied Ecology*, 52(3):675–685.

333 Capizzi, D., Bertolino, S., and Mortelliti, A. (2014). Rating the rat: global patterns and research  
334 priorities in impacts and management of rodent pests. *Mammal Review*, 44(2):148–162.

335 Chitty, D. (1960). Population processes in the vole and their relevance to general theory. *Canadian*  
336 *Journal of Zoology*, 38(1):99–113.

337 Cornulier, T., Yoccoz, N. G., Bretagnolle, V., Brommer, J. E., Butet, A., Ecke, F., Elston, D. A.,  
338 Framstad, E., Henttonen, H., Hörnfeldt, B., Huitu, O., Imholt, C., Ims, R. A., Jacob, J., Jędrze-  
339 jewska, B., Millon, A., Petty, S. J., Pietiäinen, H., Tkadlec, E., Zub, K., and Lambin, X. (2013).  
340 Europe-wide dampening of population cycles in keystone herbivores. *Science*, 340(6128):63–66.

341 Diefenbach, D. R., Conroy, M. J., Warren, R. J., James, W. E., Baker, L. A., and Hon, T. (1994).  
342 A test of the scent-station survey technique for bobcats. *The Journal of Wildlife Management*,  
343 58(1):10–17.

344 Ehrlich, D., Schmidt, N. M., Gauthier, G., Alisauskas, R., Angerbjörn, A., Clark, K., Ecke, F.,  
345 Eide, N. E., Framstad, E., Frandsen, J., Franke, A., Gilg, O., Giroux, M.-A., Henttonen, H.,

346 Hörnfeldt, B., Ims, R. A., Kataev, G. D., Kharitonov, S. P., Killengreen, S. T., Krebs, C. J.,  
347 Lanctot, R. B., Lecomte, N., Menyushina, I. E., Morris, D. W., Morrisson, G., Oksanen, L.,  
348 Oksanen, T., Olofsson, J., Pokrovsky, I. G., Popov, I. Y., Reid, D., Roth, J. D., Saalfeld, S. T.,  
349 Samelius, G., Sittler, B., Sleptsov, S. M., Smith, P. A., Sokolov, A. A., Sokolova, N. A., Soloviev,  
350 M. Y., and Solovyeva, D. V. (2019). Documenting lemming population change in the Arctic: can  
351 we detect trends? *Ambio*, 49(3):786–800.

352 Ehrlich, D., Yoccoz, N. G., and Ims, R. A. (2009). Multi-annual density fluctuations and habitat  
353 size enhance genetic variability in two northern voles. *Oikos*, 118(10):1441–1452.

354 Eisenhart, C. (1939). The interpretation of certain regression methods and their use in biological  
355 and industrial research. *The Annals of Mathematical Statistics*, 10(2):162–186.

356 Fidino, M., Simonis, J. L., and Magle, S. B. (2019). A multistate dynamic occupancy model to  
357 estimate local colonization–extinction rates and patterns of co-occurrence between two or more  
358 interacting species. *Methods in Ecology and Evolution*, 10(2):233–244.

359 Gilbert, N. A., Clare, J. D. J., Stenglein, J. L., and Zuckerberg, B. (2021). Abundance estimation of  
360 unmarked animals based on camera-trap data. *Conservation biology : the journal of the Society  
361 for Conservation Biology*, 35(1):88–100.

362 Gopaldaswamy, A. M., Delampady, M., Karanth, K. U., Kumar, N. S., and Macdonald, D. W. (2015).  
363 An examination of index-calibration experiments: counting tigers at macroecological scales.  
364 *Methods in Ecology and Evolution*, 6(9):1055–1066.

365 Greenwell, B. M. and Schubert Kabban, C. M. (2014). investr: An R package for inverse estimation.  
366 *The R Journal*, 6(1):90.

367 Hansen, T. F., Stenseth, N. C., and Henttonen, H. (1999). Multiannual vole cycles and popula-  
368 tion regulation during long winters: an analysis of seasonal density dependence. *The American  
369 Naturalist*, 154(2):129–139. PMID: 29578785.

- 370 Hanski, I., Henttonen, H., and Hansson, L. (1994). Temporal variability and geographical patterns  
371 in the population density of microtine rodents: A reply to Xia and Boonstra. *The American*  
372 *Naturalist*, 144(2):329–342.
- 373 Hansson, L. and Henttonen, H. (1988). Rodent dynamics as community processes. *Trends in*  
374 *Ecology & Evolution*, 3(8):195–200.
- 375 Henden, J.-A., Ehrlich, D., Soininen, E. M., and Ims, R. A. (2021). Accounting for food web  
376 dynamics when assessing the impact of mesopredator control on declining prey populations.  
377 *Journal of Applied Ecology*, 58(1):104–113.
- 378 Hörnfeldt, B., Hipkiss, T., and Eklund, U. (2005). Fading out of vole and predator cycles? *Pro-*  
379 *ceedings of the Royal Society B: Biological Sciences*, 272(1576):2045–2049.
- 380 Horvitz, D. G. and Thompson, D. J. (1952). A generalization of sampling without replacement  
381 from a finite universe. *Journal of the American Statistical Association*, 47(260):663–685.
- 382 Huggins, R. and Hwang, W.-H. (2011). A review of the use of conditional likelihood in capture-  
383 recapture experiments. *International Statistical Review*, 79(3):385–400.
- 384 Ims, R. and Andreassen, H. (1999). Demographic synchrony in fragmented populations. In Barrett,  
385 G. and Peles, J., editors, *The ecology of small mammals at the landscape level: experimental*  
386 *approaches*, pages 129–145. Springer-Verlag.
- 387 Ims, R. A. (1987a). Male spacing systems in microtine rodents. *The American Naturalist*,  
388 130(4):475–484.
- 389 Ims, R. A. (1987b). Responses in spatial organization and behaviour to manipulations of the food  
390 resource in the vole *Clethrionomys rufocanus*. *The Journal of Animal Ecology*, pages 585–596.
- 391 Ims, R. A. and Fuglei, E. (2005). Trophic interaction cycles in tundra ecosystems and the impact  
392 of climate change. *BioScience*, 55(4):311–322.

- 393 Ims, R. A., Killengreen, S. T., Ehrich, D., Flagstad, Ø., Hamel, S., Henden, J.-A., Jensvoll, I., and  
394 Yoccoz, N. G. (2018). Ecosystem drivers of an Arctic fox population at the western fringe of the  
395 Eurasian Arctic. *Polar Research*, 36((sup1)).
- 396 Jennelle, C. S., Runge, M. C., and MacKenzie, D. I. (2002). The use of photographic rates to  
397 estimate densities of tigers and other cryptic mammals: a comment on misleading conclusions.  
398 *Animal Conservation*, 5(2):119–120.
- 399 Jensen, P., Stenseth, N., and E., F. (1993). Trappability of the norwegian lemming (*Lemmus lem-*  
400 *mus*). In Stenseth, N. and R.A., I., editors, *The Biology of Lemmings*, pages 547–554. Academic  
401 Press, London.
- 402 King, C. M. and Powell, R. A. (2006). *The natural history of weasels and stoats: ecology, behavior,*  
403 *and management*. Oxford University Press.
- 404 Kleiven, E. F., Henden, J.-A., Ims, R. A., and Yoccoz, N. G. (2018). Seasonal difference in temporal  
405 transferability of an ecological model: near-term predictions of lemming outbreak abundances.  
406 *Scientific Reports*, 8(1).
- 407 Kolowski, J. M., Oley, J., and McShea, W. J. (2021). High-density camera trap grid reveals lack of  
408 consistency in detection and capture rates across space and time. *Ecosphere*, 12(2):e03350.
- 409 Korpela, K., Delgado, M., Henttonen, H., Korpimäki, E., Koskela, E., Ovaskainen, O., Pietiäinen,  
410 H., Sundell, J., Yoccoz, N. G., and Huitu, O. (2013). Nonlinear effects of climate on boreal  
411 rodent dynamics: mild winters do not negate high-amplitude cycles. *Global Change Biology*,  
412 19(3):697–710.
- 413 Krebs, C. J. (1996). Population cycles revisited. *Journal of Mammalogy*, 77(1):8–24.
- 414 Krebs, C. J. (2013). *Population fluctuations in rodents*. University of Chicago Press.

- 415 Krebs, C. J., Boonstra, R., Gilbert, S., Reid, D., Kenney, A. J., and Hofer, E. J. (2011). Density  
416 estimation for small mammals from livetrapping grids: rodents in northern Canada. *Journal of*  
417 *Mammalogy*, 92(5):974–981.
- 418 Lambin, X., Petty, S. J., and Mackinnon, J. L. (2000). Cyclic dynamics in field vole populations  
419 and generalist predation. *Journal of Animal Ecology*, 69(1):106–119.
- 420 Legagneux, P., Gauthier, G., Lecomte, N., Schmidt, N. M., Reid, D., Cadieux, M.-C., Berteaux,  
421 D., Bêty, J., Krebs, C. J., Ims, R. A., Yoccoz, N. G., Morrison, R. I. G., Leroux, S. J., Loreau,  
422 M., and Gravel, D. (2014). Arctic ecosystem structure and functioning shaped by climate and  
423 herbivore body size. *Nature Climate Change*, 4(5):379–383.
- 424 MacKenzie, D. I., Nichols, J. D., Lachman, G. B., Droege, S., Andrew Royle, J., and Langtimm,  
425 C. A. (2002). Estimating site occupancy rates when detection probabilities are less than one.  
426 *Ecology*, 83(8):2248–2255.
- 427 Marolla, F., Aarvak, T., Øien, I. J., Mellard, J. P., Henden, J.-A., Hamel, S., Stien, A., Tveraa, T.,  
428 Yoccoz, N. G., and Ims, R. A. (2019). Assessing the effect of predator control on an endan-  
429 gered goose population subjected to predator-mediated food web dynamics. *Journal of Applied*  
430 *Ecology*, 56(5):1245–1255.
- 431 Meerburg, B. G., Singleton, G. R., and Kijlstra, A. (2009a). Rodent-borne diseases and their risks  
432 for public health. *Critical Reviews in Microbiology*, 35(3):221–270. PMID: 19548807.
- 433 Meerburg, B. G., Singleton, G. R., and Leirs, H. (2009b). The Year of the Rat ends — time to fight  
434 hunger!. *Pest Management Science*, 65(4):351–352.
- 435 Mölle, J. P., Kleiven, E. F., Ims, R. A., and Soininen, E. M. (2021). Using subnivean camera traps  
436 to study arctic small mammal community dynamics during winter. *Arctic Science*, pages 1–17.

- 437 Nicolau, P. G., Sørbye, S. H., and Yoccoz, N. G. (2020). Incorporating capture heterogeneity in the  
438 estimation of autoregressive coefficients of animal population dynamics using capture–recapture  
439 data. *Ecology and Evolution*, 10(23):12710–12726.
- 440 Otis, D. L., Burnham, K. P., White, G. C., and Anderson, D. R. (1978). Statistical inference from  
441 capture data on closed animal populations. *Wildlife Monographs*, (62):3–135.
- 442 Øvrejorde, A. (2007). Calibrating abundance indices of small rodents in subarctic tundra. *MSci*  
443 *thesis, Univ. of Tromsø*.
- 444 Palencia, P., Rowcliffe, J. M., Vicente, J., and Acevedo, P. (2021). Assessing the camera trap  
445 methodologies used to estimate density of unmarked populations. *Journal of Applied Ecology*,  
446 58(8):1583–1592.
- 447 Palmer, M. S., Swanson, A., Kosmala, M., Arnold, T., and Packer, C. (2018). Evaluating rela-  
448 tive abundance indices for terrestrial herbivores from large-scale camera trap surveys. *African*  
449 *Journal of Ecology*, 56(4):791–803.
- 450 Parsons, M. A., Orloff, A. E., and Prugh, L. R. (2021). Evaluating livetrapping and camera-based  
451 indices of small-mammal density. *Canadian Journal of Zoology*, 99(6):521–530.
- 452 Powell, R. A. and Proulx, G. (2003). Trapping and marking terrestrial mammals for research: Inte-  
453 grating ethics, performance criteria, techniques, and common sense. *ILAR Journal*, 44(4):259–  
454 276.
- 455 Rendall, A. R., Sutherland, D. R., Cooke, R., and White, J. (2014). Camera trapping: A contem-  
456 porary approach to monitoring invasive rodents in high conservation priority ecosystems. *PLoS*  
457 *ONE*, 9(3):e86592.
- 458 Rota, C. T., Ferreira, M. A. R., Kays, R. W., Forrester, T. D., Kalies, E. L., McShea, W. J., Parsons,



- 459 A. W., and Millspaugh, J. J. (2016). A multispecies occupancy model for two or more interacting  
460 species. *Methods in Ecology and Evolution*, 7(10):1164–1173.
- 461 Soinen, E. M., Henden, J.-A., Ravolainen, V. T., Yoccoz, N. G., Bråthen, K. A., Killengreen,  
462 S. T., and Ims, R. A. (2018). Transferability of biotic interactions: Temporal consistency of  
463 arctic plant–rodent relationships is poor. *Ecology and Evolution*, 8(19):9697–9711.
- 464 Soinen, E. M., Jensvoll, I., Killengreen, S. T., and Ims, R. A. (2015). Under the snow: a new  
465 camera trap opens the white box of subnivean ecology. *Remote Sensing in Ecology and Conser-  
466 vation*, 1(1):29–38.
- 467 Stenseth, N. C. (1999). Population cycles in voles and lemmings: Density dependence and phase  
468 dependence in a stochastic world. *Oikos*, 87(3):427–461.
- 469 Tabak, M. A., Norouzzadeh, M. S., Wolfson, D. W., Sweeney, S. J., Vercauteren, K. C., Snow, N. P.,  
470 Halseth, J. M., Di Salvo, P. A., Lewis, J. S., White, M. D., Teton, B., Beasley, J. C., Schlichting,  
471 P. E., Boughton, R. K., Wight, B., Newkirk, E. S., Ivan, J. S., Odell, E. A., Brook, R. K., Lukacs,  
472 P. M., Moeller, A. K., Mandeville, E. G., Clune, J., and Miller, R. S. (2019). Machine learning  
473 to classify animal species in camera trap images: applications in ecology. *Methods in Ecology  
474 and Evolution*, 10(4):585–590.
- 475 Tast, J. (1966). The root vole, *Microtus oeconomus* (Pallas), as an inhabitant of seasonally flooded  
476 land. In *Annales Zoologici Fennici*, volume 3, pages 127–171. JSTOR.
- 477 Turchin, P. and Hanski, I. (2001). Contrasting alternative hypotheses about rodent cycles by trans-  
478 lating them into parameterized models. *Ecology Letters*, 4(3):267–276.
- 479 Turchin, P., Oksanen, L., Ekerholm, P., Oksanen, T., and Henttonen, H. (2000). Are lemmings prey  
480 or predators? *Nature*, 405(6786):562–565.

- 481 Villette, P., Krebs, C. J., Jung, T. S., and Boonstra, R. (2015). Can camera trapping provide accurate  
482 estimates of small mammal (*Myodes rutilus* and *Peromyscus maniculatus*) density in the boreal  
483 forest? *Journal of Mammalogy*, 97(1):32–40.
- 484 Wearn, O. R. and Glover-Kapfer, P. (2019). Snap happy: camera traps are an effective sampling  
485 tool when compared with alternative methods. *Royal Society Open Science*, 6(3):181748.
- 486 Wilson, D. E. and Reeder, D. M. (2005). *Mammal species of the world: a taxonomic and geo-*  
487 *graphic reference*, volume 2. JHU Press.
- 488 Yoccoz, N. G. and Ims, R. A. (2004). Spatial population dynamics of small mammals: some  
489 methodological and practical issues. *Animal Biodiversity and Conservation*, 27(1):427–435.
- 490 Yoccoz, N. G., Nichols, J. D., and Boulinier, T. (2001). Monitoring of biological diversity in space  
491 and time. *Trends in Ecology and Evolution*, 16(8):446–453.

## A Supplementary Methods

### A.1 Temporal distribution of data sampling

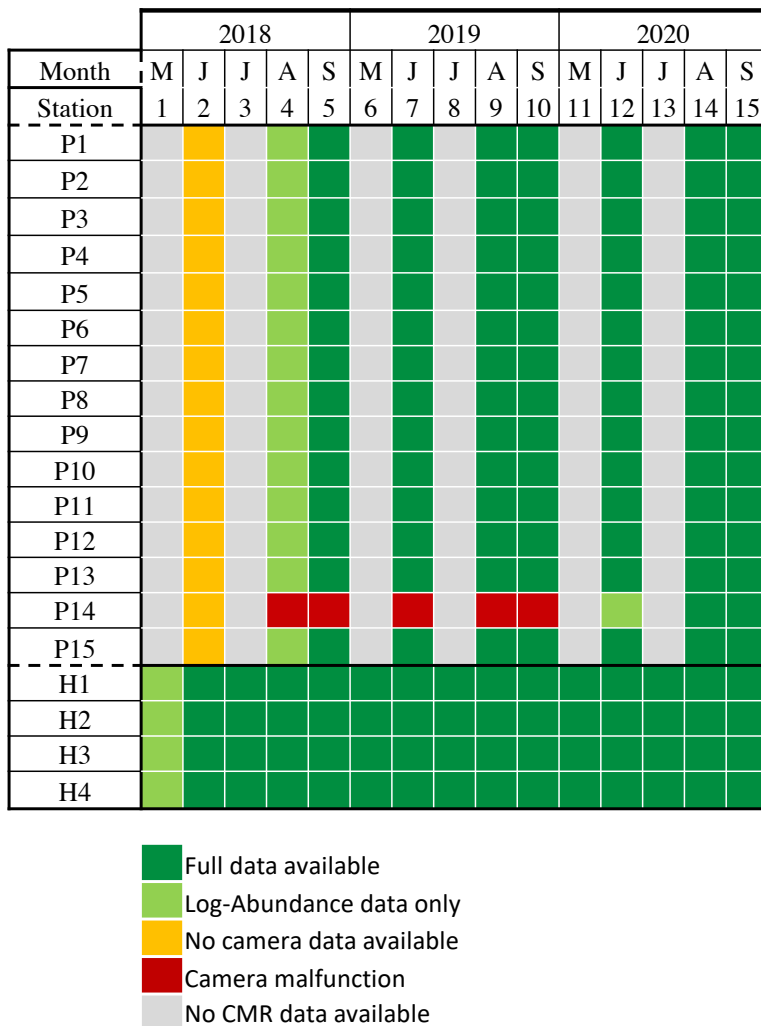


Figure 8: Temporal distribution of the index-calibration data for each of the stations for the different regions.

## 494 **A.2 Camera Trap sampling**

495 We used *Reconyx<sup>TM</sup> SM750 Hyperfire<sup>TM</sup>* (Reconyx Inc., Holmen, WI, USA) with a passive in-  
496 frared (PIR) motion sensor. Each camera trap was placed at the roof of an artificial metal tunnel,  
497 facing down. These tunnels were deployed in natural small mammal runways without any kind of  
498 lure, simulating natural tunnels/cavities which small mammals typically enter. For a more detailed  
499 description of the small mammal camera setup see (Soininen et al., 2015) and (Möller et al., 2021).  
500 At Porsanger, where the capture-recapture was done in standardized trapping grids, the camera  
501 traps were always deployed close to the center of the grid. At Håkøya, where the shape of the  
502 capture-recapture grids did not follow a structured design, the camera traps were deployed within  
503 the trapping grid.

504 This methodology allowed us to collect continuous camera trap data from the small rodent  
505 populations monitored by the capture-recapture design, with a total of 15 camera traps (and capture-  
506 recapture grids) in Porsanger and 4 in Håkøya. The camera traps collected data continuously and  
507 were checked once a year to replace batteries and collect memory cards. To avoid multiple camera  
508 trap counts from the same trigger event and to save power so that battery would not run out before  
509 next check, the cameras were set to not be triggered more than once per minute.

### 510 **A.2.1 Camera trap image annotations**

511 Once collected, all the camera trap images were annotated using the *MLWIC* package in R  
512 (Tabak et al., 2019) for automatic image classification. We set the classification threshold at 95%  
513 confidence for positive identification of a species in a photo. For the images from Håkøya, an  
514 area only inhabited by a single vole species, the images were classified to species level with high  
515 accuracy. For the Porsanger dataset, which contains multiple vole species, it was not possible to  
516 obtain sufficient classification results using the *MLWIC* package, as it did not separate different

517 species of voles accurately (only possible at genus level). Therefore, we manually annotated the  
518 images for the Porsanger analysis to species level.

519

## B Supplementary Results

In this section we present the calibration model coefficients for the different CT-indices tested in this study, as well as the predictive metrics, separately for the Gray-sided Vole (B.1) and for the Tundra Vole (B.2). Finally, we show the photo counts of all the species detected in the camera traps (B.3).

### B.1 Gray-sided Vole

#### B.1.1 Linear Regression Coefficients

Table 3: Coefficients for region Porsanger for all the CMR-encompassing windows.

Window	$\beta_0 (\pm \text{s.e.})$	$\beta_1 (\pm \text{s.e.})$	p-value ( $\beta_1$ )	$R^2$
$Y_{[0,0]}$	$0.05 \pm 0.1$	$1.45 \pm 0.15$	$< 0.001$	0.466
$Y_{[-1,1]}$	$0.14 \pm 0.09$	$1.41 \pm 0.13$	$< 0.001$	0.521
$Y_{[-2,2]}$	$0.15 \pm 0.08$	$1.44 \pm 0.12$	$< 0.001$	0.578
$Y_{[-3,3]}$	$0.16 \pm 0.08$	$1.39 \pm 0.11$	$< 0.001$	0.569
$Y_{[-4,4]}$	$0.16 \pm 0.08$	$1.34 \pm 0.11$	$< 0.001$	0.569
$Y_{[-5,5]}$	$0.15 \pm 0.08$	$1.32 \pm 0.11$	$< 0.001$	0.564
$Y_{[-6,6]}$	$0.16 \pm 0.08$	$1.28 \pm 0.11$	$< 0.001$	0.545
$Y_{[-7,7]}$	$0.16 \pm 0.08$	$1.27 \pm 0.11$	$< 0.001$	0.546
$Y_{[-8,8]}$	$0.16 \pm 0.08$	$1.25 \pm 0.11$	$< 0.001$	0.541
$Y_{[-9,9]}$	$0.16 \pm 0.08$	$1.24 \pm 0.11$	$< 0.001$	0.534
$Y_{[-10,10]}$	$0.15 \pm 0.08$	$1.23 \pm 0.11$	$< 0.001$	0.535
$Y_{[-11,11]}$	$0.14 \pm 0.07$	$1.2 \pm 0.11$	$< 0.001$	0.535

Table 4: Coefficients for region Porsanger for all the CMR-preceding windows.

Window	$\beta_0$ ( $\pm$ s.e.)	$\beta_1$ ( $\pm$ s.e.)	p-value ( $\beta_1$ )	$R^2$
$Y_{[-2,-2]}$	$-0.01 \pm 0.09$	$1.05 \pm 0.13$	$< 0.001$	0.3732
$Y_{[-3,-2]}$	$0.05 \pm 0.08$	$0.96 \pm 0.12$	$< 0.001$	0.3626
$Y_{[-4,-2]}$	$0.04 \pm 0.08$	$0.98 \pm 0.11$	$< 0.001$	0.3938
$Y_{[-5,-2]}$	$0.04 \pm 0.08$	$0.99 \pm 0.12$	$< 0.001$	0.3964
$Y_{[-6,-2]}$	$0.06 \pm 0.09$	$0.98 \pm 0.12$	$< 0.001$	0.3636
$Y_{[-7,-2]}$	$0.07 \pm 0.08$	$1.03 \pm 0.12$	$< 0.001$	0.3901
$Y_{[-8,-2]}$	$0.09 \pm 0.08$	$1.02 \pm 0.12$	$< 0.001$	0.3889
$Y_{[-9,-2]}$	$0.09 \pm 0.08$	$1.01 \pm 0.12$	$< 0.001$	0.3894
$Y_{[-10,-2]}$	$0.09 \pm 0.08$	$1.03 \pm 0.12$	$< 0.001$	0.3955
$Y_{[-11,-2]}$	$0.08 \pm 0.08$	$1 \pm 0.12$	$< 0.001$	0.3945

## B.1.2 Predictive Performance

Table 5: Predictive performance of the calibration models for Porsanger, using the CT-index for the CMR-encompassing windows to predict log-abundance.

Window	Coverage	ECM	Bias	RMSE
$Y_{[0,0]}$	0.957	0.617	-0.008	0.483
$Y_{[-1,1]}$	0.957	0.600	-0.007	0.431
$Y_{[-2,2]}$	0.957	0.661	-0.004	0.385
$Y_{[-3,3]}$	0.957	0.652	-0.004	0.394
$Y_{[-4,4]}$	0.948	0.670	-0.003	0.394
$Y_{[-5,5]}$	0.948	0.652	-0.004	0.399
$Y_{[-6,6]}$	0.957	0.609	-0.005	0.415
$Y_{[-7,7]}$	0.957	0.617	-0.004	0.415
$Y_{[-8,8]}$	0.948	0.609	-0.005	0.421
$Y_{[-9,9]}$	0.948	0.617	-0.005	0.427
$Y_{[-10,10]}$	0.939	0.609	-0.005	0.427
$Y_{[-11,11]}$	0.939	0.626	-0.005	0.427



Table 6: Predictive performance of the calibration models for Porsanger, using the CT-index for the CMR-preceding windows to predict log-abundance.

Window	Coverage	ECM	Bias	RMSE
$Y_{[-2,-2]}$	0.930	0.617	-0.011	0.599
$Y_{[-3,-2]}$	0.948	0.548	-0.011	0.611
$Y_{[-4,-2]}$	0.983	0.548	-0.009	0.571
$Y_{[-5,-2]}$	0.965	0.557	-0.009	0.568
$Y_{[-6,-2]}$	0.965	0.574	-0.009	0.605
$Y_{[-7,-2]}$	0.957	0.591	-0.007	0.570
$Y_{[-8,-2]}$	0.948	0.591	-0.007	0.574
$Y_{[-9,-2]}$	0.948	0.591	-0.007	0.573
$Y_{[-10,-2]}$	0.957	0.609	-0.007	0.566
$Y_{[-11,-2]}$	0.957	0.583	-0.007	0.566

528 **B.2 Tundra Vole**

529 **B.2.1 Linear regression coefficients**

Table 7: Coefficients for region Håkøya for all the CMR-encompassing windows.

Window	$\beta_0 (\pm \text{s.e.})$	$\beta_1 (\pm \text{s.e.})$	p-value ( $\beta_1$ )	$R^2$
$Y_{[0,0]}$	$0.43 \pm 0.25$	$0.96 \pm 0.37$	0.012	0.104
$Y_{[-1,1]}$	$0.46 \pm 0.24$	$1.13 \pm 0.35$	0.002	0.150
$Y_{[-2,2]}$	$0.53 \pm 0.23$	$1.1 \pm 0.34$	0.002	0.152
$Y_{[-3,3]}$	$0.58 \pm 0.23$	$1.1 \pm 0.34$	0.003	0.145
$Y_{[-4,4]}$	$0.64 \pm 0.22$	$1.0 \pm 0.33$	0.004	0.137
$Y_{[-5,5]}$	$0.70 \pm 0.22$	$0.91 \pm 0.32$	0.007	0.120
$Y_{[-6,6]}$	$0.71 \pm 0.22$	$0.89 \pm 0.32$	0.008	0.117
$Y_{[-7,7]}$	$0.73 \pm 0.22$	$0.87 \pm 0.32$	0.008	0.114
$Y_{[-8,8]}$	$0.72 \pm 0.22$	$0.89 \pm 0.32$	0.007	0.118
$Y_{[-9,9]}$	$0.72 \pm 0.21$	$0.91 \pm 0.31$	0.005	0.126
$Y_{[-10,10]}$	$0.72 \pm 0.21$	$0.89 \pm 0.31$	0.006	0.124
$Y_{[-11,11]}$	$0.73 \pm 0.21$	$0.89 \pm 0.31$	0.005	0.126

Table 8: Coefficients for region Håkøya for all the CMR-preceding windows.

Window	$\beta_0$ ( $\pm$ s.e.)	$\beta_1$ ( $\pm$ s.e.)	$R^2$	p-value ( $\beta_1$ )
$Y_{[-2,-2]}$	$0.37 \pm 0.22$	$1.28 \pm 0.33$	0.2109	< 0.001
$Y_{[-3,-2]}$	$0.54 \pm 0.22$	$1.09 \pm 0.32$	0.1692	0.001
$Y_{[-4,-2]}$	$0.61 \pm 0.21$	$1.00 \pm 0.32$	0.1471	0.002
$Y_{[-5,-2]}$	$0.68 \pm 0.22$	$0.88 \pm 0.32$	0.1162	0.008
$Y_{[-6,-2]}$	$0.71 \pm 0.21$	$0.83 \pm 0.32$	0.1056	0.011
$Y_{[-7,-2]}$	$0.75 \pm 0.22$	$0.82 \pm 0.32$	0.1025	0.013
$Y_{[-8,-2]}$	$0.75 \pm 0.22$	$0.84 \pm 0.32$	0.1039	0.012
$Y_{[-9,-2]}$	$0.76 \pm 0.22$	$0.86 \pm 0.32$	0.1097	0.010
$Y_{[-10,-2]}$	$0.78 \pm 0.22$	$0.85 \pm 0.32$	0.1082	0.010
$Y_{[-11,-2]}$	$0.76 \pm 0.22$	$0.87 \pm 0.32$	0.1136	0.008

530 **B.2.2 Predictive performance**

Table 9: Predictive performance of the calibration models for Håkøya, using the CMR-encompassing windows.

Window	Coverage	ECM	Bias	RMSE
$Y_{[0,0]}$	0.933	0.283	0.022	1.109
$Y_{[-1,1]}$	0.933	0.367	-0.003	0.860
$Y_{[-2,2]}$	0.933	0.333	0.003	0.886
$Y_{[-3,3]}$	0.950	0.300	0.013	0.921
$Y_{[-4,4]}$	0.967	0.300	0.012	0.942
$Y_{[-5,5]}$	0.950	0.267	0.037	1.040
$Y_{[-6,6]}$	0.950	0.250	0.045	1.073
$Y_{[-7,7]}$	0.950	0.250	0.038	1.077
$Y_{[-8,8]}$	0.950	0.250	0.026	1.050
$Y_{[-9,9]}$	0.950	0.250	0.020	0.996
$Y_{[-10,10]}$	0.933	0.283	0.011	0.988
$Y_{[-11,11]}$	0.933	0.283	0.010	0.987

Table 10: Predictive performance of the calibration models for Håkøya, using the CMR-preceding windows.

Window	Coverage	ECM	Bias	RMSE
$Y_{[-2,-2]}$	0.933	0.350	0.013	0.701
$Y_{[-3,-2]}$	0.967	0.383	0.017	0.793
$Y_{[-4,-2]}$	0.950	0.317	0.034	0.891
$Y_{[-5,-2]}$	0.950	0.283	0.070	1.072
$Y_{[-6,-2]}$	0.983	0.267	0.084	1.178
$Y_{[-7,-2]}$	0.983	0.217	0.065	1.164
$Y_{[-8,-2]}$	0.983	0.217	0.059	1.127
$Y_{[-9,-2]}$	0.967	0.233	0.048	1.075
$Y_{[-10,-2]}$	0.983	0.233	0.028	1.056
$Y_{[-11,-2]}$	0.967	0.233	0.022	1.021

531 **B.3 Other species**

532 The camera traps provide information on more species than the two vole species used in this cal-  
533 ibration. Figure 9 displays counts of all species observed in the camera during the course of the  
534 study. In Porsanger, the Norwegian Lemming (*Lemmus lemmus*) is regularly observed (it is absent  
535 on Håkøya). This is a rodent species that has been considered particularly difficult to trap, and  
536 in fact no lemmings have been trapped by the live traps during this study (and only one during  
537 the previous 20 years in the same grids). Shrews are also observed in about the same numbers as  
538 voles in both study regions. Moreover, small mustelids (stoat (*Mustela erminea*) and least weasel  
539 (*Mustela nivalis*)) are also frequently observed in the regions where they exist (least weasel is not  
540 present on Håkøya).

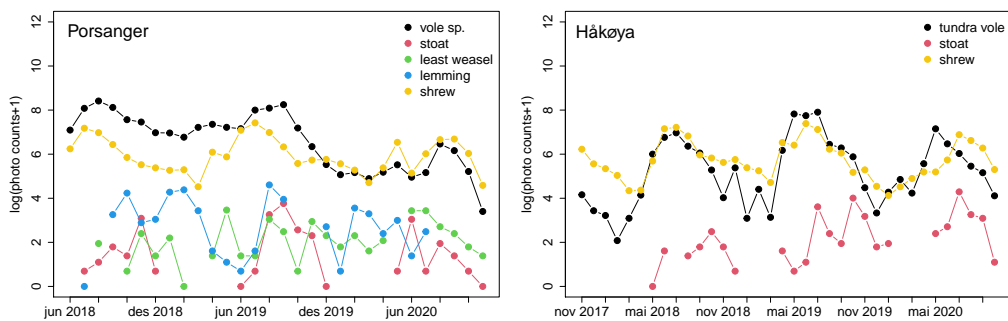


Figure 9: Number of trigger events for all species recorded by the camera traps as a monthly total for the two regions Håkøya and Porsanger, using automated classification data.

## Paper III

**Seasonality, density dependence and spatial population synchrony**

Pre-print available at [arXiv.org](https://arxiv.org). doi: 10.48550/arXiv.2203.16118





# Seasonality, density dependence and spatial population synchrony

Pedro G. Nicolau<sup>\*1</sup>, Sigrunn H. Sørbye<sup>1</sup>, Rolf A. Ims<sup>2</sup> and Nigel G. Yoccoz<sup>2</sup>

<sup>1</sup>Department of Mathematics and Statistics, Faculty of Science, UiT The Arctic University of Norway

<sup>2</sup>Department of Arctic and Marine Biology, Faculty of Biosciences, Fisheries and Economics, UiT The Arctic University of Norway

---

*\*Address for correspondence:* Pedro Guilherme Nicolau, Department of Mathematics and Statistics, Faculty of Science, UiT The Arctic University of Norway, 9037 Tromsø, Norway. E-mail: pedro.nicolau@uit.no

## Abstract

Spatial population synchrony has been the focus of theoretical and empirical studies for decades, in the hopes of understanding mechanisms and interactions driving ecological dynamics. In many systems, it is well-known that seasonality plays a critical role in the density-dependence structure of the populations, yet this has hardly received any attention in synchrony studies. Here, we propose a protocol that allows to elucidate deterministic and stochastic sources of spatial synchrony, while accounting for geographic- and season-specific density dependence. We apply our protocol to seasonally-sampled time series of sub-arctic gray-sided voles, known for marked spatial synchrony. Dissociating seasonal density-dependence contributions to the total observed synchrony reveals differential strength and shape of synchrony patterns by season. Mild winter weather reveals to be an important driver of vole spatial synchrony, with lagged effects in the fall. This has direct implications to the future population dynamics of such species when facing climate change.

## 1 Introduction

Spatial synchrony – referring to the extent local populations display simultaneous changes across space – is a universal characteristic of geographically distributed populations. The strength and scale of population synchrony, which varies tremendously between species and ecosystems, has been the subject of a large number of theoretical and empirical studies (reviewed by Liebhold et al. (2004); Hansen et al. (2020)). These studies are motivated by their potential to provide unique insights into the mechanisms that drive ecological dynamics across a range of spatial scales (Bjørnstad et al., 1999; Koenig, 1999; Walter et al., 2017). The study of spatial population synchrony is one of the fields within ecology that is, both conceptually and methodologically, most tightly linked to other sciences that also deal with spatio-temporal dynamics (Nareddy et al., 2020; Pérez-García et al., 2021).

P.A.P. Moran (1953) developed the first formal theory of spatial population synchrony. Moran’s theorem postulates that populations subjected to the same regulatory biotic mechanisms (i.e. log-linear density dependence), and influenced by the same (or perfectly correlated) abiotic environmental variation (e.g. stochastic weather), will display a synchrony that mirrors the synchrony of the environmental variation (Moran, 1953; Hudson and Cattadori, 1999; Hansen et al., 2020). While this theorem has become a cornerstone of the study of population synchrony, Moran himself expressed the need for relaxing some of its restrictive assumptions in order to be more applicable to empirical case studies. Subsequently, many studies have contributed to a “generalization of the Moran effect” (sensu Hansen et al. (2020)) by, for instance, allowing for non-linear density dependence (Blasius et al., 1999; Engen and Sæther, 2005), spatially heterogeneous (Royama, 2005; Hugueny, 2006) and temporally autocorrelated environmental variation (Massie et al., 2015), and inclusion of other synchronizing mechanisms (e.g. dispersal Ripa (2000) and trophic interactions Jarillo et al. (2020)). Analytical approaches to elucidate the effect of climatic variation on population synchrony have become particularly timely in the current era of anthropogenic climate change (Sheppard et al., 2015; Koenig and Liebhold, 2016).

Accounting for seasonality was a fundamental aspect highlighted by Moran (1953) when assessing the effect of meteorological conditions on population synchrony. This became clear to him when analyzing population time series of lynx from boreal Canada, which is a region with strikingly different climate in summer and winter. Moran realized that season-specific biotic mechanisms were important, because different demographic parameters are involved in the two

seasons (e.g. reproduction only in summer). However, because the lynx population time series were based on only one census per year, Moran was not able to analytically account for season-specific population processes (i.e. density dependence). More modern studies of seasonally-sampled boreal and arctic rodent populations have shown that marked season-specific density dependence is indeed present and a crucially important determinant of local population dynamics (Hansen et al., 1999; Stenseth et al., 2003; Fauteux et al., 2021). Although seasonality is such a critical aspect of most ecological systems (White and Hastings, 2020), and changing seasonality is one of the most profound consequences of global warming in the northern hemisphere (Xu et al., 2013), we are not aware of any study of population synchrony that has explicitly incorporated seasonality. On the contrary, it has even been argued that one should use yearly averages to remove the influence of seasonality when estimating synchrony (e.g. Dallas et al. (2020)).

The purpose of the present study is to devise a general stepwise analytical protocol, that accounts for season-dependent and geographic context-dependent population processes, to identify which aspects of climatic variation and change are most influential to spatial population synchrony (Fig. 1). We illustrate the applicability and potential of the protocol through a case study of the gray-sided vole (*Myodes rufocanus*). This boreal-arctic rodent species is renowned for its important role in ecosystem functioning (Boonstra et al., 2016) and multi-annual population cycles (Hansen et al., 1999; Turchin et al., 2000), with suspected impacts of climate change on these cycles (Ims et al., 2008; Cornulier et al., 2013).

## 2 Results

Local gray-sided vole abundances were estimated every spring and fall over 21 years based on capture-recapture sampling in northern Norway (Fig. 2 a, b). Nineteen sampling locations (i.e. live-trapping grids) were spaced along a 170 km transect in boreal mountain birch forest and encompassed three predefined geographic regions ( $R_1$ : coast,  $R_2$ : fiord and  $R_3$ : inland; Fig. 2a) which were expected to influence the density dependent structure of vole population dynamics.

The 21-year population time series encompass five multi-annual cycles, exhibiting profound overall synchrony across the extent of the study area (Fig. 2b). However, despite visible spatial synchrony, and relative temporal stationarity, there is also some variation in timing and amplitude of the cyclic peaks among the localities. This regards especially the spring series, which have lower and more variable abundance estimates than the fall series (Fig. 2b).

Previous studies have demonstrated that local boreal and Arctic vole populations are adversely affected by winter weather phenomena, such as thaw-freeze cycles (Aars and Ims, 2002; Kausrud et al., 2008) and rain-on-snow events (Fauteux et al., 2021). Hence, we derived local time series of the number of days the temperature crossed zero degrees (Celsius), and the total amount of rainfall (mm) during winter (Fig. 2d). The two weather variables exhibit spatial synchrony, with a tendency for milder (more zero crosses) and wetter (more rainfall) climate towards the coastal area.

### 2.1 Density-dependence structure

Following Stenseth et al. (2003), we fitted second-order log-linear autoregressive models to the population time series, according to the density-dependent (DD) models described in Fig. 1 (models II-IV). As we use a Bayesian framework to conduct the data analysis, we selected Bayesian  $R^2$  (Gelman et al., 2019) as a measure of explained variance (i.e. the fit) of the different linear autoregressive models. In general, the models explained more of the abundance variance in the fall than the spring (Fig. 3). The inclusion of geographic region-specific DD parameters

(when comparing model II and III; Fig. 3) did not improve the model fit much, suggesting there are small differences in the DD structure between the three geographic regions. However, a large improvement of the model fit was achieved when including including season-specific DD parameters (model IV; Fig. 3), especially concerning the fall abundances. This implies that season-specific biotic interactions are strongly influential components of the overall population dynamics.

## 2.2 Spatial population synchrony

The spatial correlograms, based on the four population metrics (I-IV) outlined in Fig. 1, clearly show that much of the overall spatial population synchrony (Fig. 4, I) is due to a common DD structure across the study area (Fig. 4, II-IV). Moreover, when accounting for season-specific DD (model IV), the synchrony in the residuals drops substantially in comparison to that from models II and III, which only account for annual DD (Fig. 4, IV). The reduction in spatial synchrony due to seasonal DD is particularly sharp for the fall abundances, for which the synchrony between the most distant populations approaches zero. Accounting for the slight differences in density dependence among the three geographic regions provides almost no contribution to the synchrony pattern (i.e., comparison between II and III in Fig. 4).

### 2.2.1 Weather synchrony vs. population synchrony

The synchrony of both of the weather variables declined steeply as a function of distance between the sampling stations. However, there was more scattering in the cross-correlations in rainfall when compared to the correlations in the zero crosses (Fig. 5a). The synchrony of number of zero crosses was positively and significantly associated to population synchrony corrected for DD structure (model IV) both in fall and spring, while the synchrony in winter rainfall was only related to the population synchrony in the fall (Fig. 5b,c).

## 3 Discussion

We have here proposed and exemplified an analytical protocol, that based on time series data, allows for elucidating deterministic and stochastic sources of spatial population synchrony. Potential deterministic sources include density dependence, climatic seasonality and geographic ecological context, while influential stochastic sources are likely weather variables. Spatial covariance in stochastic weather events amounts to the Moran effect provided that the deterministic components of local population dynamics are linear and identical. Nonetheless, under most circumstances, correlated weather events are expected to exert synchronizing effects when the local density-dependent structure is non-linear and spatially heterogeneous (i.e., the generalized Moran effect; cf. Engen and Sæther (2005); Royama (2005); Hansen et al. (2020)).

Moran (1953) showed that a key step to make “meteorological phenomena show up more clearly” in statistical analyses of population synchrony is to remove the density-dependent structure from the population time series before making further statistical inferences (e.g., by analyzing the residuals of an autoregressive model). Many studies have used Moran’s approach to remove serial autocorrelation in order to fulfill the independence requirement for significance tests of synchrony (Buonaccorsi et al., 2001; Liebhold et al., 2004). However, there appears to be a lack of studies that have followed Moran’s suggestion to formally analyze whether the scale of synchrony in the population residuals is dependent on synchrony in the weather (but see Grøtan et al. (2005)); i.e., as achieved by step IV in our analytical protocol. Accordingly, Hansen et al.

(2020) conclude that there has been an “analytical deficiency” in empirical Moran-effect studies in terms of making formal inferences about how population synchrony is environmentally forced. We show in the present study that by focusing on residuals which by definition depend on an adequate model structure, we draw more accurate inferences regarding the strength and scale of synchrony.

By applying our analytical protocol to bi-annually sampled time series of gray-sided vole populations we demonstrate winter weather contributions to spatial synchrony. We found that both the amount of rainfall and the frequency of mild-spells in winter contribute to spatial synchrony. These two weather variables have previously been found to affect local population dynamics of boreal and arctic vole species by enhancing winter declines (Aars and Ims, 2002; Fauteux et al., 2021). However, the present study is the first to analytically link large-scale spatial synchrony – a phenomenon that appears to be ubiquitous in boreal and arctic cyclic small rodent populations (cf. Stenseth and Ims (1993); Krebs (2013)) – to any form of stochastic environmental forcing; i.e. Moran effects.

An interesting result arising from our analysis is the time-lagged effect of the winter weather on synchrony of fall abundances. Moran (1953) found similar time-lagged weather effects on an annual time-scale for Canada lynx and speculated about which biological mechanisms could be involved. In voles, environmental conditions in the non-breeding seasons may have lasting effects, for instance, by delaying the onset of reproduction and thereby reducing population growth over the summer (Ergon et al., 2001). The combination of direct and lagged effects of winter weather amounts to an enhanced Moran effect. As increased frequencies of rain-on-snow events and thaw-freeze cycles are very likely outcomes of climate warming in boreal and Arctic ecosystems (AMAP, 2017), we predict that the strength and scale of spatial synchrony of rodent populations will change in these ecosystems.

Climatic seasonality is an externally forced oscillator that acts on the dynamics of most natural systems (Fretwell, 1972). Yet both empirical and theoretical studies of ecological dynamics mostly ignore this fact (White and Hastings, 2020). While seasonality has been shown to be a very important component of spatio-temporal disease dynamics (Earn et al., 1998; Grenfell et al., 2001; Moustakas et al., 2018), we are not aware of empirical studies that have explicitly investigated how such seasonal forcing acts on the strength and scale of synchrony in animal population dynamics. Our analytical protocol provides means for filling this knowledge gap. Specifically, the role of seasonality becomes evident by comparing the correlograms of residuals from models with and without seasonal density dependence (i.e. compare correlograms III and IV in Fig. 4). In the case of sub-arctic gray-sided voles, seasonality is evidently an important determinant of the region-scale spatial synchrony. This regards especially the fall abundances, for which both the overall synchrony becomes reduced and the distance effect is enhanced when seasonal density dependence is accounted for. In this case, it appears that the exact nature of such season-specific effects is contingent on the relative magnitude of the spring and fall noise term of the bi-variate autoregressive model (see Appendix C).

The role of seasonality may be a particularly forceful determinant of spatio-temporal population dynamics in species with multivoltine life cycles, like voles. For instance, the length of winter seasons has been found to exert a strong effect on the local vole population dynamics by acting through density dependent structure (Batzli, 1999; Stenseth, 1999; Stenseth et al., 2003; Bierman et al., 2006) and likely also through season-specific noise terms (Vasseur (2007), Appendix C). Hence, it may not be surprising that seasonality also exerts an effect on regional population dynamics (e.g. large-scale spatial synchrony) as here shown for sub-arctic gray-sided voles. However, as demographic processes are typically season-specific also in univoltine species (Boyce et al., 1999) – including how they are affected by density-dependent and inde-

pendent factors –, we believe that our analytical protocol (Fig. 1) will help advance empirical studies of spatial population synchrony for a wide range of species.

## 4 Methods

The methods section follows the structure outlined in Fig. 1, with the five steps required to investigate weather effects on the spatial population synchrony of a gray-sided vole population, after accounting for the geographical- and seasonal-DD structure of the population.

### 4.1 Sampling and Time Series (Steps 1 and 2)

#### 4.1.1 Data and Study Area

We use data from a long-term running monitoring program of the rodent community in the region of Porsanger, northern Norway, between 2000-2020. The data collection consisted of a capture-mark-recapture methodology with two trapping days at 19 individual stations, scattered along a linear transect of approximately 170 km of road. Trapping sessions were conducted twice per year, once in late spring after snow melt, and once at the end of the summer, at the end of the vole reproductive season (see Ehrich et al. (2009) for precise trapping specifications). The Porsanger region contains different landscapes and is subject to a strong climatic contrast (in both temperature and precipitation). The different stations can be sorted into  $m = 3$  regions according to their landscape affinities: coastal region ( $R_1$ ), fjord region ( $R_2$ ) and inland region ( $R_3$ ). Stations 1–5 were included in  $R_1$  ( $n_1 = 5$ ), stations 6–12 were included in  $R_2$  ( $n_2 = 7$ ) and stations 13–19 were included in  $R_3$  ( $n_3 = 7$ ). Fig. 2 summarizes spatial features of the study area and data.

#### 4.1.2 Abundance estimation from mark-capture-recapture data

To reduce a potential bias when estimating synchrony (Santin-Janin et al., 2014), we incorporated the sampling error from capture heterogeneity in our estimates of seasonal abundances (Nicolau et al., 2020). Specifically, we fitted a multinomial regression model to the capture history data to estimate the probability of obtaining a given capture history as a function of individual features registered during the live trapping. These features included the *weight* and *sex* of the individuals. We also added a random effect for station in the predictor of the regression model. Individual capture probabilities were subsequently estimated by assuming a temporal effect on the capture process (model  $M_{th}$ , Otis et al. (1978)). Finally, the individual probabilities were used to estimate seasonal abundances using an empirical Horvitz-Thompson estimator, which is a function of the estimated individual capture probabilities. Denote the resulting estimated log abundances by  $\{X_{s,t}\}$  and  $\{Y_{s,t}\}$ , for spring and fall, respectively, at spatial locations  $s = 1, \dots, n_s$  and year  $t = 1, \dots, n_t$ . For the case study,  $n_s = 19$  and  $n_t = 21$ .

#### 4.1.3 Weather variables

To explore the effect of the weather on the spatial synchrony, we should ideally look into the winter snow conditions (i.e, snow depth and ice formation) as they can be considered the most relevant climatic variables affecting rodent population cycles (Hansson and Henttonen, 1985; Hansen et al., 2013; Stien et al., 2012; Fauteux et al., 2021), being an interaction of different weather variables, including temperature and precipitation. As this information was not directly

available, we resorted to proxy variables of snow conditions, using the temperature and precipitation estimates from the Norwegian Meteorological Institute between 2000-2020. These measurements correspond to model estimates (not measured at station level) and are prone to large uncertainties, particularly the precipitation (Lussana et al., 2019). For our proxies of snow conditions, we derived two variables: winter *zero crosses*, as the total number of times the mean daily temperature crossed 0 °C during winter (21 Dec – 20 Mar); and *winter rainfall*, as the precipitation sum in days where the mean temperature surpassed 0 °C, during winter.

## 4.2 Statistical Framework

We describe the statistical framework to decompose density-dependence contributions into the spatial synchrony of populations, and isolate the weather effects on population synchrony, described in steps 3–5 in Fig. 1.

### 4.2.1 Density-dependence structure (Step 3)

The general protocol (Fig. 1, step 3) specifies three different models for the DD structure of the estimated time series. Here, we assume that the general function  $f(\cdot)$  is linear, describing the log-DD structure in terms of direct and delayed effects up to lag  $p$ . Specifically, the three models either include or exclude regional- and seasonal-dependent effects as specified below.

In general, the spatial locations  $s$  are assumed to be within a closed geographical region  $R$ , which can be partitioned into  $m$  mutually exclusive subregions,  $R = R_1 \cup \dots \cup R_m$ . For the gray-sided vole case study, this corresponds to  $m = 3$  regions. The most general model includes both regional-specific and seasonal-specific terms (Fig. 1, model (IV)), and the assumed log-linear dependency structure up to order  $p$  can be expressed by

$$X_{s,t} = \beta_{r1}Y_{s,t-1} + \beta_{r2}X_{s,t-1} + \dots + \beta_{r,2p-1}Y_{s,t-p} + \beta_{r,2p}X_{s,t-p} + \epsilon_{s,t} \quad (1)$$

$$Y_{s,t} = \gamma_{r1}X_{s,t} + \gamma_{r2}Y_{s,t-1} + \dots + \gamma_{r,2p-1}X_{s,t-1} + \gamma_{r,2p}Y_{s,t-p} + \omega_{s,t} \quad (2)$$

where  $t = p + 1, \dots, n_t$  and  $s \in R_r$ . The terms  $\epsilon_{st}$  and  $\omega_{st}$  denote individual random environmental noise at each spatial location  $s$  for each time point  $t$ , while the sets of regional- and seasonal-specific coefficients can be summarized as  $\Theta_{R_x} = \{\beta_{r1}, \dots, \beta_{r,2p}\}$  and  $\Theta_{R_y} = \{\gamma_{r1}, \dots, \gamma_{r,2p}\}$ .

Simplifications of the given model will yield more simplistic measures of the DD structure. According to the general protocol in Fig. 1, Model (I) corresponds to assuming no DD structure, in which all of the given coefficients are equal to 0. This corresponds to simply using the estimated raw log-abundance series,  $\{X_{s,t}\}$  and  $\{Y_{s,t}\}$ , in further analysis.

Following (Stenseth et al., 2003), we included delayed effects up to order  $p = 2$  for the case study. Model (II) refers to a second-order annual autoregressive processes including coefficients  $\Theta = \{\beta_2, \beta_4, \gamma_2, \gamma_4\}$  which are neither regional-specific ( $m = 1$ ; disregarding spatial heterogeneity), nor seasonal-specific ( $\beta_1 = \beta_3 = \gamma_1 = \gamma_3 = 0$ ; assuming yearly dynamics). Such AR(2) models are often used in literature (e.g. Turkia et al. (2020); Dallas et al. (2020)). Model (III) is characterized by incorporating regional-specific effects  $\{\beta_{r2}, \beta_{r4}, \gamma_{r2}, \gamma_{r4}\}_{r=1}^m$ . This corresponds to AR(2) models which allow for spatial differences in the DD structure which can account for some of the observed synchrony (Hugueny, 2006). Finally, by including the seasonal-specific effects  $\{\beta_{r1}, \beta_{r3}, \gamma_{r1}, \gamma_{r3}\}_{r=1}^m$ , we get the bivariate model (IV) which is very similar to a second-order vector autoregressive model (VAR). The difference to a VAR-model, however, is that the time series  $\{X_{s,t}\}$  and  $\{Y_{s,t}\}$  are observed at two different time points in year  $t$ , and the fall log-abundances are modeled in terms of the spring observations within the

same year. Seasonal-specific DD has been recognized as fundamental to model small rodent population dynamics (Hansen et al., 1999), but to our knowledge seasonal DD contributions to spatial synchrony have not been assessed.

#### 4.2.2 Measuring the scale and shape of spatial population synchrony (Step 4)

To assess the scale and shape of the spatial synchrony, we can consider the spatial correlations of the environmental noise terms in Models (I–IV) as a function of geographical distance. The following analysis is repeated using the four different models for DD structure, specified in section 4.2.1. A major goal is then to understand how the inclusion of regional- and seasonal-specific terms influences the synchrony estimates, i.e., which part of the synchrony is explained by the different DD components.

Define the residual vectors  $\epsilon'_s = (\epsilon_{s,1}, \dots, \epsilon_{s,n_t})$  and  $\omega'_s = (\omega_{s,1}, \dots, \omega_{s,n_t})$  for all spatial locations  $s = 1, \dots, n_s$  and  $t = p+1, \dots, n_t$ . The contributions to the spatial synchrony are then characterized by the pairwise correlations between vectors within each of the sets  $\{\epsilon'_s\}_{s=1}^{n_s}$  and  $\{\omega'_s\}_{s=1}^{n_s}$ . If the associations between these residual series are expected to be linear, the degree of synchrony is typically measured using Pearson's correlation coefficient (Bjørnstad et al., 1999; Liebhold et al., 2004). To model the correlations in terms of geographical distance, let  $\delta_{i,j}$  denote the Euclidean distance between two stations  $i$  and  $j$ . In accordance with calculating the spatial correlogram (Bjørnstad et al., 1999; Bjørnstad and Falck, 2001; Liebhold et al., 2004), we discretize the  $n_s(n_s - 1)/2$  unique distances between stations into distance classes  $d_k$ ,  $k = 1, \dots, K$ , where  $K$  is the total number of classes. Specifically, a distance class  $d_k$  is defined by  $L_k < \delta_{i,j} < U_k$ , where  $L_k$  and  $U_k$  represent the lower and upper bound of the distances within that class, respectively. The corresponding averages of the pairwise correlations  $\{\rho_{i,j}\}$  for distance class  $d_k$  are then given by

$$\rho_k(d_k) = \frac{2 \sum_{i=1}^{n_k} \sum_{j=i+1}^{n_k} \rho_{i,j}}{n_k(n_k - 1)}, \quad L_k < \delta_{i,j} \leq U_k, \quad (3)$$

where  $n_k$  is the total number of distances/correlations within distance class  $d_k$ . The given formulation is analogous to the calculation of Koenig's modified correlogram (Koenig, 1999; Bjørnstad et al., 1999), as the correlations are not centered (zero synchrony is taken as the reference line of the correlogram). For the given case study, we assumed that the distance-class width is  $U_k - L_k = 1$  for all classes, which corresponds to rounding off the geographical distances to the nearest integer. We used this method to calculate the averaged correlations in (3) as a pre-processing step to reduce random noise in the estimated correlations.

As an alternative to using the non-parametric covariance function (Bjørnstad and Falck, 2001) or other non-parametric estimates of the correlation function (Liebhold et al., 2004), we chose to model the correlations in terms of the distances using the regression model

$$\rho_k(d_k) = f(d_k) + \nu_k, \quad k = 1, \dots, K. \quad (4)$$

Here,  $f$  denotes a smooth underlying function while  $\{\nu_k\}$  represents zero-mean, independent Gaussian error terms with constant variance. This model is fitted using a Bayesian framework where the function  $f$  is assigned a second-order intrinsic Gaussian Markov random field prior (Rue and Held (2005), page 110). The model is scaled according to Sørbye and Rue (2014) and the precision parameter of the model is assigned a penalized complexity prior with parameters  $U = 0.5$  and  $\alpha = 0.01$  (Simpson et al., 2017). Using the methodology of integrated nested Laplace approximation (Rue et al., 2009), both the posterior mean and credible intervals for  $f$  are calculated efficiently, without the need of resampling techniques, like Monte Carlo simulation or bootstrapping.



### 4.2.3 Effects of Weather (Step 5)

Finally, we can use the measures of synchrony accounting for the effects of geographic- and seasonal-dependent DD to investigate potential weather (or other relevant environmental variables) drivers. For this, we can model the set of correlations  $\{\rho_k(d_k)\}_{k=1}^K$  from model (IV) as a function of the corresponding spatial correlations of different weather covariates, defined by  $\{\rho_k^{(c)}(d_k)\}_{k=1}^K$ . The availability of such covariates are typically case-specific but should be measured or estimated to represent the same spatial locations and time points used for the log-abundance estimates. For the given case study, the relationship between the weather variables (*zero crosses* and *winter rainfall*) appeared to be linear, and was thus modeled using simple linear regression models.

# Figures

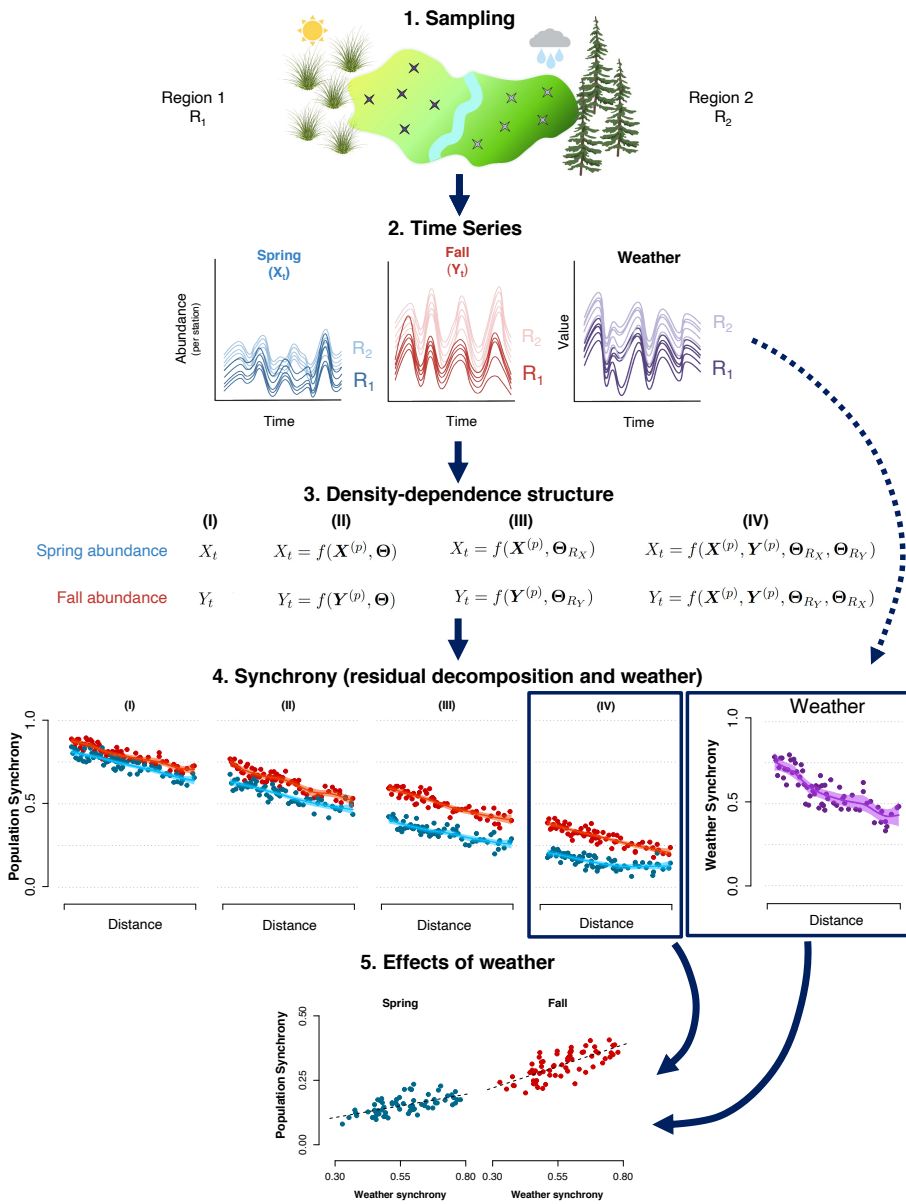


Figure 1: Methodological Protocol (cont.)

Figure 1: (cont.) The five main steps of a general methodological protocol to single out the impacts of climatic variation (weather) on spatial population synchrony, by accounting for seasonal and geographical contexts in ecological population processes (density dependence). Step 1: Seasonal (spring and fall) sampling of both local populations and a focal weather variable at different locations (crosses). The geographic sampling frame encompasses two regions ( $R_1$  and  $R_2$ ) representing different geographic ecological contexts (e.g. habitats or ecological communities). Step 2: Season- and region-specific time series of local population abundance estimates resulting from the sampling process, together with time series of the focal weather variable. The estimation of abundance ideally involves separating the observation process and the population process, accounting for detectability. Step 3: Four alternative models to further analyze spatial population synchrony. (I) corresponds to seasonal abundance estimates ( $X_t$  and  $Y_t$ ). (II-IV) correspond to the sets of  $X_t - f(\cdot)$  and  $Y_t - f(\cdot)$  from the respective general models for density-dependence, modeling state of the population at time  $t$  as a function of previous  $p$  states. Model (II) includes only one set  $\Theta$  of density-dependence parameters with annual time lags (i.e. ignoring seasonal and regional components). Model (III) includes region-specific parameters  $\Theta_R$ , again with annual time lags (i.e. ignoring seasonal components). Model (IV) is a bi-variate model (Stenseth et al., 2003) that includes both geographic- and season-specific parameters  $\Theta_{R_X}$  and  $\Theta_{R_Y}$ . Step 4: Season-specific synchrony patterns (i.e. scale and shape) of the population (derived from Step 3) and weather metrics (derived from Step 2) as function of distance. The dots are the pairwise cross-correlations of the population metrics and the weather variables, while the lines are estimated correlograms with associated uncertainty intervals (e.g., Bjørnstad et al. (1999)). Step 5: Estimated effects of weather synchrony on population synchrony. Season-specific (Fall and Spring) population synchrony with corrected for seasonal-density dependence and geographic context effects (i.e. residuals from model (IV)) are regressed against the spatial synchrony in the focal weather variable. Illustrations created with Biorender.com.

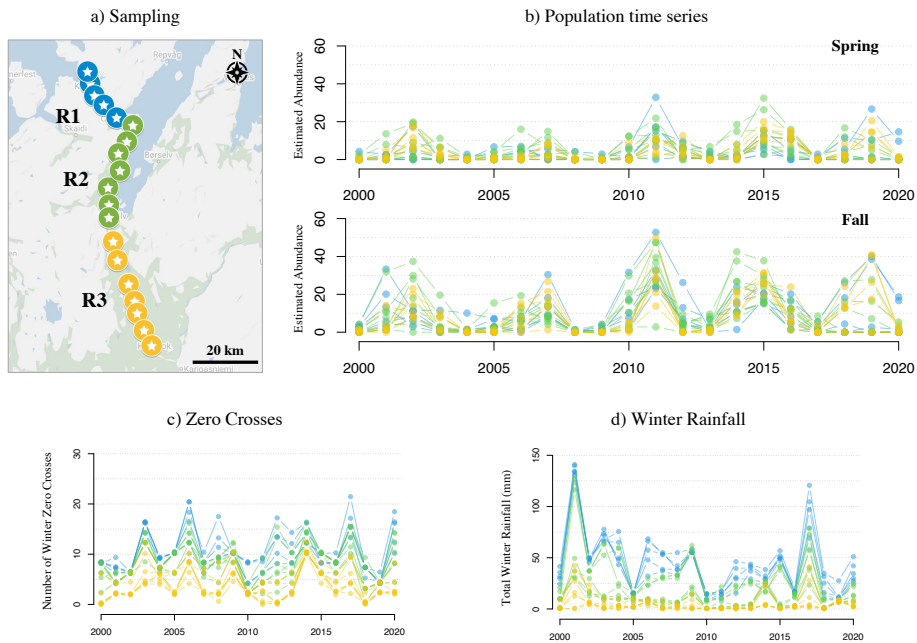


Figure 2: Sampling design and time series. a) Map with the 19 sampling stations (“dot/stars”) along the 170 km transect encompassing three geographical contexts ( $R_1$ : coast,  $R_2$ : fjord;  $R_3$ : inland). Green shade landcover denotes mountain birch forest, white denotes tundra and blue denotes water surfaces. b) Time series of abundance estimates for the 19 local grey-sided vole population in spring (lower) and fall (upper). Time series of the two focal winter weather variables are presented in c) number of zero crossings and d) total winter rainfall. Colors of curves in b)–d) correspond to the three geographic context in a).

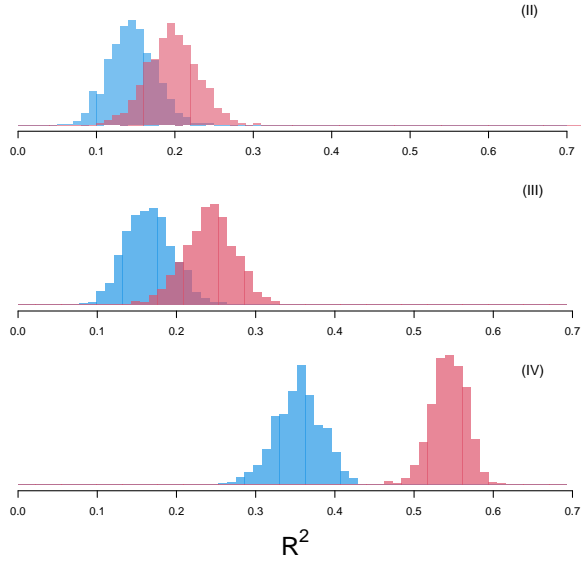


Figure 3: Distributions of Bayesian  $R^2$  values (blue for spring and red for fall abundances) for the three sets of second-order, log-linear models corresponding to the general DD models II — IV outlined Step 3 Fig. 1. As we are working in a Bayesian framework the computation of the  $R^2$  results in a distribution itself (see Gelman et al. (2019) for details).

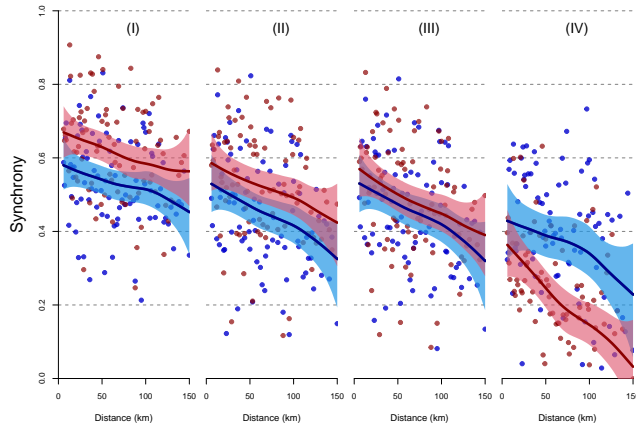


Figure 4: Correlograms depicting how the synchrony (i.e. the pairwise spatial correlations) of four different population metrics (see Fig. 1, Step 3) varies with geographical distance between local gray-sided vole populations. 95% credible intervals for spring are plotted in blue, and for fall are plotted in red, while the solid lines correspond to the median. Single dots correspond to the individual pairwise correlations used in the correlogram.

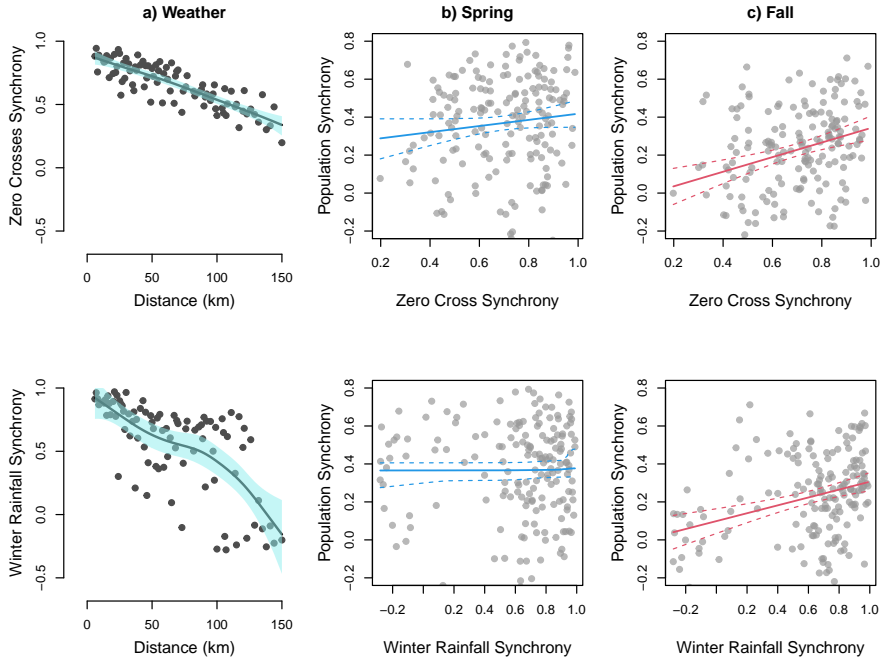


Figure 5: Weather synchrony versus population synchrony. Panels a) Correlograms of the two focal weather variables with associated 95% credible intervals, winter *zero crosses* (ZC; top) and winter rainfall (WR; bottom). Panels b) and c) correspond to linear regression lines, with associated 95% credible intervals, of population synchrony as a function of weather synchrony for spring (b) and fall abundances (c). Slope estimates for spring are  $\beta_{ZC} = 0.16$  (CI : -0.04,0.36)  $\beta_{WR} = 0.00$  (CI : -0.11,0.10). Slope estimates for fall are  $\beta_{ZC} = 0.38$  (CI : 0.20,0.56) and  $\beta_{WR} = 0.21$  (CI : 0.12,0.30). CI denotes 95% credible intervals for each regression coefficient  $\beta$ .

## References

- Aars, J. and Ims, R. A. (2002). Intrinsic and climatic determinants of population demography: the winter dynamics of tundra voles. *Ecology*, 83(12):3449–3456.
- AMAP (2017). Snow, Water, Ice and Permafrost in the Arctic (SWIPA) 2017. Arctic Monitoring and Assessment Programme (AMAP), Oslo, Norway. xiv + 269 pp.
- Batzli, G. O. (1999). Can seasonal changes in density dependence drive population cycles? *Trends in Ecology & Evolution*, 14(4):129–131.
- Bierman, S. M., Fairbairn, J. P., Petty, S. J., Elston, D. A., Tidhar, D., and Lambin, X. (2006). Changes over time in the spatiotemporal dynamics of cyclic populations of field voles (*Microtus agrestis* L.). *The American Naturalist*, 167(4):583–590.
- Bjørnstad, O. N. and Falck, W. (2001). Nonparametric spatial covariance functions: estimation and testing. *Environmental and Ecological Statistics*, 8(1):53–70.
- Bjørnstad, O. N., Ims, R. A., and Lambin, X. (1999). Spatial population dynamics: analyzing patterns and processes of population synchrony. *Trends in Ecology & Evolution*, 14(11):427–432.
- Blasius, B., Huppert, A., and Stone, L. (1999). Complex dynamics and phase synchronization in spatially extended ecological systems. *Nature*, 399(6734):354–359.
- Boonstra, R., Andreassen, H. P., Boutin, S., Hušek, J., Ims, R. A., Krebs, C. J., Skarpe, C., and Wabakken, P. (2016). Why do the boreal forest ecosystems of northwestern Europe differ from those of western North America? *BioScience*, 66(9):722–734.
- Boyce, M. S., Sinclair, A. R. E., and White, G. C. (1999). Seasonal compensation of predation and harvesting. *Oikos*, 87(3):419.
- Buonaccorsi, J. P., Elkinton, J. S., Evans, S. R., and Liebhold, A. M. (2001). Measuring and testing for spatial synchrony. *Ecology*, 82(6):1668–1679.
- Cornulier, T., Yoccoz, N. G., Bretagnolle, V., Brommer, J. E., Butet, A., Ecke, F., Elston, D. A., Framstad, E., Henttonen, H., Hörnfeldt, B., Huitu, O., Imholt, C., Ims, R. A., Jacob, J., Jędrzejewska, B., Millon, A., Petty, S. J., Pietiäinen, H., Tkadlec, E., Zub, K., and Lambin, X. (2013). Europe-wide dampening of population cycles in keystone herbivores. *Science*, 340(6128):63–66.
- Dallas, T. A., Antão, L. H., Pöyry, J., Leinonen, R., and Ovaskainen, O. (2020). Spatial synchrony is related to environmental change in finnish moth communities. *Proceedings of the Royal Society of London. Series B: Biological Sciences*, 287(1927):20200684.
- Earn, D. J., Rohani, P., and Grenfell, B. T. (1998). Persistence, chaos and synchrony in ecology and epidemiology. *Proceedings of the Royal Society of London. Series B: Biological Sciences*, 265(1390):7–10.
- Ehrich, D., Yoccoz, N. G., and Ims, R. A. (2009). Multi-annual density fluctuations and habitat size enhance genetic variability in two northern voles. *Oikos*, 118(10):1441–1452.

- Engen, S. and Sæther, B.-E. (2005). Generalizations of the Moran effect explaining spatial synchrony in population fluctuations. *The American Naturalist*, 166(5):603–612.
- Ergon, T., Lambin, X., and Stenseth, N. C. (2001). Life-history traits of voles in a fluctuating population respond to the immediate environment. *Nature*, 411(6841):1043–1045.
- Fauteux, D., Stien, A., Yoccoz, N. G., Fuglei, E., and Ims, R. A. (2021). Climate variability and density-dependent population dynamics: Lessons from a simple High Arctic ecosystem. *Proceedings of the National Academy of Sciences*, 118(37):e2106635118.
- Fretwell, S. D. (1972). *Populations in a Seasonal Environment*. Princeton University Press, Princeton.
- Gelman, A., Goodrich, B., Gabry, J., and Vehtari, A. (2019). R-squared for Bayesian regression models. *The American Statistician*, 73(3):307–309.
- Grenfell, B. T., Bjørnstad, O. N., and Kappey, J. (2001). Travelling waves and spatial hierarchies in measles epidemics. *Nature*, 414(6865):716–723.
- Grøtan, V., Sæther, B.-E., Engen, S., Solberg, E. J., Linnell, J. D. C., Andersen, R., Brøseth, H., and Lund, E. (2005). Climate causes large-scale spatial synchrony in population fluctuations of a temperate herbivore. *Ecology*, 86(6):1472–1482.
- Hansen, B. B., Grøtan, V., Aanes, R., Sæther, B.-E., Stien, A., Fuglei, E., Ims, R. A., Yoccoz, N. G., and Pedersen, A. O. (2013). Climate events synchronize the dynamics of a resident vertebrate community in the high arctic. *Science*, 339(6117):313–315.
- Hansen, B. B., Grøtan, V., Herfindal, I., and Lee, A. M. (2020). The Moran effect revisited: spatial population synchrony under global warming. *Ecography*, 43(11):1591–1602.
- Hansen, T. F., Stenseth, N. C., and Henttonen, H. (1999). Multiannual vole cycles and population regulation during long winters: an analysis of seasonal density dependence. *The American Naturalist*, 154(2):129–139.
- Hansson, L. and Henttonen, H. (1985). Gradients in density variations of small rodents: the importance of latitude and snow cover. *Oecologia*, 67(3):394–402.
- Hudson, P. J. and Cattadori, I. M. (1999). The Moran effect: a cause of population synchrony. *Trends in Ecology & Evolution*, 14(1):1–2.
- Hugueny, B. (2006). Spatial synchrony in population fluctuations: extending the Moran theorem to cope with spatially heterogeneous dynamics. *Oikos*, 115(1):3–14.
- Ims, R., Henden, J.-A., and Killengreen, S. (2008). Collapsing population cycles. *Trends in Ecology & Evolution*, 23(2):79–86.
- Jarillo, J., Sæther, B.-E., Engen, S., and Cao-García, F. J. (2020). Spatial scales of population synchrony in predator-prey systems. *The American Naturalist*, 195(2):216–230.
- Kausrud, K. L., Mysterud, A., Steen, H., Vik, J. O., Østbye, E., Cazelles, B., Framstad, E., Eikeset, A. M., Mysterud, I., Solhøy, T., and Stenseth, N. C. (2008). Linking climate change to lemming cycles. *Nature*, 456(7218):93–97.



- Koenig, W. D. (1999). Spatial autocorrelation of ecological phenomena. *Trends in Ecology & Evolution*, 14(1):22–26.
- Koenig, W. D. and Liebhold, A. M. (2016). Temporally increasing spatial synchrony of North American temperature and bird populations. *Nature Climate Change*, 6(6):614–617.
- Krebs, C. J. (2013). *Population fluctuations in rodents*. University of Chicago Press.
- Liebhold, A., Koenig, W. D., and Bjørnstad, O. N. (2004). Spatial synchrony in population dynamics. *Annual Review of Ecology, Evolution, and Systematics*, 35(1):467–490.
- Lussana, C., Tveito, O. E., Dobler, A., and Tunheim, K. (2019). seNorge\_2018, daily precipitation, and temperature datasets over norway. *Earth System Science Data*, 11(4):1531–1551.
- Massie, T. M., Weithoff, G., Kuckländer, N., Gaedke, U., and Blasius, B. (2015). Enhanced Moran effect by spatial variation in environmental autocorrelation. *Nature Communications*, 6(1).
- Moran, P. (1953). The statistical analysis of the Canadian Lynx cycle. 2. Synchronization and meteorology. *Australian Journal of Zoology*, 1(3):291.
- Moustakas, A., Evans, M. R., Daliakopoulos, I. N., and Markonis, Y. (2018). Abrupt events and population synchrony in the dynamics of bovine tuberculosis. *Nature Communications*, 9(1).
- Nareddy, V. R., Machta, J., Abbott, K. C., Esmaili, S., and Hastings, A. (2020). Dynamical ising model of spatially coupled ecological oscillators. *Journal of The Royal Society Interface*, 17(171):20200571.
- Nicolau, P. G., Sørbye, S. H., and Yoccoz, N. G. (2020). Incorporating capture heterogeneity in the estimation of autoregressive coefficients of animal population dynamics using capture–recapture data. *Ecology and Evolution*, 10(23):12710–12726.
- Otis, D. L., Burnham, K. P., White, G. C., and Anderson, D. R. (1978). Statistical inference from capture data on closed animal populations. *Wildlife Monographs*, (62):3–135.
- Pérez-García, S., García-Navarrete, M., Ruiz-Sanchis, D., Prieto-Navarro, C., Avdovic, M., Puciarriello, O., and Wabnik, K. (2021). Synchronization of gene expression across eukaryotic communities through chemical rhythms. *Nature Communications*, 12(1).
- Ripa, J. (2000). Analysing the Moran effect and dispersal: their significance and interaction in synchronous population dynamics. *Oikos*, 89(1):175–187.
- Royama, T. (2005). Moran effect on nonlinear population processes. *Ecological Monographs*, 75(2):277–293.
- Rue, H. and Held, L. (2005). *Gaussian Markov random fields: theory and applications*. Chapman and Hall/CRC.
- Rue, H., Martino, S., and Chopin, N. (2009). Approximate Bayesian inference for latent Gaussian models by using integrated nested Laplace approximations. *Journal of the Royal Statistical Society: Series B (Statistical Methodology)*, 71(2):319–392.

- Santin-Janin, H., Hugueny, B., Aubry, P., Fouchet, D., Gimenez, O., and Pontier, D. (2014). Accounting for sampling error when inferring population synchrony from time-series data: A bayesian state-space modelling approach with applications. *PLoS ONE*, 9(1):e87084.
- Sheppard, L. W., Bell, J. R., Harrington, R., and Reuman, D. C. (2015). Changes in large-scale climate alter spatial synchrony of aphid pests. *Nature Climate Change*, 6(6):610–613.
- Simpson, D., Rue, H., Riebler, A., Martins, T. G., and Sørbye, S. H. (2017). Penalising model component complexity: A principled, practical approach to constructing priors. *Statistical Science*, 32:1–28.
- Sørbye, S. H. and Rue, H. (2014). Scaling intrinsic Gaussian Markov random field priors in spatial modelling. *Spatial Statistics*, 8:39–51.
- Stenseth, N. C. (1999). Population cycles in voles and lemmings: Density dependence and phase dependence in a stochastic world. *Oikos*, 87(3):427.
- Stenseth, N. C. and Ims, R. A. (1993). Population dynamics of lemmings: Temporal and spatial variations. In Stenseth, N. C. and Ims, R. A., editors, *The biology of Lemmings*, page 61–97. Academic Press.
- Stenseth, N. C., Viljugrein, H., Saitoh, T., Hansen, T. F., Kittilsen, M. O., Bølviken, E., and Glockner, F. (2003). Seasonality, density dependence, and population cycles in Hokkaido voles. *Proceedings of the National Academy of Sciences*, 100:11478–11483.
- Stien, A., Ims, R. A., Albon, S. D., Fuglei, E., Irvine, R. J., Ropstad, E., Halvorsen, O., Langvatn, R., Loe, L. E., Veiberg, V., and Yoccoz, N. G. (2012). Congruent responses to weather variability in high arctic herbivores. *Biology Letters*, 8(6):1002–1005.
- Turchin, P., Oksanen, L., Ekerholm, P., Oksanen, T., and Henttonen, H. (2000). Are lemmings prey or predators? *Nature*, 405(6786):562–565.
- Turkia, T., Jousimo, J., Tiainen, J., Helle, P., Rintala, J., Hokkanen, T., Valkama, J., and Selonen, V. (2020). Large-scale spatial synchrony in red squirrel populations driven by a bottom-up effect. *Oecologia*, 192(2):425–437.
- Vasseur, D. A. (2007). Environmental colour intensifies the moran effect when population dynamics are spatially heterogeneous. *Oikos*, 116(10):1726–1736.
- Walter, J. A., Sheppard, L. W., Anderson, T. L., Kastens, J. H., Bjørnstad, O. N., Liebhold, A. M., and Reuman, D. C. (2017). The geography of spatial synchrony. *Ecology Letters*, 20(7):801–814.
- White, E. R. and Hastings, A. (2020). Seasonality in ecology: Progress and prospects in theory. *Ecological Complexity*, 44:100867.
- Xu, L., Myneni, R. B., III, F. S. C., Callaghan, T. V., Pinzon, J. E., Tucker, C. J., Zhu, Z., Bi, J., Ciais, P., Tømmervik, H., Euskirchen, E. S., Forbes, B. C., Piao, S. L., Anderson, B. T., Ganguly, S., Nemani, R. R., Goetz, S. J., Beck, P. S. A., Bunn, A. G., Cao, C., and Stroeve, J. C. (2013). Temperature and vegetation seasonality diminishment over northern lands. *Nature Climate Change*, 3(6):581–586.

## A Winter Weather Patterns

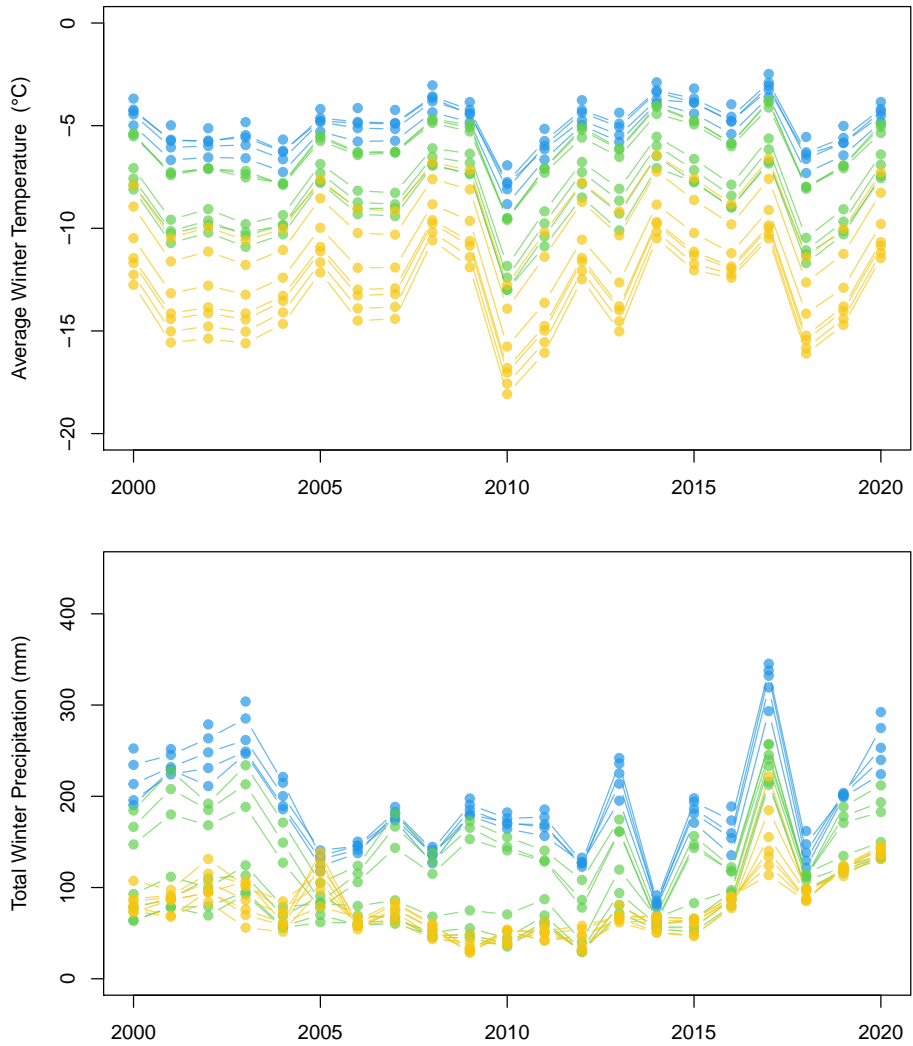


Figure 6: Winter mean temperature and winter total precipitation for the 19 stations, color-coded according to their region.

## B Model coefficients (section 2.1)

### Model II

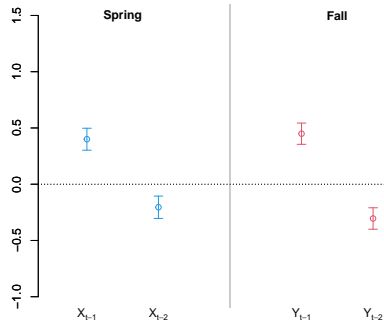


Figure 7: Autoregressive coefficient estimates for model II. Associated 95% credible intervals are represented by the bars.

### Model III

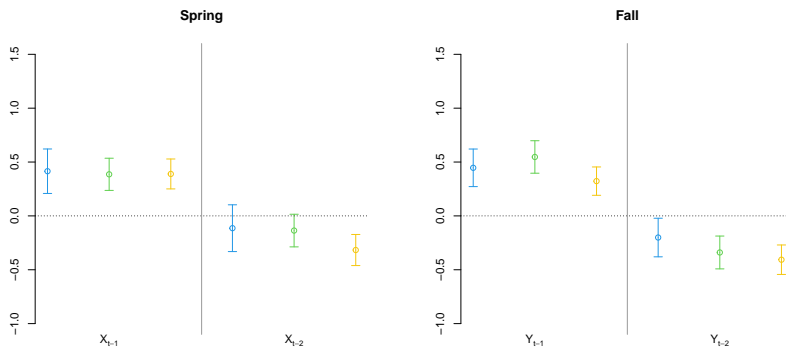


Figure 8: Autoregressive coefficient estimates for model III. Associated 95% credible intervals correspond to the bars, with the coefficients associated with each region represented with the respective color (blue for  $R_1$ , green for  $R_2$  and yellow for  $R_3$ ).

## Model IV

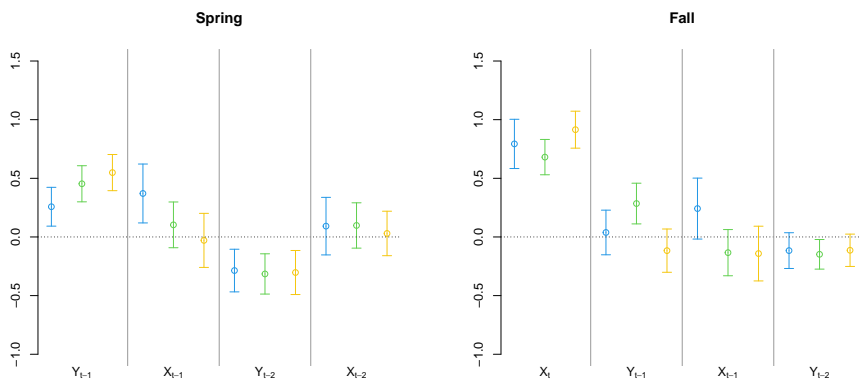


Figure 9: Autoregressive coefficient estimates for model IV, according to the different seasons. Associated 95% credible intervals correspond to the bars, with the coefficients associated with each region represented with the respective color (blue for  $R_1$ , green for  $R_2$  and yellow for  $R_3$ ).

## C Simulations

To assess when the observed changes in seasonal correlations can occur, we made a short simulation study. We simulated 100.000 pairs of time series, each pair corresponding to 2 populations with a true process described by model IV (see Methods), with regression parameters approximating those of the real data set (section B; parameter values were  $\{\beta_1 = 0.5, \beta_2 = 0.1, \beta_3 = -0.4, \beta_4 = 0.1, \gamma_1 = 0.8, \gamma_2 = 0.1, \gamma_3 = -0.1, \gamma_4 = -0.1\}$ ). We then compared (a) the true correlation in the noise terms for each pair (which corresponds to a parameter in the simulation; we used  $r=0.5$  for the spring correlation and  $r=0.3$  for the fall correlation), against: (b) the correlations when using year-to-year raw abundances for either spring and fall (model I); and (c) correlations in the residuals of yearly AR(2) for each season separately (model II).

Figure 10 displays the noise correlation estimates for each of the approaches, using different variances of spring and fall noise. We can infer that the decrease we have observed for fall densities (i.e., summer season) happens when the winter noise is as large or larger than the summer noise, which is expected by the case in study system (the estimated variances were 0.86 for spring and 0.86 for fall). If the summer noise is larger than the winter noise, the patterns are reversed compared to the case when winter noise is larger than summer noise. Note that correlations based on annual models can be higher than the true ones. This confirms that the observed changes come from considering the seasonal model (IV) instead of the annual models (I–III), rather than artifacts related to the data. This shows that fluctuating (i.e., seasonal) environments can enhance synchrony, but the exact pattern obtained using annual time series will depend on the noise structure and which season is monitored (Vasseur, 2007).

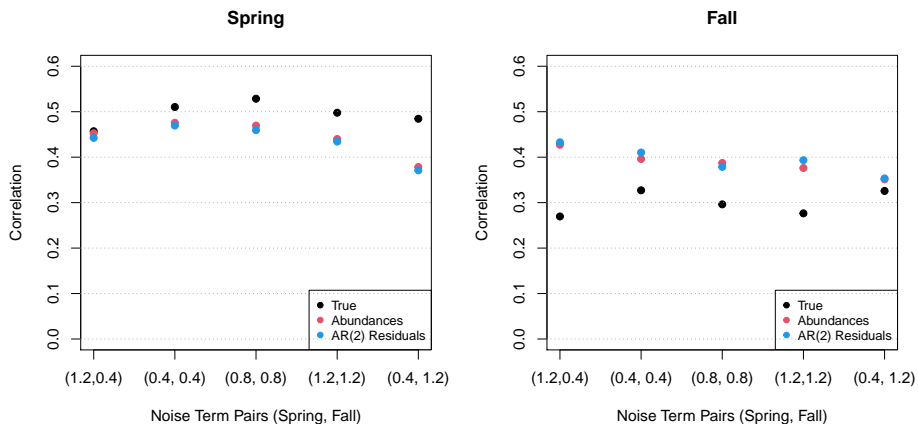


Figure 10: Simulating noise term correlations for either Spring and Fall. X-axis corresponds to the noise terms of either Spring (left) and Fall processes (right). This corresponds to the  $\epsilon$  and  $\omega$  terms in equations 1–2. The mean true correlations in the noise terms (a) are the black dots; the mean correlations in the raw abundances are the red dots; are the mean correlations in the AR(2) model residuals (c) are the blue dots.

Abundance

Time

